

# Dynamical Processes for Descriptive Ocean Circulation

---

This is the complete chapter concerning dynamical processes; a truncated version appears in the print text. Many additional figures are included here, along with expanded descriptions and derivations. Tables for Chapter 7 appear only on this Web site.

Water in the ocean at all time and space scales is subject to the same small set of forces and accelerations. What distinguishes one type of motion from another, for instance a surface wave from the Gulf Stream, is the relative importance of the different accelerations and forces within this small set. In this chapter we introduce a basic dynamical framework for the major circulation and water mass structures described in ensuing chapters. We use as little mathematics as possible, relying principally on word descriptions of the physical processes. Students are directed to dynamical oceanography textbooks for complete coverage of these topics, including scale analysis and derivations, such as Gill (1982), Pedlosky (1987), Cushman-Roisin (1994), Knauss (1997), Salmon (1998), Vallis (2006), and Huang (2010).

We proceed from the basic equations of motion (Sections 7.1 and 7.2) and density evolution (Section 7.3) to mixing layers (Section 7.4); direct wind response including Ekman layers (Section 7.5); geostrophic flow (Section

7.6); vorticity, potential vorticity, and Rossby waves (Section 7.7); wind-driven circulation models of the gyre circulations (Section 7.8); equatorial and eastern boundary circulations (Section 7.9); and finally thermohaline forcing, abyssal circulation, and overturning circulation (Section 7.10).

## 7.1. INTRODUCTION: MECHANISMS

---

Ultimately, motion of water in the ocean is driven by the sun, the moon, or tectonic processes. The sun's energy is transferred to the ocean through buoyancy fluxes (heat fluxes and water vapor fluxes) and through the winds. Tides create internal waves that break, creating turbulence and mixing. Earthquakes and turbidity currents create random, irregular waves including tsunamis. Geothermal processes heat the water very gradually with little effect on circulation.

Earth's rotation profoundly affects almost all phenomena described in this text. Rotating fluids behave differently from non-rotating fluids in ways that might be counterintuitive. In a non-rotating fluid, a pressure difference between two points in the fluid drives the fluid

toward the low pressure. In a fluid dominated by rotation, the flow can be *geostrophic*, perpendicular to the pressure gradient force, circling around centers of high or low pressure due to the Coriolis effect.

Ocean circulation is often divided conceptually into two parts, the *wind-driven* and the *thermohaline* (or buoyancy-dominated) components. Wind blowing on the ocean initially causes small capillary waves and then a spectrum of waves and swell in the ocean (Chapter 8). Impulsive changes in wind lead to short time-scale inertial currents and Langmuir cells. Steady or much more slowly changing wind (in speed and direction) creates the ocean's near-surface frictional Ekman layer, which involves the Coriolis effect. As the wind momentum transfer persists, the geostrophic, wind-driven circulation results.

Thermohaline circulation is associated with heating and cooling (“thermo”), and evaporation, precipitation, runoff, and sea ice formation — all of which change salinity (“haline”). Thermohaline-dominated circulation is mostly weak and slow compared with wind-driven circulation. Thermohaline forcing ranges from very local to very broad scale. An example of local forcing is the deep overturn driven by cooling and/or evaporation in which the horizontal scale of convection is at most a few kilometers. Broad-scale buoyancy forcing is associated with vertical diffusion that acts on the large-scale temperature and salinity structure. Vertical diffusion is very weak in the interior of the ocean, but is essential for maintaining the ocean's vertical stratification. In discussing thermohaline effects, it is common to refer to the meridional overturning circulation (MOC) (Section 14.2.3). Overturning does not have to be meridional to be of interest, and it is generally useful to simply refer to overturning circulation. The energy source for thermohaline circulation importantly includes the wind and tides that produce the turbulence essential for the diffusive upwelling across isopycnals that closes the

thermohaline overturning. Both the wind-driven and thermohaline circulations are almost completely in geostrophic balance, with the forcing that drives them occurring at higher order.

## 7.2. MOMENTUM BALANCE

Fluid flow in three dimensions is governed by three equations expressing how velocity (or momentum) changes, one for each of the three physical dimensions. Each of the three momentum equations includes an acceleration term (how velocity changes with time), an advection term (see Section 5.1.3), and forcing terms. These are the same Newton's Laws taught in physics. Since a fluid is continuous, the mass of a single object is replaced by the mass per unit volume (density); forces are also expressed per unit volume. In “word” equations:

$$\begin{aligned} & \text{Density} \times (\text{Acceleration} + \text{Advection}) \\ & = \text{Forces per unit volume} \end{aligned} \quad (7.1)$$

$$\begin{aligned} & \text{Forces per unit volume} \\ & = \text{Pressure gradient force} + \text{Gravity} \\ & \quad + \text{Friction} \end{aligned} \quad (7.2)$$

Expressions (7.1) and (7.2) are each three equations, one for each of the three directions (e.g., east, north, and up). The terms in Eqs. (7.1) and (7.2) are illustrated in Figure S7.1. For ocean dynamics, these equations are usually written in Cartesian coordinates ( $x, y, z$ ), where  $x$  and  $y$  are west–east and south–north, and  $z$  is upward. Atmospheric dynamicists and some ocean modelers use spherical coordinates instead (longitude, latitude, and the local vertical).

The inclusion of advection means that Eq. (7.1) is the expression of momentum change in a *Eulerian* framework, where the observer sits at a fixed location relative to Earth.

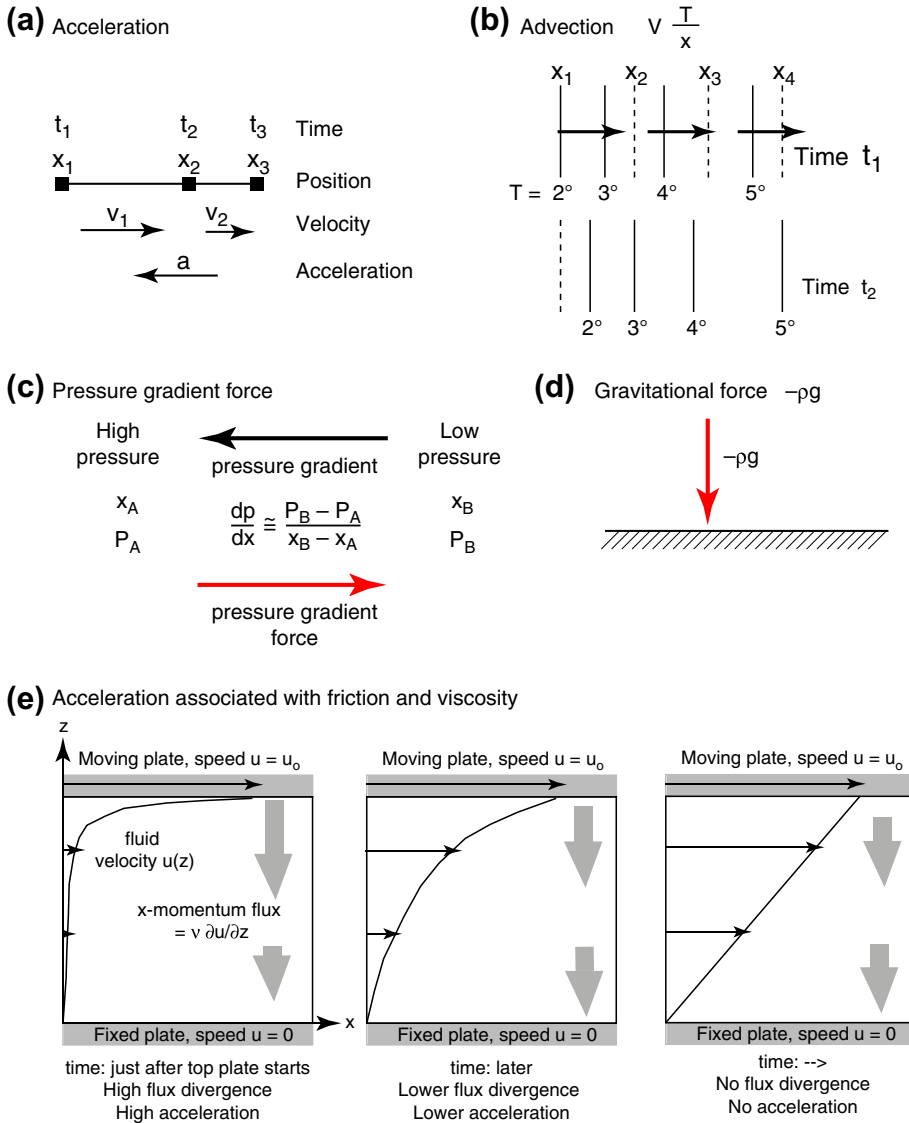


**FIGURE S7.1** Forces and accelerations in a fluid: (a) acceleration, (b) advection, (c) pressure gradient force, (d) gravity, and (e) acceleration associated with viscosity  $\nu$ .

Equation (7.1) can be written without the advection term, in a *Lagrangian* framework, where the observer drifts along with the fluid flow. (See also Section S16.5 in the online supplement.)

For a rotating geophysical flow, we, as observers, sit within a rotating “frame of reference” attached to the rotating Earth. For this reference frame, the acceleration term on the left-hand side of Eq. (7.1) is

rewritten to separate local acceleration due to an actual local force from the effects of rotation. The effects that are separated out are the *centrifugal* and *Coriolis accelerations* (Section 7.2.3).

The “pressure gradient” force in Eq. (7.2) arises from external forcing. The frictional force in Eq. (7.1) leads to *dissipation* of energy due to the fluid’s *viscosity*.

### 7.2.1. Acceleration and Advection

*Acceleration* is the change in velocity with time. If the vector velocity is expressed in Cartesian coordinates as  $\mathbf{u} = (u, v, w)$  where the bold  $\mathbf{u}$  indicates a vector quantity, and  $u, v,$  and  $w$  are the positive eastward (x-direction), northward (y-direction), and positive upward (z-direction) velocities, then

$$\text{x-direction acceleration} = \partial u / \partial t \quad (7.3a)$$

with similar expressions for the y- and z-directions. In a rotating frame of reference, such as on the surface of Earth, the acceleration term includes two additional terms: centrifugal and Coriolis acceleration (Section 7.2.3).

*Advection* is defined in Section 5.1.3. Advection is how the flow moves properties (including scalars such as temperature or salinity) and vectors (such as the velocity). Advection can change the flow property if there is a gradient in the property through which the fluid moves. The advection term thus is a product of the velocity and the difference in the property from one location to another. There are three advection terms in each momentum equation, since the flow bringing in a different property can come from any of the three directions. (The vertical advection term is sometimes called convection.) In the x-momentum equation, the advection term is

$$\begin{aligned} \text{x-direction advection} \\ = u \partial u / \partial x + v \partial u / \partial y + w \partial u / \partial z \end{aligned} \quad (7.3b)$$

The *substantial derivative* is the sum of the acceleration and advection terms:

$$\begin{aligned} Du/Dt = \partial u / \partial t + u \partial u / \partial x \\ + v \partial u / \partial y + w \partial u / \partial z \end{aligned} \quad (7.4)$$

Eq. (7.4) represents the change in  $u$  at a fixed point (Eulerian framework). In a Lagrangian framework, following the particle of water, only the time derivative appears; the three advection terms do not appear since they are contained in the movement of the particle.

### 7.2.2. Pressure Gradient Force and Gravitational Force

*Pressure* is defined in Section 3.2. The flow of fluid due to spatial variations in pressure (the *pressure gradient force*) is also described. In mathematical form, the pressure gradient force is

$$\begin{aligned} \text{x-direction pressure gradient force} \\ = -\partial p / \partial x \end{aligned} \quad (7.5)$$

The pressure gradient force has a negative sign because the force goes from high pressure to low pressure.

The *gravitational force* between Earth and the object or fluid parcel is directed toward the center of mass of Earth. Gravitational force is mass of the object  $\times$  gravitational acceleration  $g$ , equal to  $9.780318 \text{ m}^2/\text{sec}$  (at the equator). The gravitational force per unit volume is

$$\begin{aligned} \text{z-direction gravitational force per unit volume} \\ = -\rho g \end{aligned} \quad (7.6)$$

### 7.2.3. Rotation: Centrifugal and Coriolis Forces

Earth rotates at a rate of  $\Omega = 2 \pi / T$  where  $T$  is the length of the (sidereal) day, which has 86,164

seconds; hence  $\Omega = 0.729 \times 10^{-4} \text{ sec}^{-1}$ .<sup>1</sup> We look at motions and write our theories sitting in a “rotating reference frame,” that is, attached to the rotating Earth. However, the reference frame that is correct for Newton’s Laws (Eq. 7.1) is an “inertial reference frame,” which is not rotating. To look at motions from within our rotating reference frame, we must add two terms due to the Earth’s rotation. The first is the “Coriolis force” and the second is the “centrifugal force” (Figure S7.2). A derivation of these two pseudo-forces is given at the end of this section.

### 7.2.3.1. Centrifugal and Centripetal Force

*Centrifugal force* is the apparent outward force on a mass when it is rotated. Think of a ball on the end of a string that is being twirled around, or the outward motion you feel when turning a curve in a car. In an inertial frame, there is no outward acceleration since the system is not rotating. The ball or your body just moves in the straight line that they were following originally. But in the rotating reference frame of the string or the car, they appear to be accelerated away. Since Earth rotates around a fixed axis, the direction of centrifugal force is always outward away from the axis. Thus it is opposite to the direction of gravity at the equator; at Earth’s poles it is zero. (*Centripetal force* is the necessary inward force that keeps the mass from moving in a straight line; it is the same size as centrifugal force, with the opposite sign. Centripetal force is real; centrifugal force is just an apparent force. For the rotating Earth, centripetal force is supplied by the gravitational force towards Earth’s center.)

If Earth was a perfect, rigid sphere, the ocean would be 20 km deeper at the equator than at the poles. But this is not observed, because the

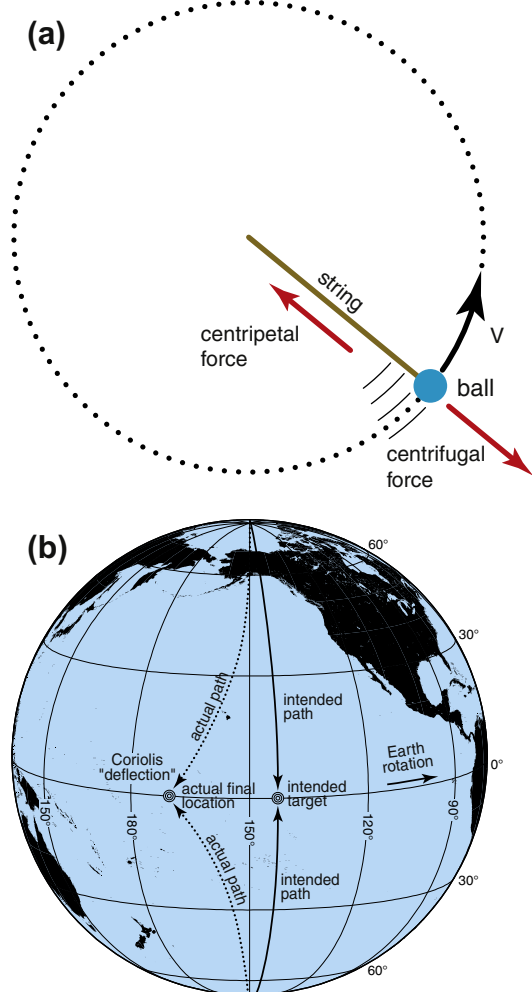


FIGURE S7.2 (a) Centrifugal and centripetal forces and (b) Coriolis force.

solid Earth is deformed by centrifugal force. That is, Earth is a spheroid rather than a sphere, with the radius at the equator approximately 20 km greater than at the poles. Therefore the

<sup>1</sup> The *solar day*, which is the time between consecutive highest points of the sun in the sky, is 24 hours, or 86,400 seconds. The *sidereal day* is the rotation period relative to the fixed stars, which is the inertial reference frame. The sidereal day is slightly shorter than the solar day, with 23 hours, 56 minutes, and 4.1 seconds. One *pendulum day* is one sidereal day /  $\sin\phi$ , where a sidereal day is the time it takes for Earth to rotate 360 degrees and where  $\phi$  = latitude. For  $\phi = 10^\circ, 45^\circ, 60^\circ$ , 1 pendulum day = 5.7, 1.4, 1.2 sidereal days.

centrifugal force at the equator is balanced (canceled) by the extra gravitational force there (this is referred to as “effective gravity”).

The mathematical expression for centrifugal acceleration (force divided by density) is

$$\text{centrifugal acceleration} = \Omega^2 r \quad (7.7)$$

where  $\Omega$  is the rotation rate of Earth, equal to  $2\pi/T$  where  $T$  is the length of day, and  $r$  is Earth’s radius. Because the centrifugal acceleration is nearly constant in time and points outward, away from Earth’s axis of rotation, we usually combine it formally with the gravitational force, which points toward Earth’s center. We replace  $g$  in Eq. (7.6) with the effective gravity  $g$ , which has a weak dependence on latitude. Hereafter, we do not refer separately to the centrifugal force. The surface perpendicular to this combined force is called the *geoid*. If the ocean were not moving relative to Earth, its surface would align with the geoid.

### 7.2.3.2. Coriolis Force

The second term in a rotating frame of reference included in the acceleration equation (7.1) is the *Coriolis force*. When a water parcel, air parcel, bullet, hockey puck, or any other body that has little friction moves, Earth spins out from under it. By Newton’s Law, the body moves in a straight line if there is no other force acting on it. As observers attached to Earth, we see the body appear to move relative to our location. In the Northern Hemisphere, the Coriolis force causes a moving body to appear to move to the right of its direction of motion (Figure S7.2b). In the Southern Hemisphere, it moves to the left.

The Coriolis force is non-zero only if the body is in motion, and is important only if the body travels for a significant period of time. Coriolis force is larger for larger velocities as well. For the flight of a bullet there is no need to consider the Coriolis force because the travel time is extremely short. For missiles that fly long paths

at high speeds, Coriolis force causes significant deflections. For winds in the atmosphere’s Jet Stream, the timescale of motion is several days to several weeks, so Earth’s rotation is very important and the winds do not blow from high to low pressure. The same holds true in the ocean, where currents last for weeks or years and are strongly influenced by the Coriolis force.

For large-scale ocean currents, and to some extent winds, the vertical velocity is much weaker than the horizontal velocity. Certainly the distance that a water parcel can move in the vertical is much more limited than in the horizontal, because of both the difference in depth and width of the ocean, and because of the ocean’s stratification. Therefore, Coriolis effects act mostly on the horizontal velocities and not on the vertical ones. As noted previously, the Coriolis force apparently sends objects to the right in the Northern Hemisphere and to the left in the Southern Hemisphere. At the equator, the Coriolis effect acting on horizontal velocities is zero. Its magnitude is largest at the poles.

Mathematically, the Coriolis force is

x-momentum equation:

$$-2\Omega \sin \phi v \equiv -f v \quad (7.8a)$$

y-momentum equation:

$$-2\Omega \sin \phi u \equiv f u \quad (7.8b)$$

Coriolis parameter:

$$f = 2\Omega \sin \phi \quad (7.8c)$$

where “ $\equiv$ ” denotes a definition,  $\Omega$  is the rotation rate,  $\phi$  is latitude,  $u$  is velocity in the x-direction,  $v$  is velocity in the y-direction, and where the signs are appropriate for including these terms on the left-hand side of Eq. (7.1). The *Coriolis parameter*,  $f$ , is a function of latitude and changes sign at the equator, and it has units of  $\text{sec}^{-1}$ . (The non-dimensional parameter called the *Rossby number* introduced in Section 1.2 is  $\text{Ro} = 1/fT$

or  $Ro = U/fL$ , where  $U$ ,  $L$ , and  $T$  are characteristic velocity, length, and timescales for the flow.)

### 7.2.3.3. Derivation of Centrifugal and Coriolis Terms

The Coriolis and centrifugal terms are derived by transforming Newton's law of motion (Eq. 7.1) from its true inertial system, relative to the fixed stars, to the rotating Earth-centric system. This derivation is available in advanced textbooks on classical mechanics, and is included here for completeness. Equations are numbered separately to maintain consistent numbering because they are not included in the print text. We write the three-dimensional vector version of Eq. (7.1) as

$$\frac{\partial \vec{v}_s}{\partial t} = \vec{F}/\rho \quad (S7.1)$$

where the subscript "s" means that the velocity of the particle is measured in the inertial frame of reference relative to the stars. Rewrite this velocity as the sum of the particle's velocity relative to Earth's surface and the velocity of Earth's surface due to rotation:

$$\vec{v}_s = \vec{v}_e + \vec{\Omega} \times \vec{r} \quad (S7.2)$$

where  $\vec{v}_e$  is the particle velocity relative to local coordinates on Earth's surface,  $\vec{\Omega}$  is Earth's rotation vector, pointing northward along the axis of rotation with magnitude equal to the rotation rate, and  $\vec{r}$  is the vector position of the particle. Substituting this back into Eq. (S7.1) yields

$$\begin{aligned} \left(\frac{\partial \vec{v}_s}{\partial t}\right)_s &= \left(\frac{\partial \vec{v}_e}{\partial t}\right)_s + \frac{\partial}{\partial t}(\vec{\Omega} \times \vec{r})_s \\ &= \left(\frac{\partial \vec{v}_e}{\partial t}\right)_s + \frac{\partial \vec{\Omega}}{\partial t} \times \vec{r} + \vec{\Omega} \times \left(\frac{\partial \vec{r}}{\partial t}\right)_s \end{aligned} \quad (S7.3)$$

Since Earth's rotation is essentially constant compared with the timescales of atmospheric and oceanic circulation, and using Eq. (S7.2), we find that

$$\begin{aligned} \left(\frac{\partial \vec{v}_s}{\partial t}\right)_s &= \left(\frac{\partial \vec{v}_e}{\partial t}\right)_s + \vec{\Omega} \times \left(\frac{\partial \vec{r}}{\partial t}\right)_s \\ &= \left(\frac{\partial \vec{v}_e}{\partial t}\right)_e + \vec{\Omega} \times \vec{v}_e + \vec{\Omega} \times \left(\frac{\partial \vec{r}}{\partial t}\right)_e \\ &\quad + \vec{\Omega} \times (\vec{\Omega} \times \vec{r}) \end{aligned} \quad (S7.4)$$

Since the derivative of any vector in the fixed frame is related to the derivative in the rotating frame as

$$\left(\frac{\partial \vec{q}}{\partial t}\right)_s = \left(\frac{\partial \vec{q}}{\partial t}\right)_e + \vec{\Omega} \times \vec{q} \quad (S7.5)$$

we find finally that

$$\begin{aligned} \left(\frac{\partial \vec{v}_s}{\partial t}\right)_s &= \left(\frac{\partial \vec{v}_e}{\partial t}\right)_e + 2\vec{\Omega} \times \vec{v}_e \\ &\quad + \vec{\Omega} \times (\vec{\Omega} \times \vec{r}) \end{aligned} \quad (S7.6)$$

The first term on the right-hand side is the acceleration relative to the rotating (Earth) frame of reference, the second term is the Coriolis term, and the third term is the centrifugal acceleration.

## 7.2.4. Viscous Force or Dissipation

Fluids have viscous molecular processes that smooth out variations in velocity and slow down the overall flow. These molecular processes are very weak, so fluids can often be treated, theoretically, as "inviscid" rather than viscous. However, it is observed that turbulent fluids like the ocean and atmosphere actually act as if the effective viscosity were much larger than the molecular viscosity. *Eddy viscosity* is introduced to account for this more efficient mixing (Section 7.2.4.2).

### 7.2.4.1. Molecular Viscosity

We can think of molecular viscosity by considering two very different types of coexisting

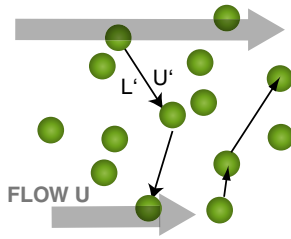


**FIGURE S7.3** Illustration of molecular processes that create viscosity. The mean flow velocity is indicated in gray ( $U$ ).  $L'$  is the distance between molecules.  $U'$  is the speed of the molecules. Random molecule motions carry information about large-scale flow to other regions, thus creating (viscous) stresses. Viscous stress depends on the mean molecular speed  $|U'|$  and mean molecular free path  $|L'|$ .

motion: the flow field of the fluid, and, due to their thermal energy, the random motion of molecules within the flow field. The random molecular motion carries (or advects) the larger scale velocity from one location to another, and then collisions with other molecules transfer their momentum to each other; this smoothes out the larger scale velocity structure (Figure S7.3).

The viscous stress within a Newtonian fluid is proportional to the velocity shear. The proportionality constant is the *dynamic viscosity*, which has meter-kilogram-second (mks) units of kg/m-sec. The dynamic viscosity is the product of fluid density times a quantity called the *kinematic viscosity*, which has mks units of  $\text{m}^2/\text{sec}$ . For water, the kinematic viscosity is  $1.8 \times 10^{-6} \text{ m}^2/\text{sec}$  at  $0^\circ\text{C}$  and  $1.0 \times 10^{-6} \text{ m}^2/\text{sec}$  at  $20^\circ\text{C}$  (Table S7.1).

Flow is accelerated or decelerated if there is a variation in viscous stress from one location

to another. This is illustrated in Figure S7.1e, where a viscous stress is produced by the motion of a plate at the top of the fluid, with a stationary plate at the bottom. The fluid must stay with each plate, so the fluid velocity at each boundary equals that plate velocity.

1. At very small times (leftmost panel), just after the top plate starts to move, there is a large variation in velocity in the fluid close to the top plate, which means there is a large stress there. The stress is associated with flux of  $x$ -momentum down into the fluid from the plate. Since there is much smaller stress farther down in the fluid, there is a net deposit of  $x$ -momentum in the fluid, which accelerates it to the right.
2. At a later time (center panel), this acceleration has produced velocity throughout the fluid and the change in viscous stress from top to bottom is reduced.
3. At a very large time (rightmost panel), the viscous stress is the same at all locations and there is no longer any acceleration; at this time the velocity varies linearly from top to bottom. (This is known as “Couette flow.”) There is a stress on the fluid as a whole, which is balanced by the frictional stress of the fluid back on the plates; there is dissipation of energy throughout the fluid even though there is no local acceleration.

Formally, for a *Newtonian fluid*, which is defined to be a fluid in which stress is proportional to strain (velocity shear), and if viscosity

**TABLE S7.1** Molecular and Eddy Viscosities and Diffusivities ( $\text{m}^2/\text{sec}$ )

	Molecular, at salinity = 35	Eddy: horizontal (along-isopycnal)	Eddy: vertical (diapycnal)
Viscosity	$1.83 \times 10^{-6} \text{ m}^2/\text{sec}$ at $0^\circ\text{C}$ $1.05 \times 10^{-6} \text{ m}^2/\text{sec}$ at $20^\circ\text{C}$	$10^2$ to $10^4 \text{ m}^2/\text{sec}$	$10^{-4} \text{ m}^2/\text{sec}$
Thermal diffusivity	$1.37 \times 10^{-7} \text{ m}^2/\text{sec}$ at $0^\circ\text{C}$ $1.46 \times 10^{-7} \text{ m}^2/\text{sec}$ at $20^\circ\text{C}$	$10^2$ to $10^4 \text{ m}^2/\text{sec}$	$10^{-5} \text{ m}^2/\text{sec}$
Haline diffusivity	$1.3 \times 10^{-9} \text{ m}^2/\text{sec}$	$10^2$ to $10^4 \text{ m}^2/\text{sec}$	$10^{-5} \text{ m}^2/\text{sec}$

has no spatial dependence, viscous stress enters the momentum equations as

$$\begin{aligned} & \text{x-momentum dissipation} \\ & = \nu(\partial^2 u/\partial x^2 + \partial^2 u/\partial y^2 + \partial^2 u/\partial z^2) \quad (7.9) \end{aligned}$$

where  $\nu$  is the molecular (kinematic) viscosity. (The dynamic viscosity is  $\rho\nu$ .) This expression comes from the divergence of the viscous stress in the x-direction. For the example shown in Figure S7.1.e, this stress is  $\nu\partial u/\partial z$ , and there is an acceleration of the fluid only if this stress varies with  $z$ .

Molecular viscosity changes flow very slowly. Its effectiveness can be gauged by a non-dimensional parameter, the *Reynolds number*, which is the ratio of the dissipation timescale to the advective timescale:  $Re = UL/\nu$ . When the Reynolds number is large, the flow is nearly inviscid and most likely very turbulent; this is the case for flows governed by molecular viscosity. However, from matching observations and theory we know that the ocean currents dissipate energy much more quickly than we can predict using molecular viscosity. How this happens is described next.

#### 7.2.4.2. Eddy Viscosity

Mixing at spatial scales larger than those quickly affected by molecular viscosity is generally a result of turbulence in the fluid. Turbulent motions stir the fluid, deforming and pulling it into elongated, narrow filaments. A stirred fluid mixes much faster than one that is calm and subjected only to molecular motion. While stirring is technically reversible, mixing is not. It is easier to think about this for a property, such as milk in a coffee cup, or salinity in the ocean, than for velocity, but the same principles apply to both. The filaments are deformed by turbulence on a smaller spatial scale. Eventually molecular viscosity takes over, when the spatial scales become very small. We refer to the effect of this turbulent stirring/mixing on the fluid as eddy viscosity.

There is no obvious way to derive the size of eddy viscosity from molecular properties. Instead, it is determined empirically, either directly from observations, or indirectly from models that work relatively well and include eddy viscosity. For large-scale ocean circulation, the “turbulent” motions are mesoscale eddies, vertical fine structure, and so on, with spatial scales smaller than the larger scales of interest. Like molecular viscosity, eddy viscosity should be proportional to the product of turbulent speed and path length. Therefore, horizontal eddy viscosity is generally much larger than vertical eddy viscosity (Table S7.1). More specifically, although we often refer to “horizontal” and “vertical” eddy viscosity, the relevant directions are along isopycnals (adiabatic surfaces) and across isopycnals (*diapycnal mixing*), since these are the natural coordinates for uninhibited quasi-lateral motion and the most inhibited quasi-vertical motion (Redi, 1982; Gent & McWilliams, 1990).

To mathematically include eddy viscosity, the viscous terms in Eqs. (7.1) and (7.9) are replaced by the eddy viscosity terms:

$$\begin{aligned} & \text{x-momentum dissipation} \\ & = A_H(\partial^2 u/\partial x^2 + \partial^2 u/\partial y^2) + A_V(\partial^2 u/\partial z^2) \quad (7.10a) \end{aligned}$$

where  $A_H$  is the horizontal eddy viscosity and  $A_V$  is the vertical eddy viscosity. (The use of the symbol  $A$  is from the early German definition of an “Austausch” or exchange coefficient to represent eddy viscosity.)  $A_H$  and  $A_V$  have units of kinematic viscosity,  $\text{m}^2/\text{sec}$  in mks units. (Although we often use these Cartesian coordinates, the most relevant stirring/mixing directions are along isopycnals (adiabatic surfaces) and across isopycnals (*diapycnal mixing*), so the coordinate system used in Eq. 7.10a is better modeled by rotating it to have the “vertical” direction perpendicular to isopycnal surfaces, and replace  $A_H$  and  $A_V$  with eddy viscosities

that are along and perpendicular to those surfaces.)

In many applications and observations, it is useful to include spatial dependence in the eddy viscosity coefficients because turbulence is unevenly distributed. Equation (7.10a) is then written in its original form, which includes spatial variation of stress:

$$\begin{aligned} \text{x-momentum dissipation} \\ = \partial/\partial x(A_H \partial u/\partial x) + \partial/\partial y(A_H \partial u/\partial y) \\ + \partial/\partial z(A_V \partial u/\partial z) \end{aligned} \quad (7.10b)$$

Eddy viscosity coefficients (Table S7.1 and Section 7.3), also called eddy momentum diffusion coefficients, are inferred from observations of microstructure (very small scale variations in velocity) and from eddy diffusivities acting on temperature and salinity that are also derived from observations, given that both are due to similar structures that mix the ocean. (Formally, in fluid mechanics, the non-dimensional ratio of viscous diffusivity to thermal diffusivity is called the *Prandtl number*; if we assume that eddy viscosity and eddy diffusivity were equal, we are assuming a turbulent Prandtl number of 1.) Numerical models typically use higher eddy viscosities than eddy diffusivities (e.g., Smith, Maltrud, Bryan, & Hecht, 2000; Treguier, 2006).

### 7.2.5. Mathematical Expression of Momentum Balance

The full momentum balance with spatially varying eddy viscosity and rotation is

$$\begin{aligned} Du/Dt - fv &= \partial u/\partial t + u \partial u/\partial x + v \partial u/\partial y \\ &+ w \partial u/\partial z - fv \\ &= -(1/\rho) \partial p/\partial x + \partial/\partial x(A_H \partial u/\partial x) \\ &+ \partial/\partial y(A_H \partial u/\partial y) \\ &+ \partial/\partial z(A_V \partial u/\partial z) \end{aligned} \quad (7.11a)$$

$$\begin{aligned} Dv/Dt + fu &= \partial v/\partial t + u \partial v/\partial x + v \partial v/\partial z \\ &+ w \partial v/\partial z + fu \\ &= -(1/\rho) \partial p/\partial y + \partial/\partial x(A_H \partial v/\partial x) \\ &+ \partial/\partial y(A_H \partial v/\partial y) \\ &+ \partial/\partial z(A_V \partial v/\partial z) \end{aligned} \quad (7.11b)$$

$$\begin{aligned} Dw/Dt &= \partial w/\partial t + u \partial w/\partial x + v \partial w/\partial y \\ &+ w \partial w/\partial z \\ &= -(1/\rho) \partial p/\partial z - g + \partial/\partial x(A_H \partial w/\partial x) \\ &+ \partial/\partial y(A_H \partial w/\partial y) \\ &+ \partial/\partial z(A_V \partial w/\partial z) \end{aligned} \quad (7.11c)$$

Here the standard notation “D/Dt” is the substantial derivative defined in Eq. (7.4).

The full set of equations describing the physical state of the ocean must also include the *mass conservation* equation (Section 5.1):

$$D\rho/Dt + \rho(\partial u/\partial x + \partial v/\partial y + \partial w/\partial z) = 0 \quad (7.11d)$$

If density changes are small, Eq. 7.11d is approximated as

$$\partial u/\partial x + \partial v/\partial y + \partial w/\partial z = 0 \quad (7.11e)$$

which is known as the *continuity* equation. The set is completed by the equations governing changes in temperature, salinity, and density, which are presented in the following section.

## 7.3. TEMPERATURE, SALINITY, AND DENSITY EVOLUTION

Evolution equations for temperature and salinity — the equation of state that relates density to salinity, temperature, and pressure, and thus an evolution equation for density — complete the set of equations (7.11a–d) that

describe fluid flow in the ocean. The boundary and initial conditions required for solving the systems of equations are beyond our scope.

### 7.3.1. Temperature, Salinity, and Density Equations

Temperature is changed by heating, cooling, and diffusion. Therefore the most basic equation would be that for heat (or enthalpy), but most dynamical treatments and models use an explicit temperature equation. Salinity is changed by addition or removal of freshwater, which alters the dilution of the salts. Most modeling uses an explicit salinity equation rather than a freshwater equation. Density is then computed from temperature and salinity using the equation of state of seawater. The “word” equations for temperature, salinity, and density forcing include:

$$\begin{aligned} & \text{temperature change} \\ & + \text{temperature advection/convection} \\ & = \text{heating/cooling term} + \text{diffusion} \end{aligned} \quad (7.12a)$$

$$\begin{aligned} & \text{salinity change} \\ & + \text{salinity advection/convection} \\ & = \text{evaporation/precipitation/runoff} \\ & \quad / \text{brine rejection} + \text{diffusion} \end{aligned} \quad (7.12b)$$

$$\begin{aligned} & \text{equation of state (dependence of density} \\ & \quad \text{on salinity, temperature, and pressure)} \end{aligned} \quad (7.12c)$$

$$\begin{aligned} & \text{density change} + \text{density advection/convection} \\ & = \text{density sources} + \text{diffusion} \end{aligned} \quad (7.12d)$$

Written in full, these are

$$\begin{aligned} DT/Dt &= \partial T/\partial t + u \partial T/\partial x + v \partial T/\partial y \\ & \quad + w \partial T/\partial z \\ &= Q_H/\rho c_p + \partial/\partial x(\kappa_H \partial T/\partial x) \\ & \quad + \partial/\partial y(\kappa_H \partial T/\partial y) + \partial/\partial z(\kappa_V \partial T/\partial z) \end{aligned} \quad (7.13a)$$

$$\begin{aligned} DS/Dt &= \partial S/\partial t + u \partial S/\partial x + v \partial S/\partial y + w \partial S/\partial z \\ &= Q_s + \partial/\partial x(\kappa_H \partial S/\partial x) \\ & \quad + \partial/\partial y(\kappa_H \partial S/\partial y) + \partial/\partial z(\kappa_V \partial S/\partial z) \end{aligned} \quad (7.13b)$$

$$\rho = \rho(S, T, p) \quad (7.13c)$$

$$\begin{aligned} D\rho/Dt &= \partial\rho/\partial t + u \partial\rho/\partial x + v \partial\rho/\partial y + w \partial\rho/\partial z \\ &= (\partial\rho/\partial S)DS/Dt + (\partial\rho/\partial T)DT/Dt \\ & \quad + (\partial\rho/\partial p)Dp/Dt \end{aligned} \quad (7.13d)$$

where  $Q_H$  is the heat source (positive for heating, negative for cooling, applied mainly near the sea surface),  $c_p$  is the specific heat of seawater, and  $Q_s$  is the salinity “source” (positive for evaporation and brine rejection, negative for precipitation and runoff, applied at or near the sea surface). (See also Chapter 5 for discussion of heat and salinity.)  $\kappa_H$  and  $\kappa_V$  are the horizontal and vertical eddy diffusivities, analogous to the horizontal and vertical eddy viscosities in the momentum equations (7.11a–d; Table S7.1. The full equation of state appears in Eq. (7.13c), from which the evolution of density in terms of temperature and salinity change can be computed (Eq. 7.13d). The coefficients for the three terms in Eq. (7.13d) are the haline contraction coefficient, the thermal expansion coefficient, and the adiabatic compressibility, which is proportional to the inverse of sound speed (Chapter 3).

### 7.3.2. Molecular and Eddy Diffusivity

The molecular diffusivity  $\kappa$  for each substance depends on the substance and the fluid. The molecular diffusivity of salt in seawater is much smaller than that for heat (Table S7.1). This difference results in a process called “double diffusion” (Section 7.4.3).

*Eddy diffusivity* is the equivalent of eddy viscosity for properties like heat and salt. Eddy diffusivity and eddy viscosity typically have similar orders of magnitude (Table S7.1) since the same turbulent processes create both. For lack of observations and for simplicity, diapycnal, quasi-vertical eddy diffusivity was once considered to be globally uniform (e.g., Stommel & Arons, 1960a, b; Section 7.10.3). A globally averaged vertical eddy diffusivity of  $\kappa_v = 1 \times 10^{-4} \text{ m}^2/\text{sec}$  accounts for the observed average vertical density structure (Section 7.10.2; Munk, 1966). However, the directly observed vertical (or diapycnal) eddy diffusivity in most of the ocean is a factor of 10 lower:  $\kappa_v \sim 1 \times 10^{-5} \text{ m}^2/\text{sec}$ , based on direct measurements of mixing rates using dye release and spread (Ledwell, Watson, & Law, 1993, 1998), measurements of very small scale vertical structure (Osborn & Cox, 1972; Gregg, 1987), and large-scale property distributions within the pycnocline (e.g., Olbers, Wenzel, & Willebrand, 1985). This implies regions of much higher diffusivity to reach the global average.

Measurements show huge enhancements of diapycnal eddy diffusivity in bottom boundary regions, especially where topography is rough (Figure S7.4; Polzin, Toole, Ledwell, & Schmitt, 1997; Kunze et al., 2006), and on continental shelves where tidal energy is focused (Lien & Gregg, 2001). In these regions, the tides move water back and forth over hundreds of meters horizontally (Egbert & Ray, 2001). If the bottom is rough, as it is over most mid-ocean ridge systems (Figures 2.5 and 2.6), the internal tide can break, causing enhanced turbulence and diffusivity. Internal tides have been directly

observed and related to turbulence along the Hawaiian Ridge (Rudnick et al., 2003). If the interaction is strong, then the enhanced diffusivity can reach high into the water column, even reaching the pycnocline, as is seen over the topographic ridges in Figure S7.4.

Diapycnal eddy diffusivity also depends on latitude (Figure S7.4b). It is small at low latitudes (order of  $10^{-6} \text{ m}^2/\text{sec}$ ), increasing to a peak at 20–30° latitude, and then declining somewhat toward higher latitudes ( $0.4$  to  $0.5 \times 10^{-4} \text{ m}^2/\text{sec}$ ). The relation of this diffusivity distribution to the actual efficiency of mixing, which also depends on the currents, has not yet been mapped.

Within the water column, away from the top and bottom boundaries, internal waves are generally relatively quiescent, without much breaking, but nonlinear interactions between internal waves and encounters with mesoscale eddies could also produce higher velocity shears that result in a low level of breaking and turbulence.

In the surface layer, eddy diffusivities and eddy viscosities are also much greater than the Munk value (e.g., Large, McWilliams, & Doney, 1994). In Section 7.5.3 on Ekman layers, we describe eddy viscosities in the surface layer on the order of 100 to  $1000 \times 10^{-4} \text{ m}^2/\text{sec}$ . Large lateral variations in diapycnal diffusivity result from the processes that create the turbulence, such as strongly sheared currents (such as the Gulf Stream) and wind-forced near-inertial motions near the base of the mixed layer.

Horizontal eddy diffusivities  $\kappa_H$  are estimated to be between  $10^3$  and  $10^4 \text{ m}^2/\text{sec}$ , with large spatial variability (e.g., Figure 14.17).  $\kappa_H$  is much larger than  $\kappa_v$ . The larger size is related to the larger horizontal length and velocity scales than in the vertical; turbulent motions and mixing are enhanced in the horizontal. Observational estimates of horizontal diffusivity have been based on dye release (Ledwell et al., 1998) and on dispersion of floats and surface drifters (Section 14.5.1). Estimates of horizontal

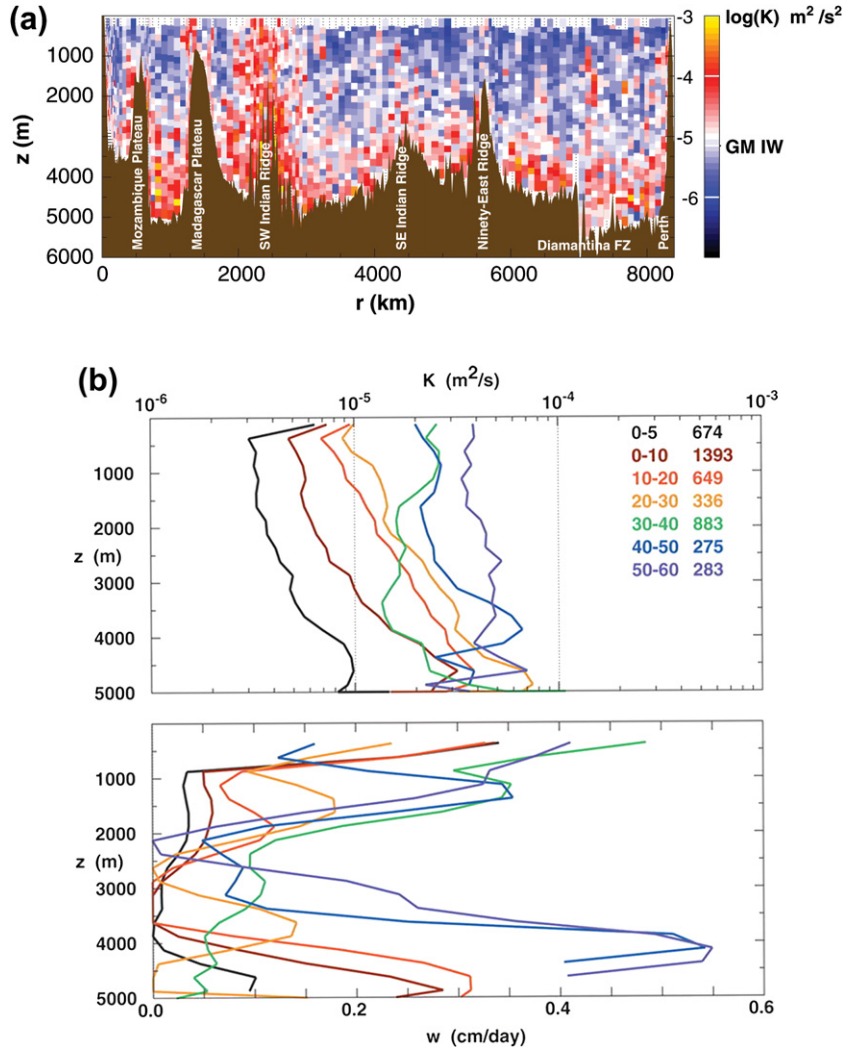


**FIGURE S7.4** (a) Observed diapycnal diffusivity ( $\text{m}^2/\text{s}^2$ ) along  $32^\circ\text{S}$  in the Indian Ocean, which is representative of other ocean transects of diffusivity. (b) Average diapycnal diffusivity as a function of latitude range (color codes). *Source: From Kunze et al. (2006).*

diffusivity are also made from choices required to match observed and theoretical phenomena such as boundary current widths. It is emphasized that, unlike molecular diffusivities, eddy diffusivities are not a property of the flow in general, but depend on which space and time-scales are “resolved” and “unresolved.”

## 7.4. MIXING LAYERS

Mixing occurs throughout the ocean. Mixing of momentum is the frictional process while mixing of properties is the diffusion process. While it is weak, it is essential for maintaining the observed stratification and can regulate the

strength of some parts of the circulation. In this section we look at mixing in the surface layer where there is direct atmospheric forcing; in bottom layers where mixing can be caused by interaction between ocean currents, tides, and waves and the bottom topography; and within the water column, away from top and bottom boundaries.

### 7.4.1. Surface Mixed Layer

The surface layer (Section 4.2.2) is forced directly by the atmosphere through surface wind stress and buoyancy (heat and freshwater) exchange. The surface “mixed layer” is seldom completely mixed, so it is sometimes difficult to define. We consider it to be the upper boundary layer of the ocean, forced directly by the atmosphere through: (1) surface stress of the wind and (2) buoyancy (heat and freshwater) exchange through the surface. Wind stress generates motion, which is strongest at the surface and decreases with depth, that is, with vertical shear in the velocity. These motions include waves that add turbulent energy to increase mixing, particularly if they break. Wind-driven Langmuir circulations (Section 7.5.2) can promote mixing, possibly through the full depth of the mixed layer.

For a surface layer that is initially stably stratified (Figure S7.5a), sufficiently large wind stress will create turbulence that mixes and creates a substantially uniform density or mixed layer (Figure S7.5b). This typically results in a discontinuity in properties at the mixed layer base.

The upper layer can also be mixed by buoyancy loss through the sea surface, increasing the density of the top of the surface layer and causing it to overturn (*convect*) to a greater depth (Figure S7.5c–e). This type of mixed layer typically has no discontinuity in density at its base. Heat or freshwater gain decreases the density of the top of the surface layer, resulting in a more stably stratified profile. If the wind then mixes

it, the final mixed layer is shallower than the initial mixed layer (Figure S7.5f–h).

Mixed layer observations typically show much more vertical structure than might be expected from these simple ideas. This is because the mixed layer is subject to greatly varying forcing, including diurnal heating that restratifies the mixed layer, cooling that convectively mixes the layer, wind-generated turbulence that mechanically stirs the layer, and small-scale instabilities of the many localized fronts within the mixed layer that can change its stratification (e.g., Boccaletti, Ferrari, & Fox-Kemper, 2007).

The thickest mixed layers occur at the end of winter (Figure 4.5), after an accumulation of months of cooling that deepens the mixed layer and increases its density. For large-scale oceanographic studies, these end-of-winter mixed layers set the properties that are subducted into the ocean interior (Section 7.8.5). Maps of late winter mixed layer depth and also maximum mixed layer depth are shown in Figure 4.5.

Several different parameterizations of surface layer mixing due to winds and buoyancy fluxes have been used. The first parameterization used (“K-T”) was developed by Kraus and Turner (1967). The Price, Weller, Pinkel (1986; PWP) model largely replaced the K-T model and is still used widely. Large et al. (1994) proposed the most commonly used modern approach, called “K-Profile Parameterization” (KPP), where “K” is shorthand for diffusivity  $\kappa$ . The KPP model extends the response to surface forcing to below the completely mixed layer, since turbulence set up at the base of the well-mixed layer penetrates downward; for instance, through near-inertial motions (Sections 7.5.1 and 14.5.3).

### 7.4.2. Bottom Mixed Layers

Near the ocean bottom, turbulence, and hence mixing, can be generated by currents or current

shear caused by the interaction with the bottom. In shallow (e.g., coastal) waters, complete mixing of the water column occurs if the depth ( $H$ ) is shallow enough and the tidal currents ( $U$ ) are fast enough (see reviews in Simpson, 1998 & Brink, 2005). Complete mixing of the water column occurs if the depth ( $H$ ) is shallow enough and the tidal currents ( $U$ ) are fast enough. From energy dissipation arguments, a useful critical parameter based on depth and velocity is  $H/U^3$ . When  $H/U^3 < a$ , where  $a$  is proportional to the empirically determined mixing efficiency and the buoyancy flux, there can be complete mixing that destroys the stratification. Considerable observational efforts have been made and are ongoing to quantify and understand the turbulence that creates the mixing (Doron, Bertuccioli, Katz & Osborn, 2001; Polzin, Toole, Ledwell, & Schmitt, 1997; Kunze et al., 2006; Lien & Gregg, 2001 and many others).

At longer timescales on the shelf, a bottom Ekman layer can develop in which frictional and Coriolis forces balance (Ekman, 1905 and Section 7.5.3), with the bottom slope also affecting the layer. The bottom slope on the shelf, and its intersection with the water column's density structure, is important for bottom Ekman layers, which can have both upslope and downslope flow. Eddy viscosity also has important variations in space and time, which affects the Ekman layer structure (Lentz, 1995).

Enhanced turbulence in a bottom boundary layer can be created by movement of water across rough topography and by breaking of internal waves that reflect off the topography and result in higher eddy diffusivity values (Figure S7.5). The higher turbulence creates locally mixed bottom boundary layers that can then be advected away from the bottom topography, creating "steppy" vertical profiles near the bottom some distance from the mixing site (Figure S7.6a).

Bottom currents due to density differences can also cause mixing. One example is

a turbidity current down an underlying bottom slope. (See Section 2.6. Another example is the overflow of dense water across a sill, as seen at the Strait of Gibraltar (Chapter 9.) The dense water flows down the continental slope as a *plume*, mixing vigorously with the lighter water around it (Figure S7.6b). This turbulent process is called *entrainment*.

As it entrains, the outflow reaches an equilibrium density with the ambient water and spreads thereafter along that isopycnal surface. The entrainment rate and the final density of the plume depend on the density of the strait outflow and the density profile in the ambient waters outside the strait.

Density differences due to the injection of lighter water into the ocean also cause mixing and entrainment. An example is hot hydrothermal water injected at mid-ocean ridges and hotspots that entrain ambient waters as the plumes rise. A man-made example is water from a sewer outfall where the discharged fluid is less dense than the seawater. In both cases, mixing (entrainment) takes place as the plumes rise due to their buoyancy.

### 7.4.3. Internal Mixing Layers

In the interior of the ocean (i.e., away from boundaries), continuous profiling instruments have shown that vertical profiles of water properties — temperature and salinity, and hence density — are often not smooth (Figure S7.5i) but "stepped" (Figure S7.5j). The vertical scale of the steps can be decimeters to many meters. Turbulence (Section 7.4.3.1) and/or double diffusion (Section 7.4.3.2) mix the water column internally and can create such steps.

#### 7.4.3.1. Turbulent Mixing

Breaking internal waves can create internal mixing (Section 8.4; Rudnick et al., 2003). Vertical shear from other sources can also result in turbulence. On the other hand, vertical stratification stabilizes the mixing. One way to

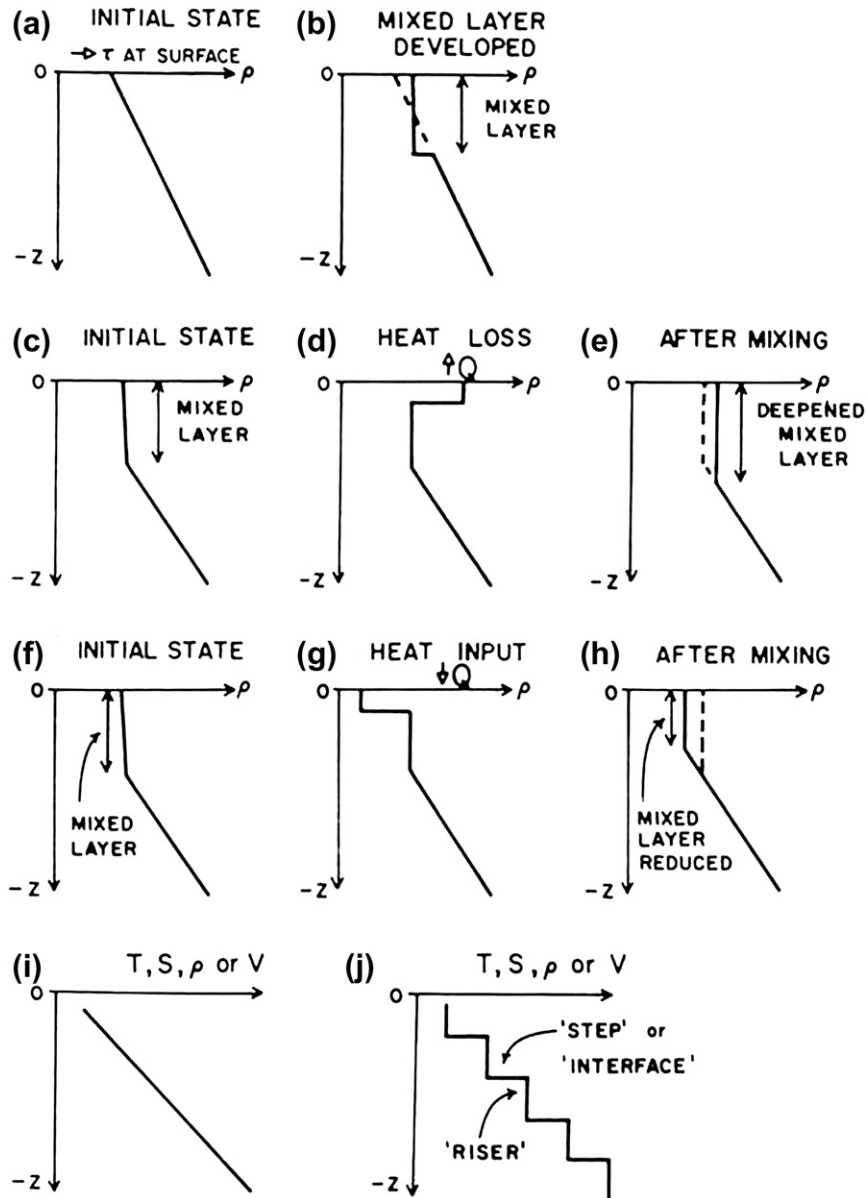


**FIGURE S7.5** Mixed layer development. (a, b) An initially stratified layer mixed by turbulence created by wind stress; (c, d, e) an initial mixed layer subjected to heat loss at the surface, which deepens the mixed layer; (f, g, h) an initial mixed layer subjected to heat gain and then to turbulent mixing presumably by the wind, resulting in a thinner mixed layer; (i, j) an initially stratified profile subjected to internal mixing, which creates a stepped profile. Notation:  $\tau$  is wind stress and  $Q$  is heat (buoyancy).

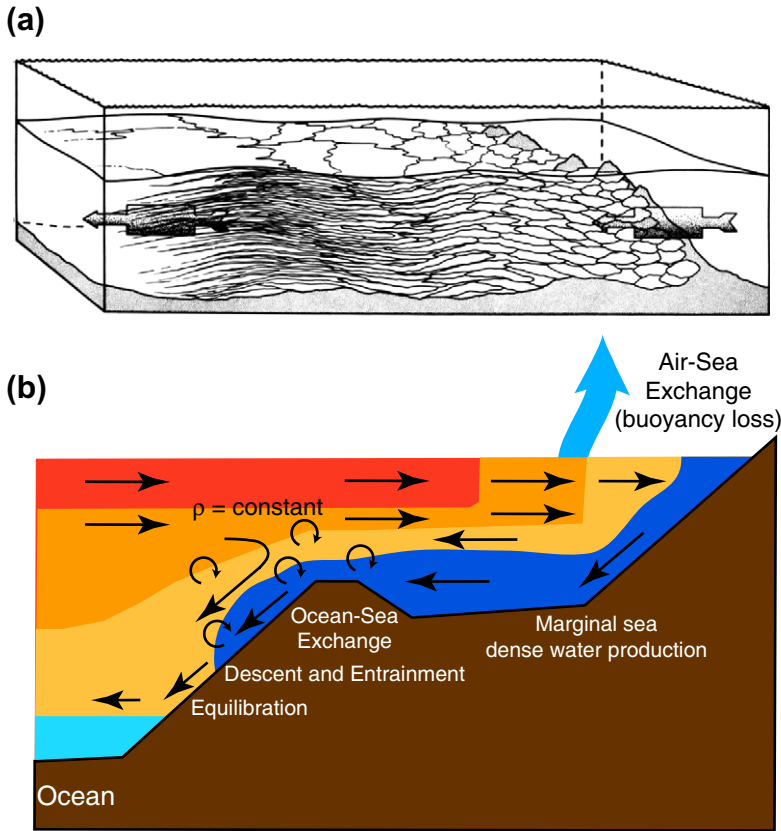


**FIGURE S7.6** (a) Bottom boundary layers and their advection away from the bottom. Source: From *Armi (1978)*. (b) Mixing of a plume of dense water as it flows out over a strait into less dense ambient waters. After *Price and Baringer (1994)*.

express this trade-off is through a non-dimensional quantity called the *Richardson number*:

$$R_i = N^2 / (\partial u / \partial z)^2 \quad (7.14)$$

where

$$N^2 = -g(\partial \rho / \partial z) / \rho_0 \quad (7.15)$$

$N$  is the Brunt-Väisälä frequency (Section 3.5.6) and the vertical shear of the horizontal speed is  $(\partial u / \partial z)$ . If the Richardson number is small, the stratification is weak and the shear is large, so we expect mixing to be vigorous. From theory and observations, vigorous mixing starts when the Richardson number falls below  $1/4$ .

The initial steps of mixing between two horizontally adjacent waters with strong temperature/salinity differences are visible at the front between the waters. Stirring at the front draws layers of the adjacent waters into each other along isopycnals, resulting in *interleaving* or *fine structure*, with layering of one to tens of meters on both sides of the front. The interleaving facilitates local vertical (diapycnal) mixing between the two water masses, which is the next step to actual mixing between them. The actual mixing can take place through turbulent processes or the double diffusive processes described in the next subsection. In both cases, much smaller scale vertical structure, on the order of centimeters (*microstructure*), is an indication of the actual mixing at

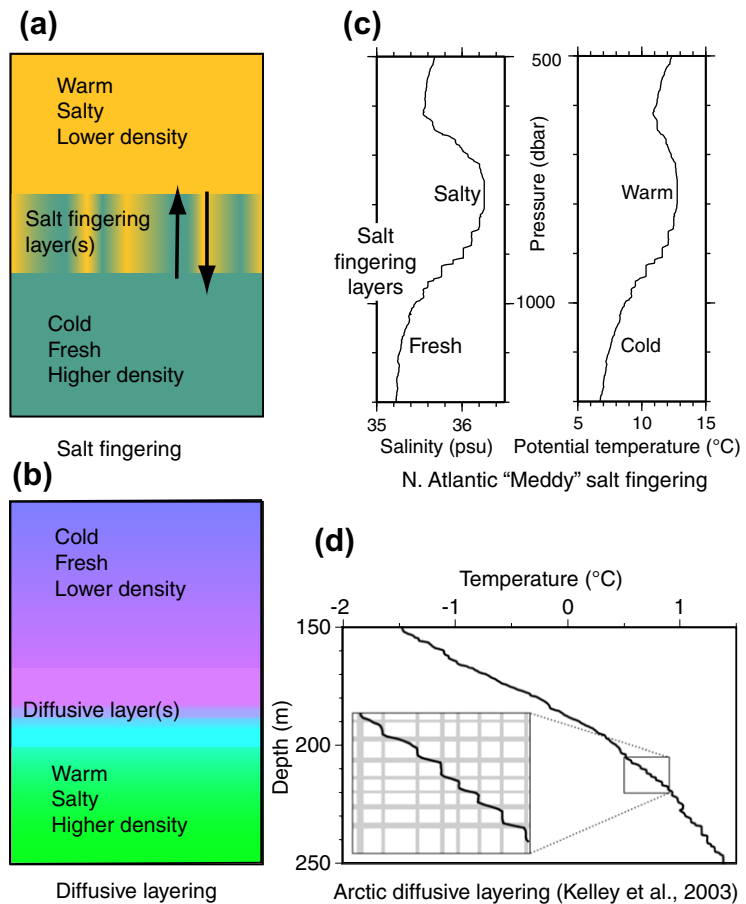
the interfaces between the interleaving layers. Such interleaving has been observed in the western equatorial Pacific, in the Antarctic Circumpolar Current (ACC), in the Kuroshio and Gulf Stream, and so forth; that is, in every region where there are strong water mass fronts.

#### 7.4.3.2. Double Diffusion

Heat diffuses about 100 times faster than salt (Table S7.1). *Double diffusion* is due to these differing molecular diffusivities, acting at scales of centimeters to meters, and can also create well-mixed internal layers. When warm, salty

water lies above cold, fresh water, and the interface between the two is disturbed so that small columns of warm, salty water are next to cold, fresh ones, the fast heat exchange between them will cool the saltier water and warm the fresher water while the salinity will mix much less. The saltier water becomes denser and tends to sink into the lower layer and vice versa (Figure S7.7a). The alternating columns are called *salt fingers*. In the laboratory, salt fingers can be produced easily and can grow to a few millimeters across and up to 25 cm long. Lateral diffusion occurs between the “fingers” and produces a uniform layer. Then the process

FIGURE S7.7 Double diffusion: (a) salt fingering interface (cold, fresh water warms and rises; warm, salty water cools and sinks). (b) Diffusive interface. (c) North Atlantic Mediterranean eddy salinity profile with steps due to salt fingering (25° 23'N, 26°W). (d) Arctic temperature profile with diffusive layering. Source: From Kelley et al. (2003).



may start again at the two interfaces that are now present, and eventually a number of individually homogeneous layers develop with sharply defined temperature and salinity interfaces (as in Figure S7.5j). In the ocean the layers may be meters to tens of meters thick, separated by thinner interface zones of sharp gradients of temperature and salinity. External horizontal velocities can disturb the growing fingers, so prediction of salt finger growth under all oceanic conditions is complex.

When cold, fresh water lies above warm, salty water (Figure S7.7b), the lower layer, losing heat through the interface but not much salt, will become denser and water will tend to sink, again within its own layer. This is called the *diffusive* form of double diffusion. The original stratification is strengthened by this double diffusive process. An important difference from salt fingering is that fluid does not cross the interface.

Salt fingering effects are observed in the ocean where there are strong contrasts in salinity, for instance, where salty Mediterranean Water enters the Atlantic through the Strait of Gibraltar (Figure S7.7c). The saline water intrudes at mid-depth (about 1000–2000 m) into the cooler, less saline Atlantic water (Section 4.3 and Figure 4.10). Step structures in temperature/depth and salinity/depth traces due to double diffusion are clear in CTD profiles below the Mediterranean water (Figures S7.7c and S9.33).. Diffusive interfaces are observed in high latitude regions where there is a fresh, cold layer at the surface with an underlying saltier temperature maximum layer (a dichothermal layer; Sections 4.2 and 4.3.2 and Figure S7.7d).

## 7.5. RESPONSE TO WIND FORCING

The wind blows over the sea surface exerting stress and causing the water to move within the top 50 m. Initially the wind excites small capillary waves that propagate in the direction of the wind. Continued wind-driven momentum exchange

excites a range of surface waves (Chapter 8). The net effect of this input of atmospheric momentum is a stress on the ocean (*wind stress*) (Section 5.8). For timescales of about a day and longer, Earth's rotation becomes important and the Coriolis effect enters in, as described in the following subsections.

### 7.5.1. Inertial Currents

The ocean responds initially to a wind stress impulse with transient motions known as “inertial currents.” These are a balance of the Coriolis force and the time derivatives of the initial horizontal velocities caused by the wind stress. In the Northern Hemisphere, Coriolis force acts to the right of the velocity. So if the current is initially to the north, then Coriolis will move it to the east, and then to the south, and so forth. Thus, the water particles trace out clockwise circles (Figure S7.8a). In the Southern Hemisphere, Coriolis force acts to the left and inertial currents are counterclockwise.

(Mathematically, inertial currents are the solution of

$$\partial u / \partial t = -fv \quad (7.16a)$$

$$\partial v / \partial t = -fu \quad (7.16b)$$

which is taken from Eq. 7.11a and b assuming that advection, pressure gradient forces, and dissipation are very small and can be neglected.)

Since the Coriolis force is involved, inertial currents vary with latitude. They have shorter time and length scales for higher latitudes. The frequency of an inertial current (time for a full circle) is the Coriolis parameter  $f$ , so the time it takes for the circle (the period) is  $2\pi/f$ . Since the rotation is to the right of the initial stress (wind impulse), the average flow over a full circle of the inertial current is perpendicular to the wind stress and to the right in the Northern Hemisphere and left in the Southern Hemisphere.

Inertial currents are often observed in surface drifter trajectories and surface velocity

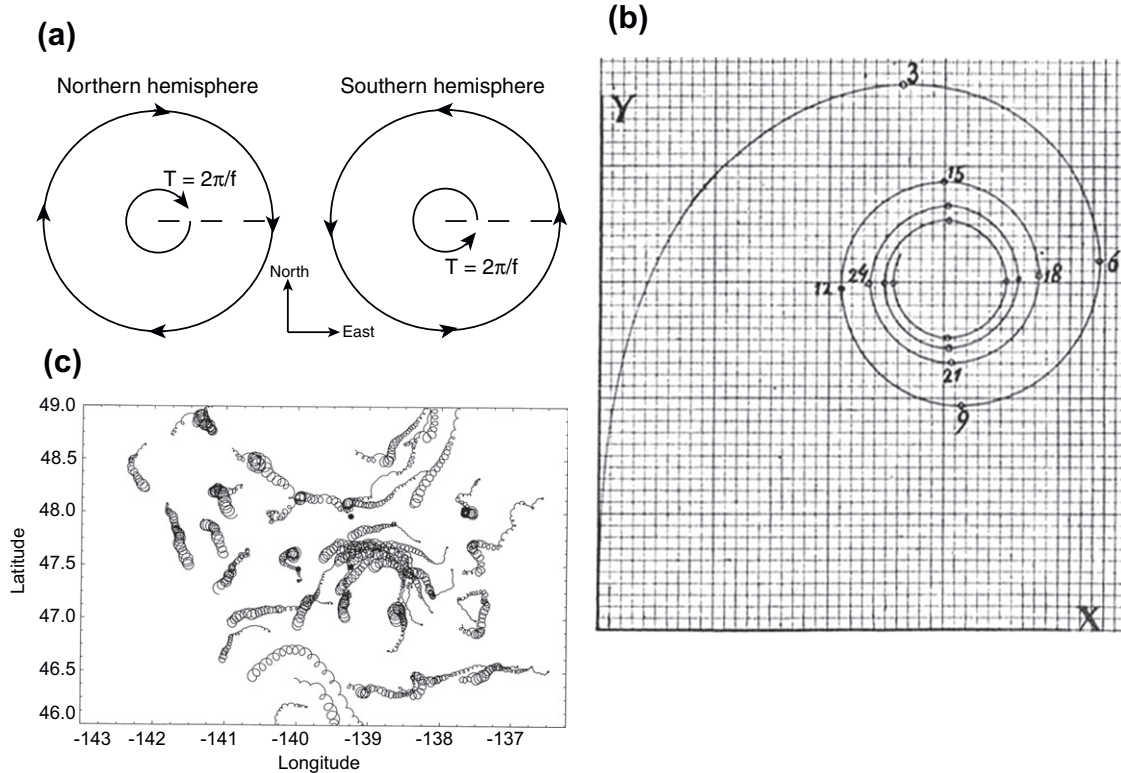


**FIGURE S7.8** (a) Schematics of inertial currents in the Northern and Southern Hemispheres. (b) Hodograph of inertial currents at  $45^\circ\text{N}$  for a wind blowing in the  $y$ -direction; the numbers are in pendulum hours. *Source: From Ekman (1905).* (c) Observations of near-inertial currents. Surface drifter tracks during and after a storm. *Source: From d'Asaro et al. (1995).*

moorings in the wake of a storm (Figure S7.8c). Inertial periods are often very close to tidal periods, so separating tidal and inertial effects in time series is sometimes difficult.

After the wind starts to blow impulsively, the current will initially oscillate around and then, after several days, settle frictionally to a steady flow at an angle to the wind (Figure S7.8b from Ekman, 1905). This becomes the surface Ekman velocity (Section 7.5.3).

### 7.5.2. Langmuir Circulation

“Langmuir circulation” is another transient response to impulsive wind forcing, in which helical vortices form near the sea surface.

Langmuir cells (LCs) were first discussed by Langmuir (1938) who carried out a number of experiments to identify their character. LCs are visually evident as numerous long parallel lines or streaks of flotsam (“windrows”) that are mostly aligned with the wind, although they can deviate by 20 degrees (Figure S7.9).

The streaks are formed by the convergence caused by the vortices (Figure S7.10). Alternate cells rotate in opposite directions so that convergence and downwelling occurs at the surface (to form streaks of flotsam) between pairs of adjacent cells, while divergence and upwelling occurs between alternate pairs. (LCs only become apparent to the eye when there is flotsam on the surface to be brought together by the



**FIGURE S7.9** “Windrows” of foam, associated with the Langmuir circulation in Loch Ness. The surface wave field suggests the wind direction, which is parallel to the narrow bands of foam. *Source: From Thorpe (2004).*

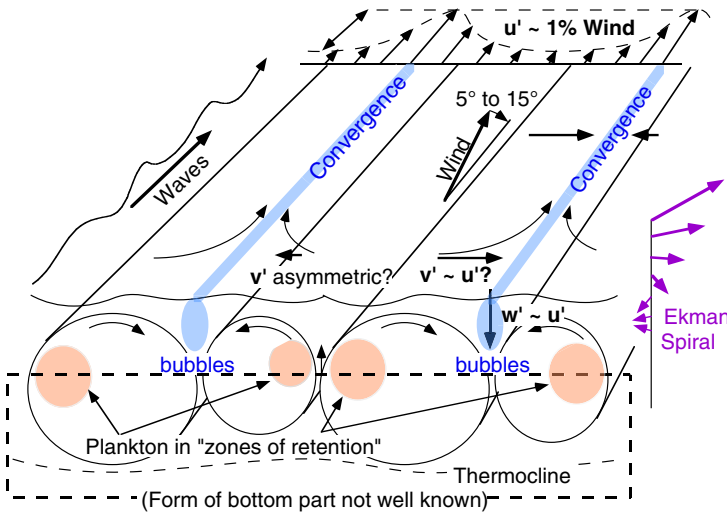


**FIGURE S7.10** Langmuir circulation, first described by Langmuir (1938). *Source: From Smith (2001).*

convergences.) The water in the cells progresses downwind as well, so that its motion is helical.

LCs have typical depth and horizontal spacing of 4–6 m and 10–50 m, but they can range up to several hundred meters horizontal

separation and up to two to three times the mixed layer depth. The cells can be many kilometers long. Multiple scales have been observed simultaneously in strong wind conditions (Assaf, Gerard, and Gordon, 1971). The

downwelling zones are concentrated in jets occupying one-third or less of the cell width under the streaks while upwelling is more widely distributed at smaller speeds. Velocities within an LC are only a fraction of the wind velocities that create them. Thus, the horizontal flow speed at the surface in the streaks can add 10 cm/sec to the non-Langmuir currents elsewhere in the surface layer. The vertical downwelling at the convergences is about one-third of the surface water speed as driven by the wind. Downwelling velocities are several centimeters per second and up to 20 cm/sec.

Langmuir circulations only appear when there are wind waves on the water surface, as in [Figure S7.9](#). Surface films that dampen small waves tend to inhibit the formation of the cells. LCs generally occur only for wind speeds greater than 3 m/sec and appear within a few tens of minutes of wind onset. The mechanism for producing Langmuir circulation is beyond the scope of this text. See [Smith \(2001\)](#) and [Thorpe \(2004\)](#) for further discussions.

Langmuir circulations provide a mechanism for converting wave energy to turbulent energy and mixing and causing the upper layer to deepen. Mixed layer observations suggest that Langmuir downwelling can penetrate to at least the middle of the mixed layer, therefore, it is expected that the downwelling plumes can penetrate to the bottom of the actively mixing layer ([Weller et al., 1985](#); [Smith, 2001](#)). Langmuir cells can generate internal waves in the stratified layer below the mixed layer that contribute to moving momentum from the mixed layer into the interior ([Polton, Smith, Mackinnon, & Tejada-Martinez, 2008](#)). Thus LCs are one of several processes that may contribute to surface mixing.

Note that Ekman's theory of the wind drift ([Section 7.5.3](#)) yields an upper layer motion that is about 45 degrees to the right of the

wind, whereas LCs are more closely aligned to the wind. This is because the timescales of the two mechanisms are quite different. LCs are generated within minutes of the wind onset and die out soon after the strong wind pulse, whereas the Ekman circulation takes many hours to develop.

### 7.5.3. Ekman Layers

Wind stress is communicated to the ocean surface layer through viscous (frictional) processes that extend several tens of meters into the ocean. For timescales longer than a day, the response is strongly affected by Coriolis acceleration. This wind-driven frictional layer is called the *Ekman layer* after [Walfrid Ekman \(1905\)](#), who based his theory on ship drift observations of the *Fram* in the Arctic.<sup>2</sup>

The classical surface Ekman layer is the steady frictional response to a steady wind stress on the ocean surface ([Figure S7.11](#)). The physical processes in an Ekman layer include only friction (eddy viscosity) and Coriolis acceleration. Velocity in the Ekman layer is strongest at the sea surface and decays exponentially downward, disappearing at a depth of about 50 m. It coexists with, but is not the same as, the mixed layer depth or euphotic zone depth.

The two most unusual characteristics of an Ekman layer (compared with a frictional flow that is not rotating) are (1) the horizontal velocity vector spirals with increasing depth ([Figure S7.11](#)) and (2) the net transport integrated through the Ekman layer is *exactly* to the right of the wind in the Northern Hemisphere (left in the Southern Hemisphere).

The surface water in an Ekman layer moves at an angle to the wind because of Coriolis acceleration. If eddy viscosity is independent of depth, the angle is 45 degrees to the right of

<sup>2</sup> Collected as part of Fridtjof Nansen's *Fram* expedition, the ship drift and wind measurements were given to Ekman to explain as his Ph.D. thesis, which focused on the response of water movement in the upper ocean to the wind stress. Later analysis of these data showed that the sea ice drifted 20 to 40 degrees to the right of the wind ([Nansen, 1922](#)).

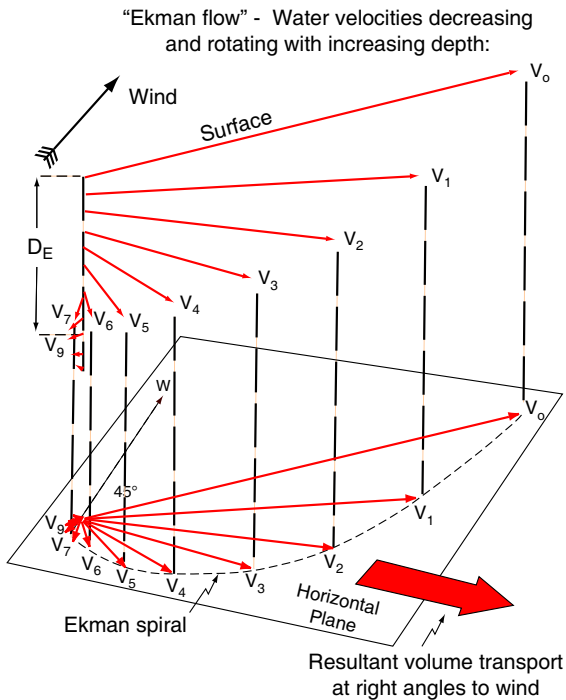


**FIGURE S7.11** Ekman layer velocities (Northern Hemisphere). Water velocity as a function of depth (upper projection) and Ekman spiral (lower projection). The large open arrow shows the direction of the total Ekman transport, which is perpendicular to the wind.

the wind in the Northern Hemisphere (and to the left of the wind in the Southern Hemisphere). If viscosity is not constant with depth, for instance, if the turbulence that creates the eddy viscosity changes with depth, then the angle between the surface velocity and the wind will differ from 45 degrees.

As the surface parcel moves, a frictional stress develops between it and the next layer below. This accelerates the layer below, which moves off to the right (Northern Hemisphere) of the surface parcel. This second layer applies stress to the third layer, and so on. The total stress decays with depth, at a rate that depends on the eddy viscosity coefficient  $A_v$ . Since each successively deeper layer is accelerated to the

right of the layer above it (Northern Hemisphere) and has a weaker velocity than the layer above it, the complete structure is a decaying "spiral." If the velocity arrows, their tips are projected onto a horizontal plane, their tips form the Ekman spiral (Figure S7.11). The whole spiral is referred to as the "Ekman layer."

The Ekman layer depth is the e-folding depth of the decaying velocity:

$$D_E = (2A_v/f)^{1/2} \quad (7.17)$$

Using a constant eddy viscosity of  $0.05 \text{ m}^2/\text{sec}$  from within the observed range (Section 7.5.5), the Ekman layer depths at latitudes 10, 45, and 80 degrees are 63, 31, and 26 m, respectively. The vertically integrated horizontal velocity in the Ekman layer is called the *Ekman transport*:

$$U_E = \int u_E(z) dz \quad (7.18a)$$

$$V_E = \int v_E(z) dz \quad (7.18b)$$

where  $u_E$  and  $v_E$  are the eastward and northward velocities in the Ekman layer, and  $U_E$  and  $V_E$  are the associated Ekman transports. (Ekman "transport" has units of depth times velocity, hence  $\text{m}^2/\text{sec}$ , rather than area times velocity.) Ekman transport in terms of the wind stress is derived from Eq. (7.11):

$$U_E = \tau^{(y)}/(\rho f) \quad (7.19a)$$

$$V_E = -\tau^{(x)}/(\rho f) \quad (7.19b)$$

where  $\tau^{(x)}$  and  $\tau^{(y)}$  are the wind stresses positive in the east and north directions, assuming no time acceleration, advection, or pressure gradient force, and setting the eddy friction stress at the sea surface equal to the wind stress. The Ekman transport is *exactly* perpendicular and to the right (left) of the wind in the Northern (Southern) Hemisphere (large arrow in Figure 7.5).

For applications of Ekman layers to general circulation (Sections 7.8 and 7.9), only the Ekman transport matters. Thus, the actual eddy viscosity and Ekman layer thickness are unimportant.

Ekman layers also form in the ocean's surface layer below sea ice. When the ice is blown by the wind, friction between the sea ice and water drives the water. If the timescale is longer than a day, the Coriolis effect is important, and an Ekman layer develops.

Ekman layers also occur at the ocean bottom (Section 7.4.2). Because of friction, the flow at the bottom must be zero. When the timescale of the deep flow is longer than a day, Coriolis acceleration is important, and an Ekman layer develops, also 50 to 100 m thick above the bottom like the surface Ekman layer. If there is a current (e.g., a geostrophic current), flowing in the lower part of the water column over the sea bottom, which we will assume for simplicity to be flat, then there is a bottom frictional stress on the water. The frictional stress at the bottom acts in the opposite direction to the current. The result of the stress is a frictional transport to the right of the stress (Northern Hemisphere). Therefore the frictional transport (bottom Ekman layer transport) is to the left of the current. The total current (interior plus Ekman) must be zero at the bottom. The net result is an Ekman current spiral in the bottom layer with the total current rotating to the left as the bottom is approached.

In shallow water, the top and bottom Ekman layers can overlap, so that the right-turning tendency in the top layer (Northern Hemisphere) will overlap the left-turning tendency in the bottom layer. The opposing right- and left-turning effects will tend to cancel more and more as the water depth decreases. If there is a wind stress at the top surface that would produce an Ekman layer of depth  $D_E$  in deep water, then in water of depth  $h$ , the approximate angle  $\alpha$  between the wind and the surface flow is as listed in Table S7.2. That is, as water

**TABLE S7.2** Angle of Surface Flow,  $\alpha$  to the Right of the Wind Direction (Northern Hemisphere), with Overlapping Surface and Bottom Ekman Layers

$h/D_E$	$\alpha$	Net flow direction in the water column
$>1$	$45^\circ$	At $90^\circ$ to right of wind
0.5	$45^\circ$	About $60^\circ$ to right of wind
0.25	$22^\circ$	About $25^\circ$ to right of wind
0.1	$3^\circ$	About $6^\circ$ to right of wind

depth decreases, the net flow is more in the direction of the wind.

Tides or internal waves (Chapter 8) rubbing against the bottom can also generate bottom Ekman-like layers, but with time-dependent spiraling currents in the frictional layer.

#### 7.5.4. Ekman Transport Convergence and Wind Stress Curl

When the wind stress varies with position so that Ekman transport varies with position, there can be a convergence or divergence of water within the Ekman layer. Convergence results in downwelling of water out of the Ekman layer. Divergence results in upwelling into the Ekman layer. This is the mechanism that connects the frictional forcing by wind of the surface layer to the interior, geostrophic ocean circulation (Section 7.8).

Divergence and convergence occur if the transport varies in the same direction as the transport. In Figure S7.12, with varying zonal (west to east) wind, the Ekman transport is to the right of the wind, and is convergent because the zonal wind varies with latitude. Note that it is not necessary for the Ekman transports to be in opposite directions to have divergence or convergence, just that the transports change.

The vertical velocity  $w_E$  at the base of the Ekman layer is obtained from the divergence of the Ekman transport, by vertically integrating

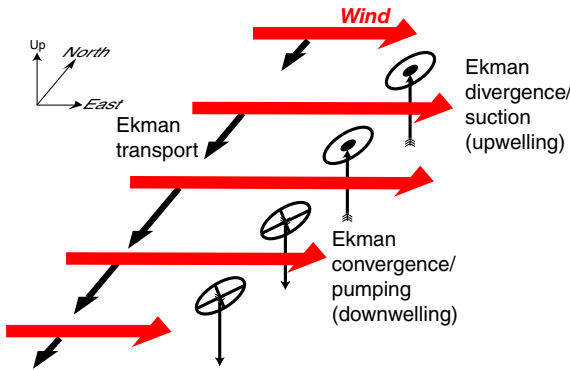


FIGURE S7.12 Ekman transport convergence and divergence in the Northern Hemisphere due to variations in a zonal (eastward) wind. Ekman transport is southward, to the right of the wind. Divergent transport causes downwelling, denoted by circles with a cross. Convergent transport causes upwelling, denoted by circles with a dot.

the continuity equation Eq. (7.11e) over the depth of the Ekman layer:

$$\begin{aligned} (\partial U_E / \partial x + \partial V_E / \partial y) &= \nabla \cdot \mathbf{U}_E \\ &= -(w_{\text{surface}} - w_E) = w_E \end{aligned} \quad (7.20)$$

where  $\mathbf{U}_E$  is the horizontal vector Ekman transport and it is assumed that the vertical velocity at the sea surface,  $w_{\text{surface}}$ , is 0. When Eq. (7.20) is negative, the transport is convergent and there must be downwelling below the sea surface (increasingly negative  $w_E$ ). The relation of Ekman transport divergence to the wind stress from Eq. (7.19a, b) is

$$\begin{aligned} \nabla \cdot \mathbf{U}_E &= \partial / \partial x (\tau^{(y)} / (\rho f)) - \partial / \partial y (\tau^{(x)} / (\rho f)) \\ &= \mathbf{k} \cdot \nabla \times (\boldsymbol{\tau} / \rho f) \end{aligned} \quad (7.21)$$

where  $\boldsymbol{\tau}$  is the vector wind stress and  $\mathbf{k}$  is the unit vector in the vertical direction. Therefore, in the Northern Hemisphere ( $f > 0$ ), upwelling into the Ekman layer results from positive wind stress curl, and downwelling results

from negative wind stress curl. Downwelling is referred to as *Ekman pumping*. Upwelling is sometimes referred to as *Ekman suction*.

A global map of wind stress curl was shown in Figure 5.16d, and is referred to frequently in subsequent chapters because of its importance for Ekman pumping/suction, although the mapped quantity should include the Coriolis parameter,  $f$ , to be related directly to upwelling and downwelling.

Equatorial upwelling due to Ekman transport results from the westward wind stress (trade winds). These cause northward Ekman transport north of the equator and southward Ekman transport south of the equator. This results in upwelling along the equator, even though the wind stress curl is small because of the Coriolis parameter dependence in Eq. (7.21).

At the equator, where the Coriolis parameter changes sign, zonal (east-west) winds can cause Ekman convergence or divergence even without any variation in the wind (Figure S7.13a,b). Right on the equator, there is no Ekman layer since the Coriolis force that would create it is zero ( $f = 0$ ). However, it has been shown from observations (Eriksen, 1982) that the Coriolis force is important quite close to the equator in the ocean, starting at about  $1/4^\circ$  latitude. If the equatorial wind is westward (a trade wind), then the Ekman transport just north of the equator is northward, and the Ekman transport just south of the equator is southward, and there must be upwelling into the surface layer on the equator. This is roughly included in Eq. (7.21) because of the variation in  $f$ , although the equation is not accurate right on the equator where  $f$  vanishes.

The coastline is the other place where Ekman transport divergence or convergence can occur, and it is *not* included in Eq. (7.21), because this divergence is due to the boundary condition at the coast and not wind stress curl. If the wind blows along the coast, then Ekman transport is perpendicular to the coast, so there must be

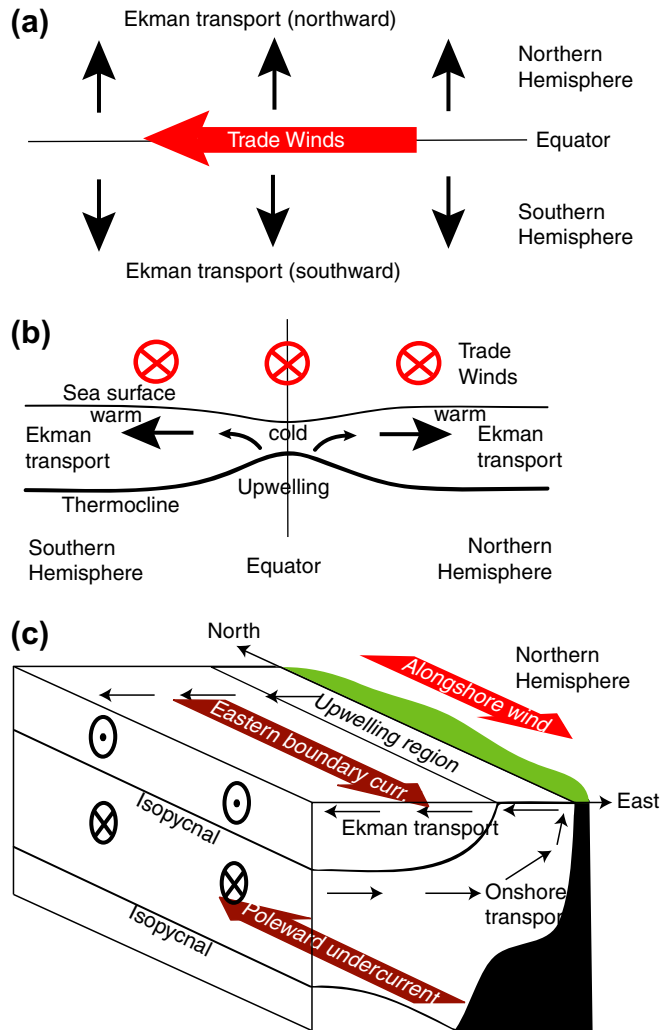


FIGURE S7.13 Ekman transport divergence near the equator driven by easterly trade winds. (a) Ekman transports. (b) Meridional cross-section showing effect on the thermocline and surface temperature. (c) Coastal upwelling system due to an alongshore wind with offshore Ekman transport (Northern Hemisphere). The accompanying isopycnal deformations and equatorward eastern boundary current and poleward undercurrent are also shown (see Section 7.9).

either downwelling or upwelling at the coast to feed the Ekman layer (Figure S7.13c). This is one mechanism for creation of coastal upwelling and subtropical eastern boundary current systems. The other mechanism is wind stress curl in the near-coastal region that drives upwelling (Section 7.9). One such

example is the California-Oregon coast, where the mean wind during most of the year includes a component that blows southward (offshore) Ekman transport to the right of the wind. This means there must be upwelling at the coast.

### 7.5.5. Observations of Ekman Response and Wind Forcing

The Ekman theory has major consequences for wind-driven ocean circulation. Thus it has been important to confirm and refine Ekman's theory with ocean observations, beyond the original ice, wind, and ship drift observations used by Ekman (1905) and Nansen (1922).

For instance, one assumption, that the eddy viscosity in the water column is constant with depth, is not accurate. (Recall that the Ekman transport is independent of viscosity, so the variability of eddy viscosity does not matter for large-scale circulation.) Eddy viscosity is highest near the sea surface because of turbulence resulting from wind waves and inertial currents generated at the surface. Also, Ekman assumed a steady wind. The speed with which the Ekman circulation develops depends on latitude, because the Coriolis force depends on latitude. Observations of Ekman spirals and Ekman response are very difficult because of the time dependence of the wind. It takes about one pendulum day for inertial and Langmuir responses (Sections 7.5.1 and 7.5.2) to die out and an essentially Ekman circulation to develop.

Ekman layer observations are also difficult because the spiral is thin compared with the usual vertical resolution of current measurements. Davis, deSzoeko, and Niiler (1981) measured currents in the mixed layer in the northeast Pacific. By filtering the data and looking at responses at short and long timescales, they found that the currents at timescales of longer than about one day looked like Ekman's theory. Chereskin (1995) measured currents in the mixed layer in the California Current using an Acoustic Doppler Current Profiler (Section S16.5.5.1 of Chapter S16 in the online supplement). Because the wind direction there was relatively steady, the Ekman-like response was clear (Figure S7.14) even without filtering the data. The high eddy viscosity values that

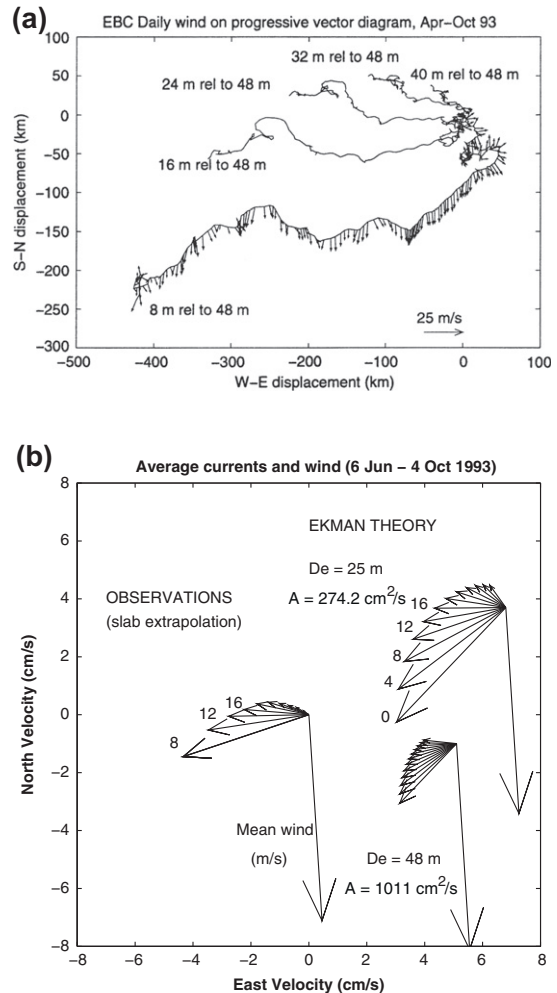


**FIGURE S7.14** Observations of an Ekman-like response in the California Current region. (a) Progressive vector diagrams (Section 6.5.2) at 8, 16, 24, 32, and 40 m depth. Because of the way the ADCP measures, the currents are shown relative to a deeper depth, rather than as absolute currents. The wind direction and speed for each day is shown by the small arrows on the 8 m progressive vector curve. (b) Observed mean velocities (left) and two theoretical Ekman spirals (offset) using different eddy diffusivities (274 and 1011  $\text{cm}^2/\text{s}$ ). The numbers on the arrows are depths. The large arrow is the mean wind. *Source: From Chereskin (1995).*

Chereskin reported (Section 7.5.3) were obtained by fitting the observed spiral to an Ekman layer with depth-dependent viscosity.

An Ekman response to the wind for a large part of the Pacific Ocean is apparent in the average 15 m velocity from surface drifters deployed in the 1980s and 1990s. The surface drifters were drogued at 15 m depth, within the Ekman layer. The drifter velocities from many years of observations were averaged and the average geostrophic velocity was subtracted. The resulting “ageostrophic” velocities, which are likely the Ekman response, are to the right of the wind stress in the Northern Hemisphere and to the left in the Southern Hemisphere (Figure S7.15).

The Ekman volume transports (horizontal and vertical) for each ocean and for the World Ocean are shown in Figure S7.16. The easterly trade winds (blowing westward) cause poleward horizontal Ekman flows in the tropical Atlantic and Pacific. The westerlies (blowing eastward) cause equatorward flows at higher latitudes. The Pacific Ekman transports are larger than the Atlantic transports mainly

because the Pacific is so much wider, not because the wind stress differs. The near-equatorial Indian transports are of the opposite sign compared with the Pacific, Atlantic, and total transports because of the large annual monsoon cycle; the westerly winds dominate the annual mean in the equatorial Indian Ocean.

Associated with the convergences and divergences of the horizontal Ekman flows are vertical flows due to Ekman pumping (Figure S7.16b). Between approximately 40°S and 40°N, downwelling prevails and the winds cause convergent Ekman transport. Poleward of about 40 degrees, there is upwelling caused by divergent Ekman transport. The narrow region of Ekman upwelling at about 5 to 10°N is associated with the Intertropical Convergence Zone in the winds. Not shown is the major upwelling along the equator that must result from the divergent Ekman transports there due to the change of sign in the Coriolis parameter. Again the Pacific and Atlantic have similar distributions and the Indian Ocean differs because of its strong annual (monsoonal) variation north of the equator.

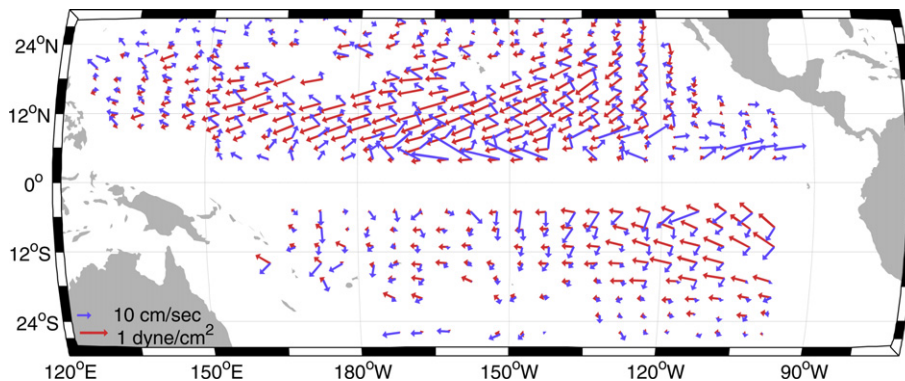


**FIGURE S7.15** Ekman response. Average wind vectors (red) and average ageostrophic current at 15 m depth (blue). The current is calculated from 7 years of surface drifters drogued at 15 m, with the geostrophic current based on average density data from Levitus, Boyer, and Antonov (1994a) removed. (No arrows were plotted within 5 degrees of the equator because the Coriolis force is small there.) This figure can also be found in the color insert. Source: From Ralph and Niiler (1999).

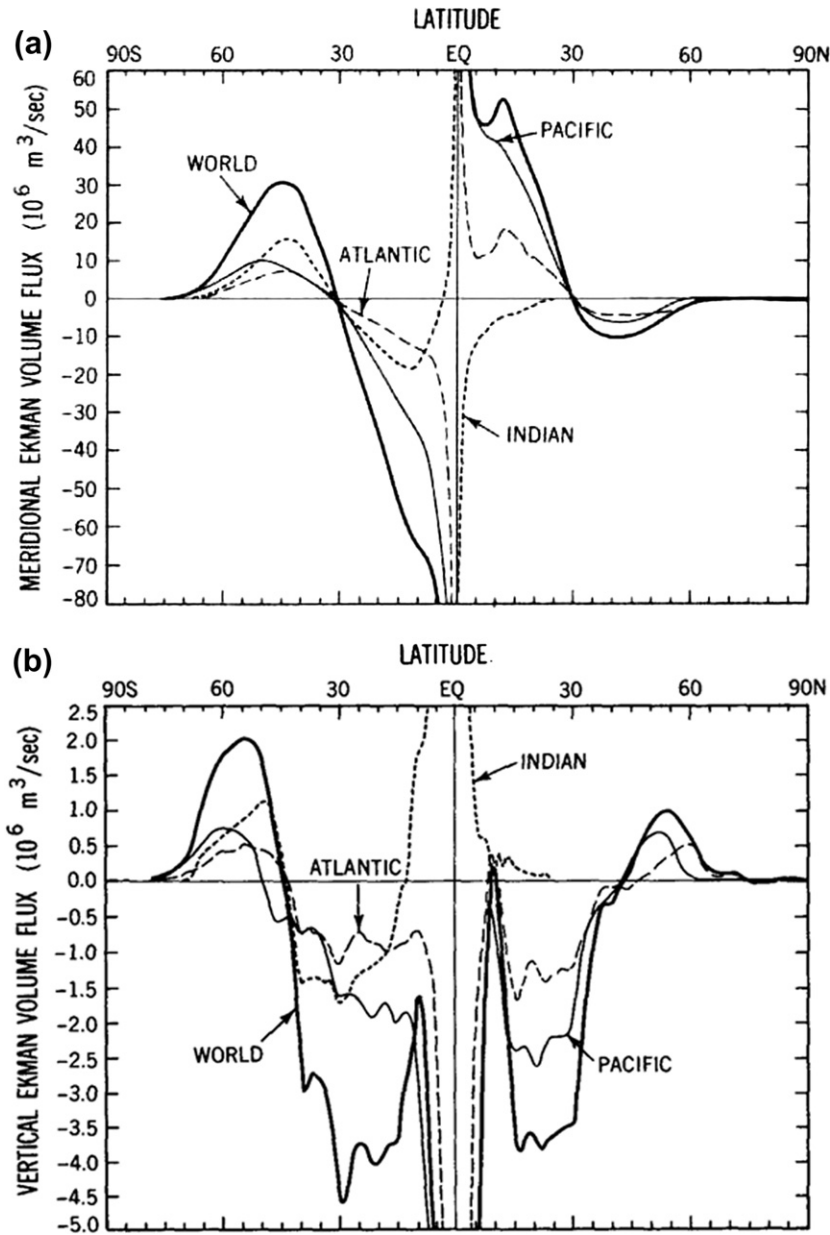


FIGURE S7.16 (a) Zonally integrated meridional Ekman fluxes (Sv) for the three oceans by latitude and month. (Positive is northward, negative is southward.) (b) Zonally integrated vertical Ekman volume flux (Sv) at the base of the Ekman layer per 10 degrees latitude belt by latitude and month. (Positive is up, negative is down.) Source: From Levitus (1988).

## 7.6. GEOSTROPHIC BALANCE

### 7.6.1. Pressure Gradient Force and Coriolis Force Balance

Throughout most of the ocean at timescales longer than several days and at spatial scales longer than several kilometers, the balance of forces in the horizontal is between the pressure gradient and the Coriolis force. This is called “geostrophic balance” or *geostrophy*.<sup>3</sup>

In a “word” equation, geostrophic balance is horizontal Coriolis acceleration

$$= \text{horizontal pressure gradient force} \quad (7.22)$$

This is illustrated in Figure S7.17. The pressure gradient force vector points from high pressure to low pressure. In a non-rotating flow, the water would then move from high to low pressure. However, with rotation, the Coriolis force exactly opposes the pressure gradient force, so that the net force is zero. Thus, the water parcel does not accelerate (relative to Earth). The parcel moves exactly perpendicular to both the pressure gradient force and the Coriolis force.

A heuristic way to remember the direction of geostrophic flow is to think of the pressure gradient force pushing the water parcel from high to low pressure, but Coriolis force moves the parcel off to the right (Northern Hemisphere) or the left (Southern Hemisphere). In the resulting steady geostrophic state, the water parcel moves exactly perpendicular to the pressure gradient force.

The vertical force balance that goes with geostrophy is *hydrostatic balance* (Section 3.2). The vertical pressure gradient force, which points upward from high pressure to low pressure, is balanced by gravity, which points downward. Thus vertical acceleration, advection, and diffusion are assumed to be very

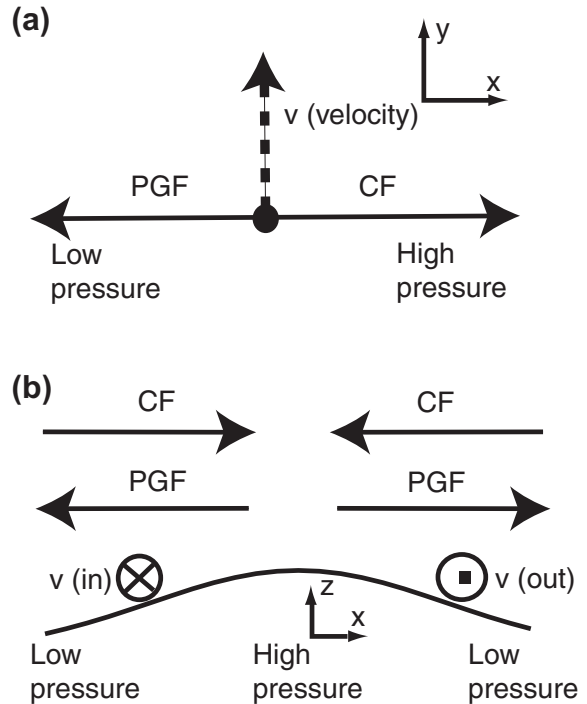


FIGURE S7.17 Geostrophic balance: horizontal forces and velocity. (a) Horizontal forces and velocity in geostrophic balance. PGF = pressure gradient force. CF = Coriolis force. (b) Side view showing elevated pressure (sea surface) in center, low pressure on sides, balance of PGF and CF, and direction of velocity  $v$  (into and out of page).

small, just as in the horizontal momentum equations. (We note that in full treatments of rotating fluid dynamics, the student will learn that hydrostatic balance holds for a very large range of fluid flows, not just those that are geostrophic.)

The mathematical expression of geostrophy and hydrostatic balance, from Eq. (7.11a, b, c), is

<sup>3</sup> The other terms in the force balance — the actual acceleration, the advection, and diffusion — never completely vanish, so no flow is exactly geostrophic.

$$-fv = -(1/\rho)\partial p/\partial x \quad (7.23a)$$

$$fu = -(1/\rho)\partial p/\partial y \quad (7.23b)$$

$$0 = -\partial p/\partial z - \rho g \quad (7.23c)$$

An alternate form for Eq. (7.23c), used for dynamic height calculations (Section 7.6.3), is

$$0 = -\alpha \partial p/\partial z - g \quad (7.23d)$$

where  $\alpha$  is specific volume. Note how many of the terms in Eq. (7.11) have been assumed to be very small and therefore are left out in Eq. 7.23a,b).<sup>4</sup>

From Eq. (7.23a,b), if the Coriolis parameter is approximately constant ( $f = f_0$ ) and if density in Eq. (7.23a,b) is also very nearly constant ( $\rho = \rho_0$ ; the “Boussinesq approximation”), the geostrophic velocities are approximately non-divergent:

$$\partial u/\partial x + \partial v/\partial y = 0 \quad (7.23e)$$

Formally in fluid dynamics, such a non-divergent velocity field can be written in terms of a *streamfunction*  $\psi$ :

$$u = -\partial\psi/\partial y \quad \text{and} \quad v = \partial\psi/\partial x \quad (7.23f)$$

From Eqs. (7.23a, b) the streamfunction for geostrophic flow is  $\psi = p/(f_0\rho_0)$ . Therefore, maps of pressure distribution (or its proxies like dynamic height, steric height, or geopotential anomaly; Section 7.6.2) are maps of the geostrophic streamfunction, and flow approximately follows the mapped contours.

Geostrophic balance is intuitively familiar to those with a general interest in weather reports. Weather maps show high and low pressure regions around which the winds blow (Figure S7.18). Low pressure regions in the atmosphere are called *cyclones*. Hurricanes, dramatic winter storms, and tornados are all cyclones. Flow around low-pressure regions is thus called *cyclonic* (counterclockwise in the Northern Hemisphere and clockwise in the Southern Hemisphere). Flow around high-pressure regions is called *anticyclonic*.

In the ocean, higher pressure can be caused by a higher mass of water lying above the observation depth. At the “sea surface,” pressure differences are due to an actual mounding of water relative to Earth’s geoid. Over the complete width of the Atlantic or Pacific Ocean anticyclonic gyres, the total contrast in sea-surface height is about 1 m.

The geostrophic velocities at the sea surface could be calculated if the appropriately time-averaged sea-surface height were known (as yet not possible for the time mean, but definitely possible from satellite altimetry for variations from the mean). The geostrophic velocity at the sea surface in terms of sea-surface height  $\eta$  above a level surface is derived from Eqs. (7.23a,b):

$$-fv = -g\partial\eta/\partial x \quad (7.24a)$$

$$fu = -g\partial\eta/\partial y \quad (7.24b)$$

<sup>4</sup> Rigorous justification of geostrophic balance is based on small Rossby and Ekman numbers, where the Rossby number is defined in Section 7.2.3, and the Ekman number is the non-dimensional parameter that is the ratio of the size of the viscous term to the size of the Coriolis term. For the vertical direction, the Ekman number is  $E_V = 2A_V/fH^2$ , where  $f$  is the Coriolis parameter and  $H$  is a characteristic vertical length scale; note the resemblance of this parameter to the Ekman layer depth in Eq. (7.17). Hydrostatic balance (Eq. 7.23c,d) is valid when the non-dimensional *aspect ratio*, which is the ratio of the vertical scale of motion ( $H$ ) to the horizontal scale of motion ( $L$ ); that is,  $\delta = H/L$ , is small. Hydrostatic balance is even more strongly justified when the Rossby number is small; that is, the substantial derivative in the  $z$ -momentum equation scales as the square of the aspect ratio times the Rossby number. Performing a complete “scale analysis” in which these assumptions are rigorously applied to the full set of momentum equations, thus deriving the balances in Eq. (7.23), is far beyond the scope of this text.

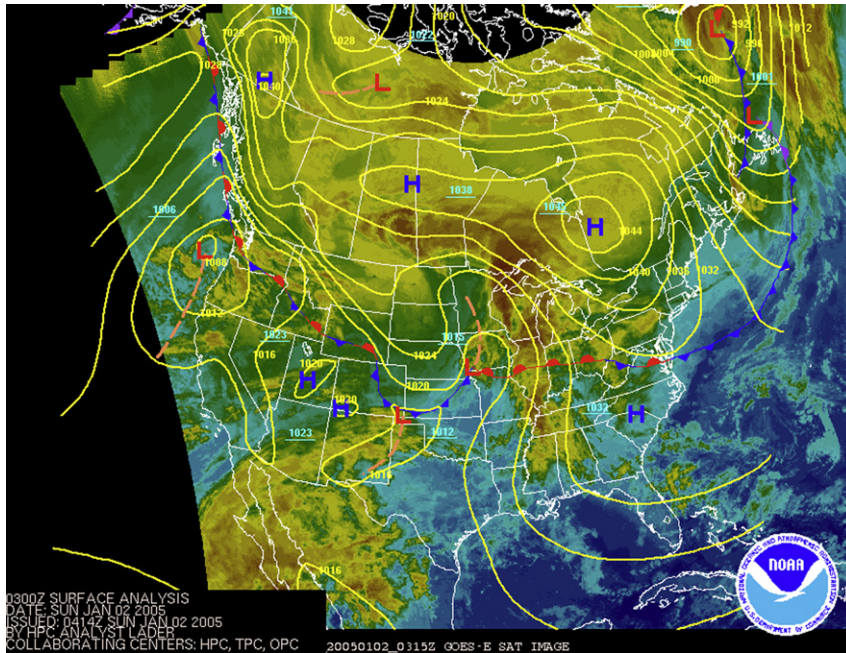


**FIGURE S7.18** Example of a daily weather map for North America, showing high- and low-pressure regions. Winds are generally not from high to low, but rather clockwise around the highs and counterclockwise around the lows. *Source: From NOAA National Weather Service (2005).*

To calculate the horizontal pressure difference below the sea surface, we have to consider both the total height of the pile of water above our observation depth and also its density, since the total mass determines the actual pressure at our observation depth (Figure S7.19). (This is where the vertical hydrostatic balance in Eq. 7.23c enters.) Therefore, if a mound of less dense water lies above us in one location and a shorter column of denser water in another location, the total mass in the two places could be the same. Close to the sea surface, there would be a pressure difference between the two places since the sea surface is higher in one location than in the other, but at depth the pressure difference would vanish because the difference in densities cancels the difference

in heights. Therefore there would be a geostrophic flow at the sea surface, which would decrease with depth until it vanishes at our observation depth ( $h_3$  in Figure S7.19a), where the total mass of the two columns of water is the same.

The variation in geostrophic flow with depth (the *geostrophic velocity shear*) is therefore proportional to the difference in density of the two water columns on either side of our observation location. The relation between the geostrophic velocity shear and the horizontal change (gradient) in density is called the *thermal wind relation*, since it was originally developed by meteorologists measuring temperature and wind, rather than by oceanographers measuring density and currents.<sup>5</sup>

<sup>5</sup> The thermal wind balance should not be confused with the thermohaline circulation, which refers to ocean overturning directly involving buoyancy fluxes (Section 7.10).

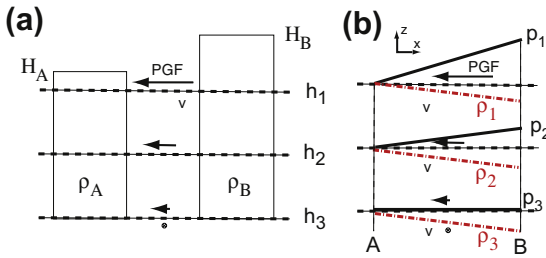


**FIGURE S7.19** Geostrophic flow and thermal wind balance. (a) Schematic of change in pressure gradient force (PGF) with depth, assuming that the left column (A) is shorter and denser than the right column (B), that is,  $\rho_A > \rho_B$  and  $H_A < H_B$ . The horizontal geostrophic velocity  $V$  is into the page for this direction of PGF and is strongest at the top, weakening with depth, as indicated by the circle sizes. (If the densities of the two columns were the same, then the PGF and velocity  $V$  are the same at all depths.) (b) Same, but for density (red) increasing with depth, and isopycnals tilted, and assuming that the sea surface at B is higher than at A so that the PGF at the sea surface ( $h_1$ ) is to the left. The PGF decreases with increasing depth, as indicated by the flattening of the isobars  $p_2$  and  $p_3$ .

The thermal wind relation is illustrated in [Figure S7.19b](#). The sea surface is sloped, with surface pressure higher to the right. This creates a pressure gradient force to the left, which drives a surface geostrophic current into the page (Northern Hemisphere). The density  $\rho$  increases with depth, and the isopycnals are tilted. Therefore the geostrophic velocity changes with depth because the pressure gradient force changes with depth due to the tilted isopycnals. Because the isopycnals are sloped in the opposite direction to the sea-surface height, the into-the-page geostrophic velocity is reduced with depth. That is, when there is light water under a high sea surface and dense water under a low sea surface, the horizontal pressure gradients become smaller with depth, since the mass of the two columns becomes more equalized with depth.

A useful rule of thumb for geostrophic flows that are surface-intensified is that, when facing downstream in the Northern Hemisphere, the

“light/warm” water is to your right. (In the Southern Hemisphere, the light water is to the left when facing downstream.) This can be safely recalled by memorizing the example for the Gulf Stream recalling that the current flows eastward with warm water to the south.

Geostrophic flow with vertical shear, which requires sloping isopycnals, is often called *baroclinic*. Geostrophic flow without any vertical shear is often called *barotropic*. Barotropic flow is driven only by horizontal variations in sea-surface height. Most oceanic geostrophic flows have both barotropic and baroclinic components.

Mathematically, the thermal wind relations are derived from the geostrophic and hydrostatic balance Eq. (7.23):

$$-f\partial v/\partial z = (g/\rho_0)\partial\rho/\partial x \quad (7.25a)$$

$$f\partial u/\partial z = (g/\rho_0)\partial\rho/\partial y \quad (7.25b)$$

(Here we have again used the Boussinesq approximation, where  $\rho$  is replaced by the constant  $\rho_0$  in the  $x$ - and  $y$ -momentum equations, whereas the fully variable density  $\rho$  must be used in the hydrostatic balance equation.)

To calculate geostrophic velocity, we must know the absolute horizontal pressure difference between two locations. If we have only the density distribution, we can calculate only the current at one level relative to that at another, that is, the geostrophic vertical shear. To convert these relative currents into absolute currents, we must determine or estimate the absolute current or pressure gradient at some level (reference level).

The selection of a reference level velocity is one of the key problems in using the geostrophic method to compute currents. A common, but usually inaccurate, referencing approach has been to assume (without measuring) that the absolute current is zero at some depth (*level of no motion*). In the case of western boundary currents or in the ACC where the currents

extend to great depth, this is not a good assumption. Nevertheless the relative geostrophic surface current calculation can be revealing since the surface currents are usually much stronger than the deep ones, and small relative error in the surface currents might be tolerated while the same amount of error in the deep currents is untenable.

In the next subsection, we introduce the “dynamic” method widely used to calculate geostrophic velocities (shear), and continue the discussion of reference velocity choices.

### 7.6.2. Geopotential and Dynamic Height Anomalies and Reference Level Velocities

Historically and continuing to the present, it has been too difficult and too expensive to instrument the ocean to directly observe velocity everywhere. Density profiles, which are much more widely and cheaply collected, are an excellent data set for estimating geostrophic velocities using the thermal wind relations and estimates of the reference level velocity. This approach to mapping ocean currents is called the “dynamic method”; it was developed in the School of Geophysics in Bergen, Norway, more than a century ago. This is the same school where both Nansen and Ekman worked, contributing some very significant ideas to physical oceanography. The dynamic method has origins in both oceanography and meteorology. In the dynamic method, the distribution of mass in the ocean is used to compute an important component of the current field. In this text the emphasis will be on how this method is commonly used in descriptive studies of ocean circulation rather than derivation of the method.

In the ocean the distribution of mass is represented by the distribution of density over both the horizontal and vertical dimensions. Once the density profiles at two locations (“stations”)

are calculated from observed temperature and salinity, the distribution of mass at the two stations can be used to calculate the vertical shear of geostrophic velocity at the midpoint between the two stations at all depths that are common to the two stations (Section 7.6.1). Then, if the velocity is known at one depth (or is assumed to have a certain value, e.g., zero), the vertical shear can be used to give the velocity at all other depths. The assumed or measured velocity at one depth is called the *reference velocity*, and its depth is called the “reference depth” or *reference level*. Thus in this method, the horizontal change in the distribution of mass creates the horizontal pressure gradient, which drives the geostrophic flow.

Oceanographers have created two closely related functions, *geopotential anomaly* and *dynamic height*, whose horizontal gradients represent the horizontal pressure gradient force. Another closely related concept, *steric height*, is used to study variations in sea level. All are calculated from the density profiles computed from the measured temperature and salinity profiles. Sverdrup, Johnson, and Fleming (1942), Gill and Niiler (1973), Gill (1982), Pond and Pickard (1983), and Stewart (2008) are a few of the many useful references for these practical quantities.

The gradient of the *geopotential*,  $\Phi$ , is in the direction of the local force due to gravity (modified to include centrifugal force). The geopotential gradient is defined from hydrostatic balance (Eq. 7.23c) as

$$d\Phi = g dz = -\alpha dp \quad (7.26a)$$

where  $\alpha$  is specific volume. The units of geopotential are  $\text{m}^2/\text{sec}^2$  or  $\text{J}/\text{kg}$ . For two isobaric surfaces  $p_2$  (upper) and  $p_1$  (lower), the geopotential is

$$\Phi = g \int dz = g(z_2 - z_1) = - \int \alpha dp \quad (7.26b)$$

Geopotential height is defined as

$$\begin{aligned} Z &= (9.8 \text{ m s}^{-2})^{-1} \int g \, dz \\ &= -(9.8 \text{ m s}^{-2})^{-1} \int \alpha \, dp \end{aligned} \quad (7.26c)$$

and is nearly equal to geometric height. This equation is in mks units; if centimeter-gram-second (cgs) units are used instead, the multiplicative constant would change from  $9.8 \text{ m s}^{-2}$  to  $980 \text{ cm s}^{-2}$ . Most practical calculations, including common seawater computer subroutines, use the specific volume anomaly

$$\delta = \alpha(S, T, p) - \alpha(35, 0, p) \quad (7.26d)$$

to compute the geopotential anomaly

$$\Delta\Phi = - \int \delta \, dp. \quad (7.26e)$$

The geopotential height anomaly is then defined as

$$Z' = -(9.8 \text{ m s}^{-2})^{-1} \int \delta \, dp. \quad (7.26f)$$

Geopotential height anomaly is effectively identical to *steric height anomaly*, which is defined by Gill and Niiler (1973) as

$$h' = -(1/\rho_0) \int \rho' \, dz \quad (7.27a)$$

in which the *density anomaly*  $\rho' = \rho - \rho_0$ . Using hydrostatic balance and defining  $\rho_0$  as  $\rho(35, 0, p)$ , Eq. (7.27a) is equivalent to Tomczak and Godfrey's (1994) steric height (anomaly)

$$h' = \int \delta \, \rho_0 \, dz \quad (7.27b)$$

which can be further manipulated to yield

$$h' = (1/g) \int \delta \, dp. \quad (7.27c)$$

This is nearly identical to the geopotential height anomaly in Eq. (7.26f), differing only in the appearance of a standard quantity for  $g$ . In SI units, steric height is in meters.

*Dynamic height*,  $D$ , is closely related to geopotential,  $\Phi$ , differing only in sign and units of reporting. Many modern publications and common computer subroutines do not distinguish between dynamic height and geopotential anomaly. The unit traditionally used for dynamic height is the dynamic meter:

$$1 \text{ dyn m} = 10 \text{ m}^2/\text{sec}^2. \quad (7.28a)$$

Therefore dynamic height reported in dynamic meters is related to geopotential anomaly as

$$\Delta D = -\Delta\Phi/10 = \int \delta \, dp/10. \quad (7.28b)$$

Its relation to the geopotential height and steric height anomalies is

$$10 \Delta D = -9.8 Z' = gh'. \quad (7.28c)$$

The quantities  $\Delta D$  and  $Z'$  are often used interchangeably, differing only by 2%. With use of the dynamic meter, maps of dynamic topography are close to the actual geometric height of an isobaric surface relative to a level surface; for example, a horizontal variation of 1 dyn m means that the isobaric surface has a horizontal depth variation of about 1 m. Note that the geopotential height anomaly more closely reflects the actual height variation, so a variation of 1 dyn m would be an actual height variation closer to 1.02 m.

Geostrophic velocities at one depth relative to those at another depth are calculated using Eq. (7.25) with geopotential anomalies, steric height anomalies, or dynamic heights. In SI units, and using dynamic meters for dynamic height, the difference between the northward velocity  $v$  and eastward velocity  $u$  at the pressure surface  $p_2$  relative to the pressure surface  $p_1$  is

$$\begin{aligned} f(v_2 - v_1) &= 10 \partial \Delta D / \partial x = -\partial \Delta \Phi / \partial x \\ &= g \partial h' / \partial x \end{aligned} \quad (7.29a)$$

$$\begin{aligned} f(u_2 - u_1) &= -10 \partial \Delta D / \partial y = \partial \Delta \Phi / \partial y \\ &= -g \partial h' / \partial y \end{aligned} \quad (7.29b)$$

where the dynamic height or geopotential anomalies are integrated vertically from  $p_1$  to  $p_2$ . The surface  $p_1$  is the *reference level*. (Comparison of Eq. 7.29 with Eq. 7.23 shows that the dynamic height and geopotential anomalies are streamfunctions for the difference between geostrophic flows from one depth to another.)

How is the velocity at the reference level chosen? Since the strength of ocean currents decreases from the surface downward in many (but not all) regions, for practical reasons, a deep level of no motion has often been presumed. A much better alternative is to use a “level of known motion”. For example, current meter measurements, or the tracks of subsurface floats, may be used to define the current at some level, and then dynamic or steric heights can be used to compute currents at all other levels relative to the known reference level. Another modern practice is to require that the entire flow field, which is defined by many density profiles, satisfy some overall constraints. An obvious one is that there can be no net transport into a region enclosed by a set of stations (otherwise there would be an increasing mound or hole in that region). Another one is that the chemistry must make sense — there can be no net production of oxygen within the ocean outside the surface layer for instance. Another type of constraint is that the flows match measured velocities from current meters or floats, but allowing for some error in the match. The constraints then help narrow the choices of reference level velocities. Formal versions of these methods, first applied to the reference level problem by Carl Wunsch in the 1970s, are called *inverse methods* because of the mathematics used to connect the constraints

to the choices of reference velocities (see Wunsch, 1996).

Another apparently attractive option is to use satellite altimeters to measure the sea-surface height, which would give the pressure distribution and hence geostrophic currents at the sea surface. These can be used to reference the geostrophic velocities calculated at all depths below the surface using dynamic height profiles. However, while the sea surface elevation is measured very precisely by satellite altimeters, the height includes Earth’s geoid, which has large spatial variations that are not yet well measured; this leads to spurious surface currents if one simply calculates the gradient in measured surface height. The geoid does not vary in time, so satellite altimetry does provide excellent information on time changes of the surface geostrophic currents. The **GR**avity and **E**arth **C**limate **E**xperiment (GRACE) satellite, launched in 2002 to measure the shorter spatial scales of Earth’s gravity field, is helping to resolve this geoid problem. Satellite altimeters and GRACE are described in the online supplementary Chapter S16.

As an example of the geostrophic method, we calculate dynamic height and a geostrophic velocity profile from two density profiles that straddle the Gulf Stream (Figure S7.20 and Table S7.3). The isopycnals sloping upward toward the north between 38 and 39°N mark the horizontal pressure gradient associated with the Gulf Stream (Figure S7.20a). The geostrophic velocity profile is calculated between stations “A” and “B” relative to an arbitrary level of no motion at 3000 m. (If it were known, the velocity at 3000m can be added later to the full velocity profile.) Station A has lower specific volume (higher potential density) than station B (Figure S7.20b). The surface dynamic height at A is therefore lower than at B (Figure S7.20c) and the surface pressure gradient force is toward the north, from B to A. Therefore, the geostrophic velocity at the midpoint between the stations (Figure

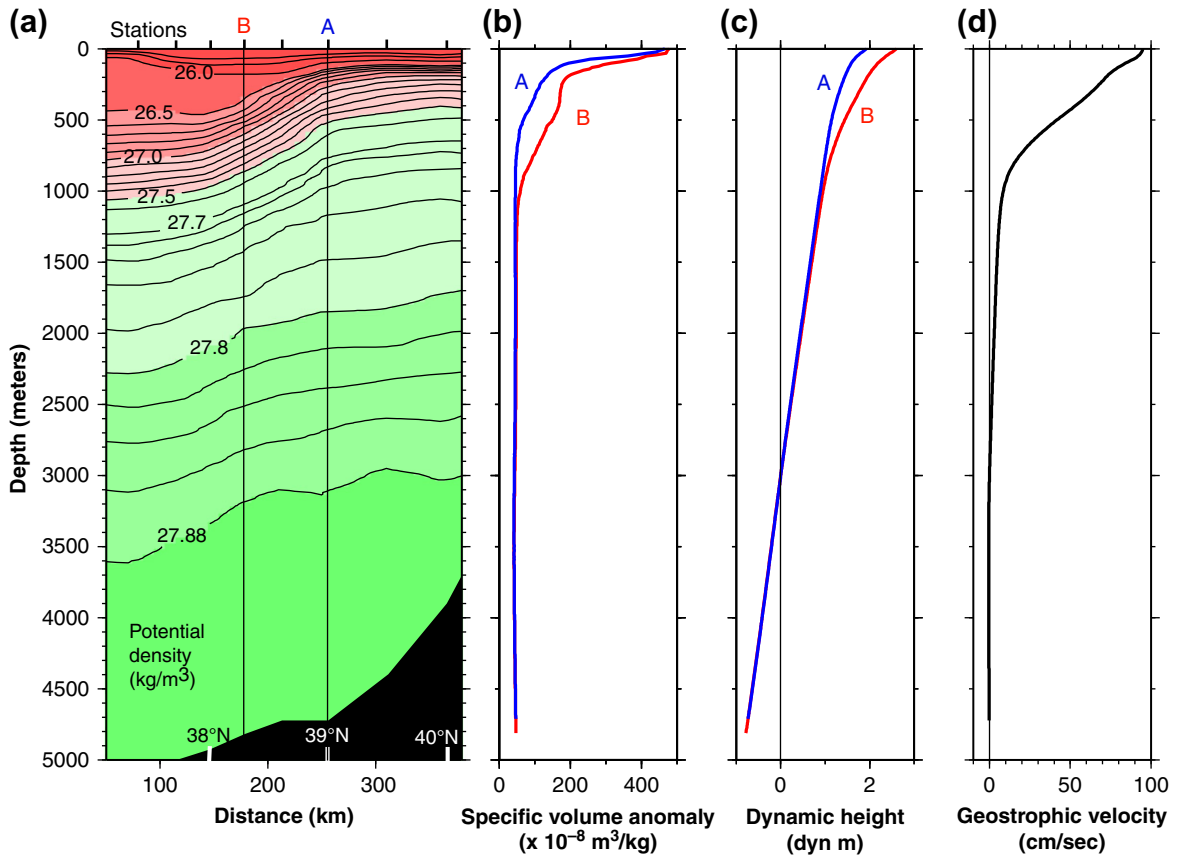


**FIGURE S7.20** (a) Potential density section across the Gulf Stream (66°W in 1997). (b) Specific volume anomaly  $\delta$  ( $\times 10^{-8}$  m<sup>3</sup>/kg) profiles at stations A and B. (c) Dynamic height (dyn m) profiles at stations A and B, assuming reference level at 3000 m. (d) Eastward geostrophic velocity (cm/sec), assuming zero velocity at 3000 m.

S7.20d) is eastward and is largest at the sea surface. This means that the sea surface must tilt downward from B to A. The vertical shear is largest in the upper 800 m where the difference in dynamic heights is largest.

For practical applications in which the maximum depths of density profiles vary, it is often most convenient to first calculate dynamic height by integrating from the surface downward for every profile (Table S7.3), and then calculate the associated geostrophic velocity relative to 0 cm/sec at the sea surface (column 4 in Table S7.3). This geostrophic velocity profile

is likely not close to the actual velocity profile, since velocities are usually small at depth and not at the sea surface. Then the assumed or independently measured velocity at the chosen deep reference level is compared with the velocity at the reference level calculated relative to 0 cm/sec at the sea surface, and the entire geostrophic velocity profile is offset by the difference. For instance, if our reference velocity choice is 0 cm/sec at 3000 m, then we look for the calculated geostrophic velocity at 3000 m relative to 0 at the sea surface and subtract this from the velocities at all depths (column 5 in Table

**TABLE S7.3** Computation of Dynamic Height and Geostrophic Current Between Stations A and B Relative to an Assumed Zero Velocity at 3000 m and at the Deepest Common Level (DCL)

Depth (m)	$D_A$ (dyn m)	$D_B$ (dyn m)	Eastward speed (cm/sec)		
			Relative to sea surface	Ref. 0 cm/sec at 3000 m	Ref. 0 cm/sec at DCL*
0	0	0	0	94.83	95.13
50	-0.230	-0.211	-2.78	92.04	92.32
100	-0.416	-0.340	-10.70	84.12	84.40
150	-0.552	-0.425	-17.89	76.94	77.22
200	-0.657	-0.495	-22.85	71.98	72.26
300	-0.835	-0.611	-31.52	63.31	63.59
400	-1.005	-0.708	-41.80	53.03	53.31
500	-1.164	-0.785	-53.27	41.56	41.84
600	-1.300	-0.846	-63.79	31.04	31.32
800	-1.511	-0.947	-79.37	15.45	15.73
1000	-1.652	-1.039	-86.29	8.53	8.81
1500	-1.904	-1.267	-90.19	4.64	4.92
2000	-2.142	-1.489	-91.87	2.96	3.24
2500	-2.377	-1.712	-93.45	1.37	1.65
3000	-2.602	-1.928	-94.85	0.0	0.28
3500	-2.814	-2.136	-95.34	-0.52	0.24
4000	-3.024	-2.347	-95.26	-0.43	0.15
4500	-3.243	-2.566	-95.13	-0.31	0.03
4710 (DCL*)	-3.343	-2.667	-95.10	-0.28	0.0

Note: Although  $D$  is called "height" and is quoted in units of "dynamic meters," it has physical dimensions of energy per unit mass as it represents work done against gravity.

Distance between the two stations = 78.0 km; latitude = 38.65°N.

The SI units for  $D$  are  $J/kg = m^2/s^2$ .

**S7.3).** If our best estimate of a reference velocity is 0 cm/sec at the bottom (deepest common level; DCL), then we offset the velocities by the value at the bottom (column 6 in [Table S7.3](#)). If we have measured the bottom current to be 5 cm/sec, then we add an offset to the complete velocity profile so as to yield 5 cm/sec at the bottom.

The DCL is the maximum depth at which geostrophic velocity can be calculated for this particular station pair, since the shallower of the two stations extends to 4710 dbar (the deeper of the pair extends to 4810 dbar). Especially for transport calculations in which the bottom current is of interest, the geostrophic velocity below the DCL is needed, but there is

only one density profile available. There are a variety of ways to assign velocity to this “bottom triangle,” including (1) no assignment, (2) assignment of velocity at the DCL, (3) extrapolation of velocity profile from above the DCL, (4) extrapolation of the velocity horizontally from the next station pair if there is one, or (5) objective mapping of the velocity field into the triangle. The last is the best way, but an objective mapping scheme might not be readily available.

### 7.6.3. Dynamic Topography and Sea-Surface Height Maps

Dynamic height at one surface relative to another is the streamfunction for the geostrophic flow at that surface relative to the other, as an extension of Eq. (7.23f). Flows are along the contours with the high “hills” to the right of the flow in the Northern Hemisphere (to the left in the Southern Hemisphere). The speed at any point is proportional to the steepness of the slope at that point; in other words, it is inversely proportional to the separation of the contours.

*Dynamic topography* maps (equivalently, steric height or sea-surface height) are shown in Chapter 14 and throughout the ocean basin chapters (9–13) to depict the geostrophic flow field. As an illustration of the common features for all basins, we show here dynamic topography maps for the Pacific and Atlantic Oceans (Figures S7.21 and S7.22). These were the first modern basin-wide maps in common use and thus have some historical interest; both show dynamic height relative to a deep level of no motion. For comparison, Figures 9.2a and 10.2a are the surface steric height maps from Reid (1994, 1997) that we use to illustrate circulation in the Pacific and Atlantic Ocean chapters. The steric height in these maps has been adjusted to represent the full flow, hence incorporating estimates of deep geostrophic velocities at all station pairs.

At the sea surface, all five ocean basins have highest dynamic topography in the west in the subtropics. The anticyclonic flows around these highs are called the *subtropical gyres*. The Northern Hemisphere oceans have low dynamic topography around 50–60°N; the cyclonic flows around these lows are the *subpolar gyres*. Tightly spaced contours along the western boundaries indicate the swift western boundary currents for each of the gyres. Low values are found all the way around Antarctica; the band of tightly spaced contours to its north marks the eastward ACC. The contrast in dynamic height and sea-surface height from high to low in a given gyre is about 0.5 to 1 dynamic meters.

In the subtropical gyres in Figures S7.21 and S7.22, close contour spacings, hence large geostrophic velocities, are found at the western boundaries. These include the energetic subtropical western boundary currents just east of Japan (Kuroshio), east of North America (Gulf Stream), east of Australia (East Australian Current), east of Brazil (Brazil Current), and east of southern Africa (Agulhas Current).

The similarity between the two Pacific surface maps (and the two Atlantic surface maps) indicates that indeed the flow at 1000 dbar (700 dbar) is relatively weak. The additional advantage of the Reid (1994, 1997) analyses is that he also produced maps of absolute dynamic topography at 1000 dbar, and at 500 dbar intervals to the ocean bottom, whereas the simple dynamic topography method assuming a level of no motion clearly does not yield a reasonable flow field at these depths.

### 7.6.4. A Two-Layer Ocean

It is frequently convenient to think of the ocean as composed of two layers in the vertical, with upper layer of density  $\rho_1$  and lower layer of density  $\rho_2$  (Figure S7.23). The lower layer is assumed to be infinitely deep. The upper layer

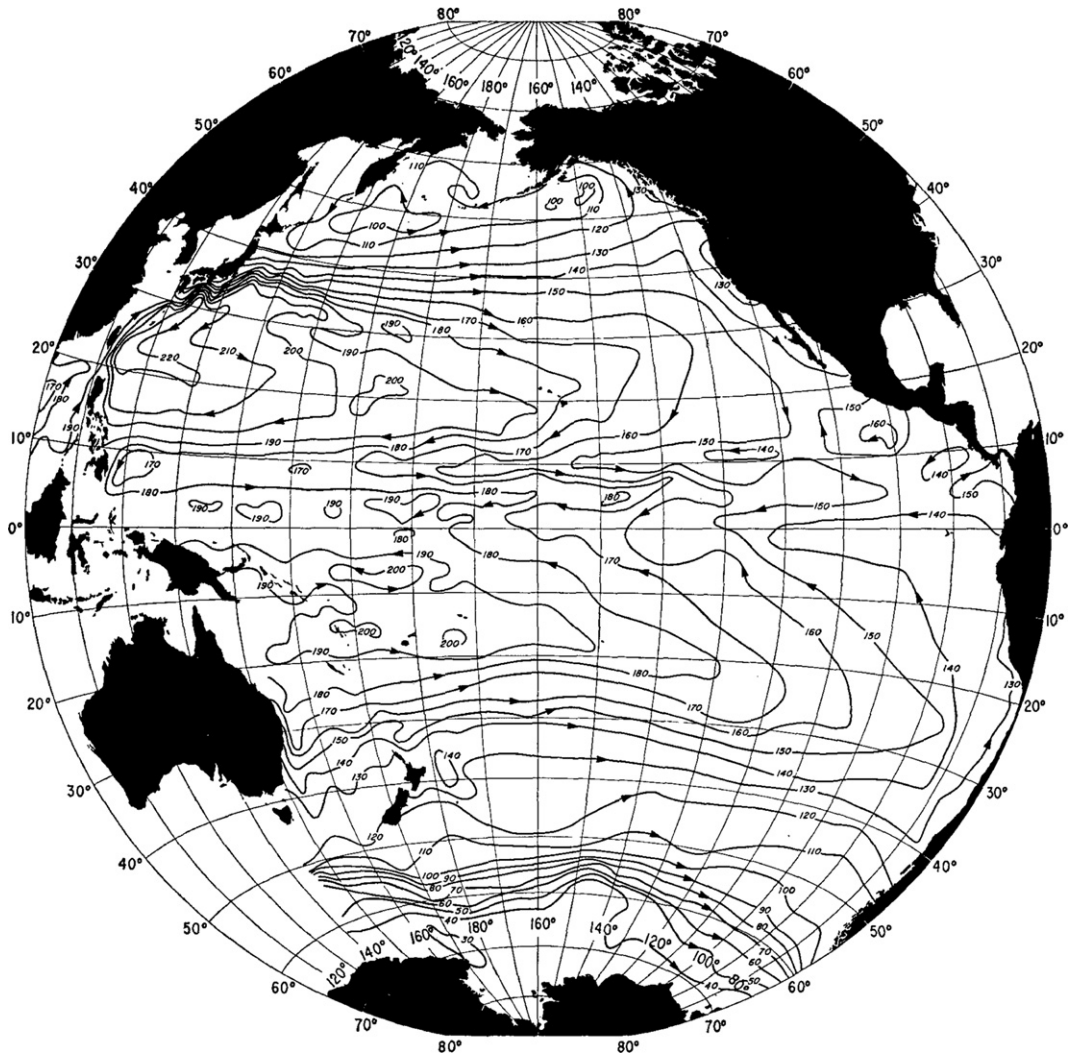


FIGURE S7.21 Mean annual dynamic topography of the Pacific Ocean sea surface relative to 1000 dbar in dyn cm ( $\Delta D = 0/1000$  dbar). Source: From Wyrki (1975).

thickness is  $h + H$ , where  $h$  is the varying height of the layer above the sea level surface and  $H$  is the varying depth of the bottom of the layer. We sample the layers with stations at "A" and "B." Using the hydrostatic equation (7.23c), we compute the pressure at a depth  $Z$  at the stations:

$$P_A = \rho_1 g(h_A + H_A) + \rho_2 g(Z - H_A) \quad (7.30a)$$

$$P_B = \rho_1 g(h_B + H_B) + \rho_2 g(Z - H_B). \quad (7.30b)$$

Here  $Z$  represents a common depth for both stations, taken well below the interface. If we

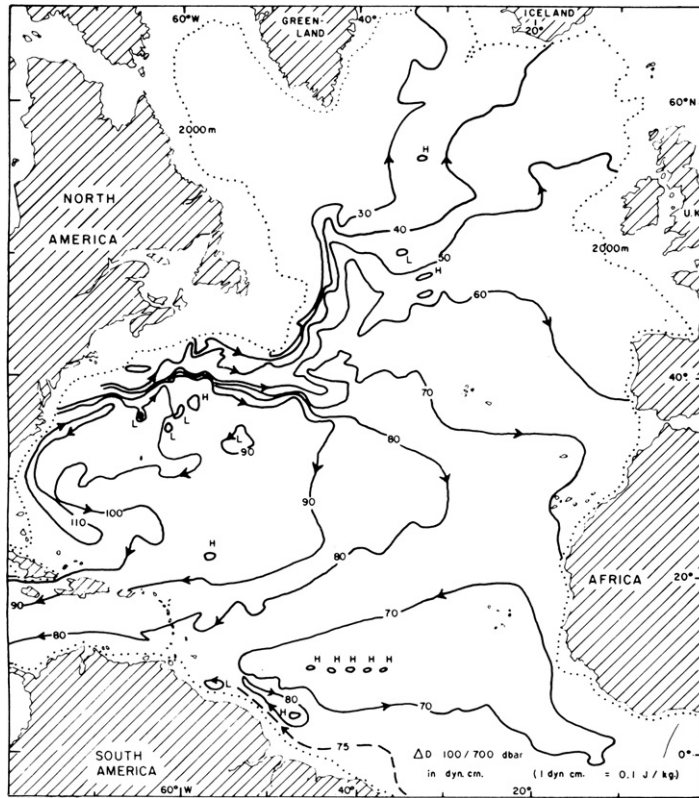


FIGURE S7.22 Dynamic topography of 100 dbar surface relative to 700 dbar surface ( $\Delta D = 100/700$  dbar) in dyn cm in the Atlantic Ocean. Source: From Stommel, Niiler, and Anati (1978).

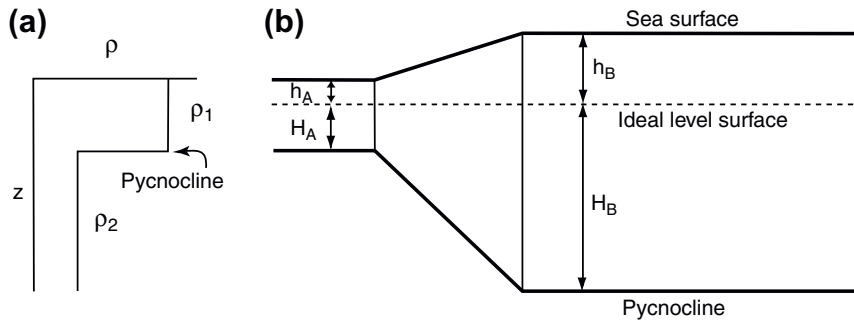
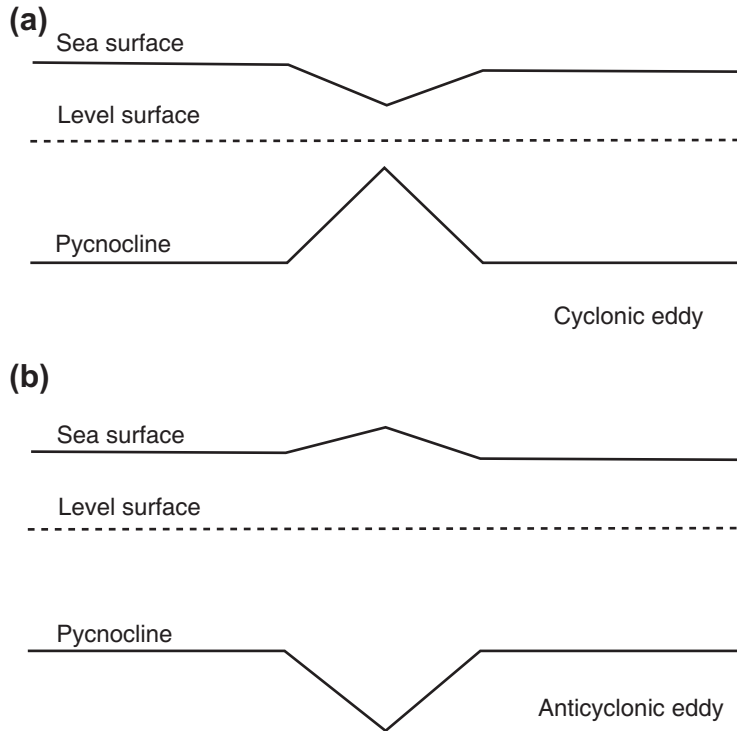


FIGURE S7.23 The two-layer ocean. (a) Vertical density profile with upper and lower layers of density  $\rho_1$  and  $\rho_2$ . (b) Sea surface and pycnocline for two stations, A and B, where the thickness of the layer above the “ideal level surface” is  $h_A$  and  $h_B$  and the thickness of the layer below the level surface is  $H_A$  and  $H_B$ , respectively. Both  $h$  and  $H$  are part of the “upper” layer shown in (a).

**FIGURE S7.24** Two-layer ocean depiction of a (a) “cold,” cyclonic ocean circulation showing the “ideal” sea surface and the subsurface thermocline structure and a (b) “warm” anticyclonic circulation.



assume that  $p_A = p_B$ , which amounts to assuming a “level of no motion” at  $Z$ , we can compute a surface slope, which we cannot measure in terms of the observed density interface slope:

$$\frac{h_A - h_B}{\Delta x} = \frac{\rho_2 - \rho_1}{\rho_1} \frac{H_A - H_B}{\Delta x} \quad (7.31a)$$

We then use Eq. (7.30a) to estimate the surface velocity  $v$ :

$$fv = g \frac{h_A - h_B}{\Delta x} = g \frac{\rho_2 - \rho_1}{\rho_1} \frac{H_A - H_B}{\Delta x} \quad (7.31b)$$

This says that we can estimate the slope of the sea surface ( $h_A - h_B$ ) from knowledge of the subsurface slope of the density interface ( $H_A - H_B$ ), which then allows us to estimate the surface flow velocity from the shape of the pycnocline.

This simple construct is also useful in depicting various forms of geostrophic circulation

features. For example, a cyclonic feature in either hemisphere is drawn in Figure S7.24a where the subsurface pycnocline slope is much greater than the surface topographic change. These cyclonic features are also known as cold features due to the upwelling of the central isopycnals in the center of the feature. This is true even if the feature is not a closed circulation. Likewise a warm feature looks like Figure S7.24b regardless of hemisphere. What will change with the hemisphere is the direction of the flow where a warm feature rotates anticyclonically (clockwise in the Northern Hemisphere) and a cold feature is cyclonic (counterclockwise). The two-layer depiction of the ocean is convenient for quickly evaluating new measurements in terms of the corresponding geostrophic currents. Note that the two-layer assumption results in a mapping of only geostrophic currents and not the entire current field.

## 7.7. VORTICITY, POTENTIAL VORTICITY, ROSSBY AND KELVIN WAVES, AND INSTABILITIES

Ocean currents are mostly geostrophic. This means that the equation for velocity includes only the pressure gradient force and Coriolis force. This poses an apparent problem: How do we insert external forces such as the wind? In formal geophysical fluid dynamics, we would show that these forces *are* in the momentum equations, but are so weak that we safely consider the flows to be geostrophic (to lowest order). To reinsert the external forces, we have to consider the “vorticity” equation, which is formally derived from the momentum equations by combining the equations in a way that eliminates the pressure gradient force terms. (It is straightforward to do.) The resulting equation gives the time change of the vorticity, rather than the velocities. It also includes dissipation, variation in Coriolis parameter with latitude, and vertical velocities, which can be set externally by Ekman pumping.

### 7.7.1. Vorticity

Vorticity in fluids is similar to angular momentum in solids, and many of the intuitions

developed about angular momentum from a standard physics course can be applied to understanding vorticity.

Vorticity is twice the angular velocity at a point in a fluid. It is easiest to visualize by thinking of a small paddle wheel immersed in the fluid (Figure S7.25). If the fluid flow turns the paddle wheel, then it has vorticity. Vorticity is a vector, and points out of the plane in which the fluid turns. The *sign* of the vorticity is given by the “right-hand” rule. If you curl the fingers on your right hand in the direction of the turning paddle wheel and your thumb points upward, then the vorticity is positive. If your thumb points downward, the vorticity is negative.

Vorticity is exactly related to the concept of curl in vector calculus. The vorticity vector  $\boldsymbol{\omega}$  is the curl of the velocity vector  $\mathbf{v}$ , expressed here — in Cartesian coordinates:

$$\begin{aligned}\boldsymbol{\omega} &= \nabla \times \mathbf{v} \\ &= \mathbf{i}(\partial v/\partial z - \partial w/\partial y) + \mathbf{j}(\partial w/\partial x - \partial u/\partial z) \\ &\quad + \mathbf{k}(\partial v/\partial x - \partial u/\partial y)\end{aligned}\tag{7.32}$$

where  $(\mathbf{i}, \mathbf{j}, \mathbf{k})$  is the unit vector in Cartesian coordinates  $(x, y, z)$  with corresponding velocity components  $(u, v, w)$ . Vorticity, therefore, has units of inverse time, for instance,  $(\text{sec})^{-1}$ .

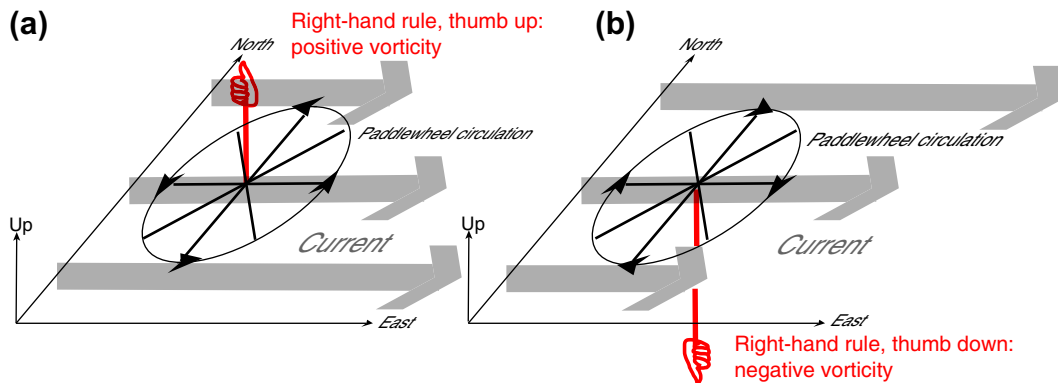


FIGURE S7.25 Vorticity. (a) Positive and (b) negative vorticity. The right-hand rule shows the direction of the vorticity by the direction of the thumb (upward for positive, downward for negative).

Fluids (and all objects) have vorticity simply because of Earth's rotation. This is called *planetary vorticity*. We do not normally appreciate this component of vorticity since it is only important if a motion lasts for a significant portion of a day, and most important if it lasts for many days, months, or years. Since geostrophic motion is essentially steady compared with the rotation time of Earth, planetary vorticity is very important for nearly geostrophic flows. The vector planetary vorticity points upward, parallel to the rotation axis of Earth. Its size is twice the angular rotation rate  $\Omega$  of Earth:

$$\omega_{\text{planetary}} = 2\Omega \quad (7.33)$$

where  $\Omega = 2\pi/\text{day} = 2\pi/86160 \text{ sec} = 7.293 \times 10^{-5} \text{ sec}^{-1}$ , so  $\omega_{\text{planetary}} = 1.4586 \times 10^{-4} \text{ sec}^{-1}$ .

The vorticity of the fluid motion relative to Earth's surface (Eq. 7.32) is called the *relative vorticity*. It is calculated from the water velocities relative to Earth's surface (which is rotating). The total vorticity of a piece of fluid is the sum of the relative vorticity and planetary vorticity. The total vorticity is sometimes called absolute vorticity, because it is the vorticity the fluid has in the non-rotating reference frame of the stars.

For large-scale oceanography, only the local vertical component of the total vorticity is used because the fluid layers are thin compared with Earth's radius, so flows are nearly horizontal. The local vertical component of the planetary vorticity is exactly equal to the Coriolis parameter  $f$  (Eq. 7.8c) and is therefore maximum and positive at the North Pole ( $\varphi = 90^\circ\text{N}$ ), maximum and negative at the South Pole ( $\varphi = 90^\circ\text{S}$ ), and 0 at the equator.

The local vertical component of the relative vorticity from Eq. (7.32) is

$$\zeta = \left( \frac{\partial v}{\partial x} - \frac{\partial u}{\partial y} \right) = \text{curl}_z \mathbf{v} \quad (7.34)$$

The local vertical component of the absolute vorticity is therefore  $(\zeta + f)$ . The geostrophic

velocities calculated from Eq. (7.23) (Section 7.6) are often used to calculate relative vorticity.

### 7.7.2. Potential Vorticity

*Potential vorticity* is a dynamically important quantity related to relative and planetary vorticity. Conservation of potential vorticity is one of the most important concepts in fluid dynamics, just as conservation of angular momentum is a central concept in solid body mechanics. Potential vorticity takes into account the height  $H$  of a water column as well as its local spin (vorticity). If a column is shortened and flattened (preserving mass), then it must spin more slowly. On the other hand, if a column is stretched and thinned (preserving mass), it should spin more quickly similar to a spinning ice skater or diver who spreads his or her arms out and spins more slowly (due to conservation of angular momentum). Potential vorticity, when considering only the local vertical components, is

$$Q = (\zeta + f)/H \quad (7.35)$$

where  $H$  is the thickness, if the fluid is unstratified. When the fluid is stratified, the equivalent version of potential vorticity is

$$Q = -(\zeta + f)(1/\rho)(\partial\rho/\partial z). \quad (7.36)$$

When there are no forces (other than gravity) on the fluid and no buoyancy sources that can change density, potential vorticity  $Q$  is conserved:

$$DQ/Dt = 0 \quad (7.37)$$

where "D/Dt" is the substantial derivative (Eq. 7.4). This means that a water parcel keeps the value of  $Q$  that it obtains wherever a force acts on it. For instance, parcels of water leaving the ocean surface layer, where they are subject to wind forcing, which changes their potential vorticity, keep the same value of potential

vorticity after they enter the ocean interior where forces (primarily friction) are much weaker.

Considering the potential vorticity (Eq. 7.35), there are three quantities that can change: relative vorticity  $\zeta$ , the Coriolis parameter  $f$ , and the thickness  $H$  (or equivalent thickness  $-(1/\rho)(\partial\rho/\partial z)$  in Eq. 7.36). The variation in  $f$  with latitude has huge consequences for ocean currents and stratification. Therefore, a special symbol  $\beta$  is introduced to denote the change in  $f$  with northward distance  $y$ , or in terms of latitude  $\phi$  and Earth's radius  $R_e$ :

$$\beta = df/dy = 2\Omega \cos \Phi/R_e \quad (7.38)$$

We often refer to the “ $\beta$ -effect” when talking about how changes in latitude affect currents, or the very large-scale, mainly horizontal Rossby waves for which the  $\beta$ -effect is the restoring force, described in Section 7.7.3.

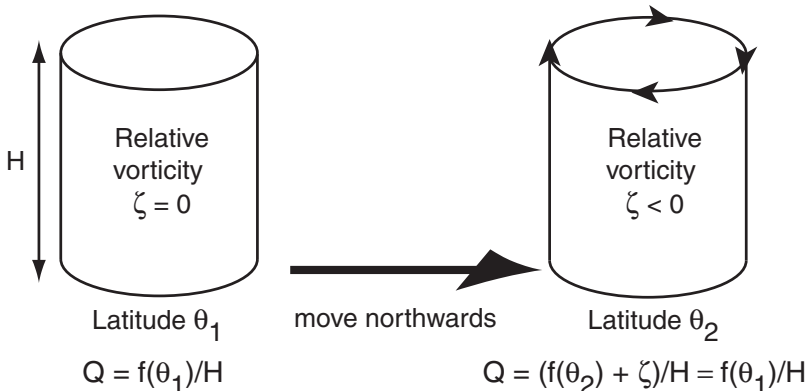
All three components of potential vorticity can change together, but we learn more about what happens if we consider just two at a time.

First we consider changes in relative vorticity  $\zeta$  and Coriolis parameter  $f$ , holding thickness  $H$  constant (Figure S7.26). When a water parcel is moved northward, it experiences an increase in  $f$ . Its relative vorticity  $\zeta$  must then decrease to

keep the numerator of Eq. (7.35) constant. If  $\zeta$  is zero to start with,  $\zeta$  will become negative and the water parcel will rotate clockwise. If the parcel is moved southward,  $f$  decreases and its relative vorticity will have to become more positive; the parcel will rotate counterclockwise.

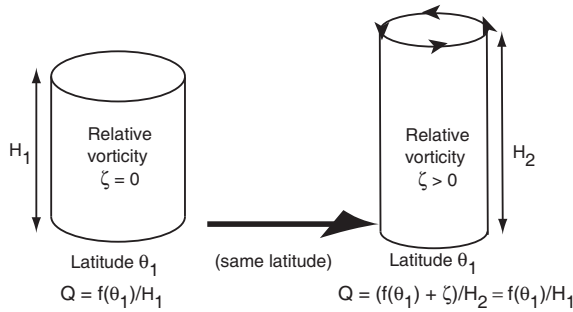
Secondly, we consider changes in relative vorticity  $\zeta$  and thickness  $H$ , holding the latitude and hence  $f$  constant (Figure S7.27). (This would be appropriate for mesoscale eddies with high relative vorticity that do not move far from their initial latitude, Arctic dynamics, or for flows in rotating laboratory tanks.) An increase in thickness  $H$  (“stretching”) must result then in an increase in relative vorticity, and the water parcel will rotate more in the counterclockwise direction. A decrease in thickness (“squashing”) results in a decrease in relative vorticity, and the water parcel will rotate more in the clockwise direction.

Thirdly, if the thickness  $H$  is allowed to vary, and if the relative vorticity is very small (such as in the very weak currents in the mid-ocean), then a northward move that increases  $f$  must result in column stretching (Figure S7.28). Similarly, a southward move would cause  $H$  to decrease or squash. (Since neither thickness



Conservation of potential vorticity  $Q$  in the absence of stretching (northern hemisphere):  
balance of planetary vorticity and relative vorticity

FIGURE S7.26 Conservation of potential vorticity: changes in relative vorticity and Coriolis parameter  $f$ , if thickness is constant.



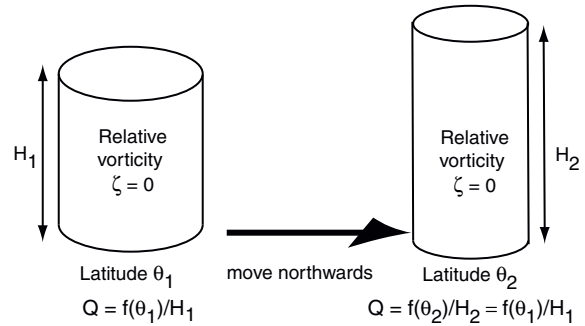
Conservation of potential vorticity  $Q$  in the absence of planetary vorticity change (northern hemisphere): balance of relative vorticity and stretching

**FIGURE S7.27** Conservation of potential vorticity: changes in thickness and relative vorticity, assuming constant latitude (constant  $f$ ).

nor relative vorticity can change without limit, there is an inherent restoring force to northward and southward movements in the ocean and atmosphere. This restoring force creates Rossby waves.)

In the Southern Hemisphere,  $f$  is negative. A southward move of a water column makes  $f$  even more negative, and requires stretching (increase in  $H$ ). A northward move makes  $f$  less negative, and requires squashing (decrease in  $H$ ). Therefore, looking at both hemispheres, we can say that poleward motion, toward larger magnitude  $f$ , requires stretching. Equatorward motion requires squashing.

The equator is a special place in terms of potential vorticity, since  $f$  changes from negative to positive crossing the equator and is zero on the equator. Any water parcels moving into the equatorial region must become more dominated by relative vorticity, as in Figure S7.28. We see this in the much stronger horizontal current shears near the equator than at higher latitudes. (Geostrophy also breaks down right on the equator; slightly off the equator, small pressure gradients result in large geostrophic currents, so we also see high velocities in the equatorial region compared with other latitudes.)



Conservation of potential vorticity  $Q$  in the absence of relative vorticity (northern hemisphere): balance of planetary vorticity and stretching

**FIGURE S7.28** Conservation of potential vorticity: changes in thickness and latitude (Coriolis parameter  $f$ ), assuming negligible relative vorticity (Northern Hemisphere).

### 7.7.3. Rossby Waves

The adjustment of any fluid to a change in forcing takes the form of waves that move out and leave behind a steady flow associated with the new forcing. We describe some general properties of waves in Chapter 8. The large-scale, almost geostrophic circulation adjusts to changing winds and buoyancy forcing mainly through “planetary” or *Rossby waves* and *Kelvin waves* (Section 7.7.6). Pure Rossby and Kelvin waves are never found except in simplified models and lab experiments. However, much of the ocean’s variability can be understood in terms of Rossby wave properties, particularly the tendency for westward propagation relative to the mean flow. We describe these waves without derivations, which can be found in the many geophysical fluid dynamics textbooks referenced at the start of this chapter.

A first important fact is that Rossby waves have wavelengths of tens to thousands of kilometers. Since the ocean is only 5 to 10 km deep and is stratified, particle motions in Rossby waves are almost completely transverse (horizontal, parallel to the surface of Earth), which

differs from intuition that we build from watching surface gravity waves.

Second, the restoring force for Rossby waves is the variation in Coriolis parameter  $f$  with latitude, so all dispersion information includes  $\beta$  (Eq. 7.38). As a water column is shoved off to a new latitude, its potential vorticity must be conserved (Eq. 7.35). As with all waves, the column overshoots, and then has to be restored again, creating the wave. Therefore the water column height or relative vorticity begin to change. These cannot change indefinitely without external forcing, so the water column is restored back toward its original latitude. As with all waves, the column overshoots, and then has to be restored back again, creating the wave. For a short wavelength Rossby wave, the relative vorticity changes in response to the change in Coriolis parameter  $f$  as in Figure S7.26 — for a parcel moving northward to higher  $f$ , the relative vorticity becomes negative. This pushes columns to the east of the parcel toward the south and pulls columns to the west of parcel toward the north. The net effect

is a westward propagation of the wave. For a long wavelength Rossby wave (Figure S7.29) the column height changes in response to the change in  $f$ , as in Figure S7.28. For northward motion of the parcel, height increases; the downward slope in height to the east causes southward geostrophic flow on that side while the downward slope in height to the west of the perturbation causes northward geostrophic flow on the west. The net effect again is westward propagation of the disturbance.

Third, Rossby wave crests and troughs move only westward (relative to any mean flow, which could advect them to the east) in both the Northern and Southern Hemispheres; that is, the phase velocity is westward (plus a northward or southward component). On the other hand, the group velocity of Rossby waves can be either westward or eastward. The group velocity of Rossby waves is westward for long wavelengths (more than about 50 km) and eastward for short wavelengths (even though the zonal phase velocity is westward).

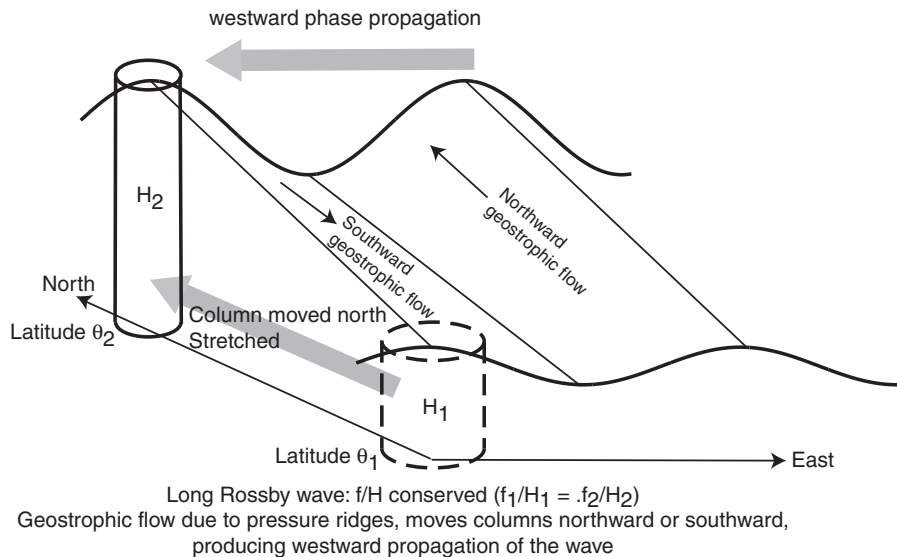


FIGURE S7.29 Schematic of a long wavelength Rossby wave.

Fourth, velocities in Rossby waves are almost geostrophic. Therefore, they can be calculated from variations in pressure; for instance, as measured by a satellite altimeter, which observes the sea-surface height. Behavior similar to a Rossby wave (westward phase propagation) can be seen at almost all latitudes in each of the subtropical oceans in the satellite altimetry images in Figures 14.18 and 14.19.

Although pure Rossby waves do not occur, many variable flows such as eddies or meanders of currents like the Gulf Stream Extension or AAC can be interpreted in terms of Rossby wave properties, in the sense that Rossby waves are the basic set of linear wave solutions for flows with a small Rossby number and small aspect ratio. If the mean flows are removed from observed variability, the variability often appears to move westward. The atmosphere has the same Rossby-wave-like phenomena, such as those seen in daily weather maps showing large loops or meanders in the Jet Stream (Figure S7.18).

#### 7.7.4. Rossby Deformation Radius and Rossby Wave Dispersion Relation

Turning slightly more analytical, we introduce, again without derivation, the Rossby deformation radius and the dispersion relation for Rossby waves with simple stratification.

The length scale that separates long from short wavelength Rossby waves is called the *Rossby deformation radius*. It is the intrinsic horizontal length scale for geostrophic or nearly geostrophic flows, relative to which all length scales are compared. The Rossby radius characterizes the observed mesoscale (eddy) length scales and also the spatial decay scale of boundary-trapped waves such as Kelvin waves (Section 7.7.6) and the latitudinal width of equatorially trapped waves.

The Rossby deformation radius in an unstratified ocean is

$$R_E = (gH)^{1/2}/f \quad (7.39a)$$

where  $H$  is the ocean depth scale.  $R_E$  is called the *barotropic Rossby deformation radius* or “external” deformation radius. Barotropic deformation radii are on the order of thousands of kilometers. In an unstratified ocean, the horizontal velocities for geostrophic flows are the same (in magnitude and direction) from the top of the ocean to the bottom. In the more realistic stratified ocean, there is a similar “barotropic mode,” with velocities in the same direction at all depths, and with a barotropic Rossby deformation radius also given by Eq. (7.39a).

The Rossby deformation radius associated with the ocean’s stratification is

$$R_I = NH_s/f \quad (7.39b)$$

where  $N$  is the Brunt-Väisälä frequency (Eq. 7.14), and  $H_s$  is an intrinsic scale height for the flow.  $R_I$  is called the *baroclinic deformation radius* (or “internal” deformation radius). “Baroclinic” means that the velocity structure changes within the water column, associated with isopycnal slopes. The first baroclinic mode has a single velocity reversal within the water column. The vertical length scale  $H_s$  associated with the first baroclinic mode is about 1000 m, which is the typical pycnocline depth. (The second baroclinic mode has two velocity reversals and hence a shorter vertical length scale, and so on for the higher modes.) The vertical length scale  $H_s$  associated with the first baroclinic mode is about 1000 m, which is the typical pycnocline depth.  $R_I$  for the first baroclinic mode varies from more than 200 km in the tropics to around 10 km at high latitudes (Figure S7.30a; Chelton et al., 1998).

The dispersion relation (Section 8.2) for first mode baroclinic Rossby waves is

$$\omega = \frac{-\beta k}{k^2 + l^2 + (1/R_I)^2} \quad (7.40)$$

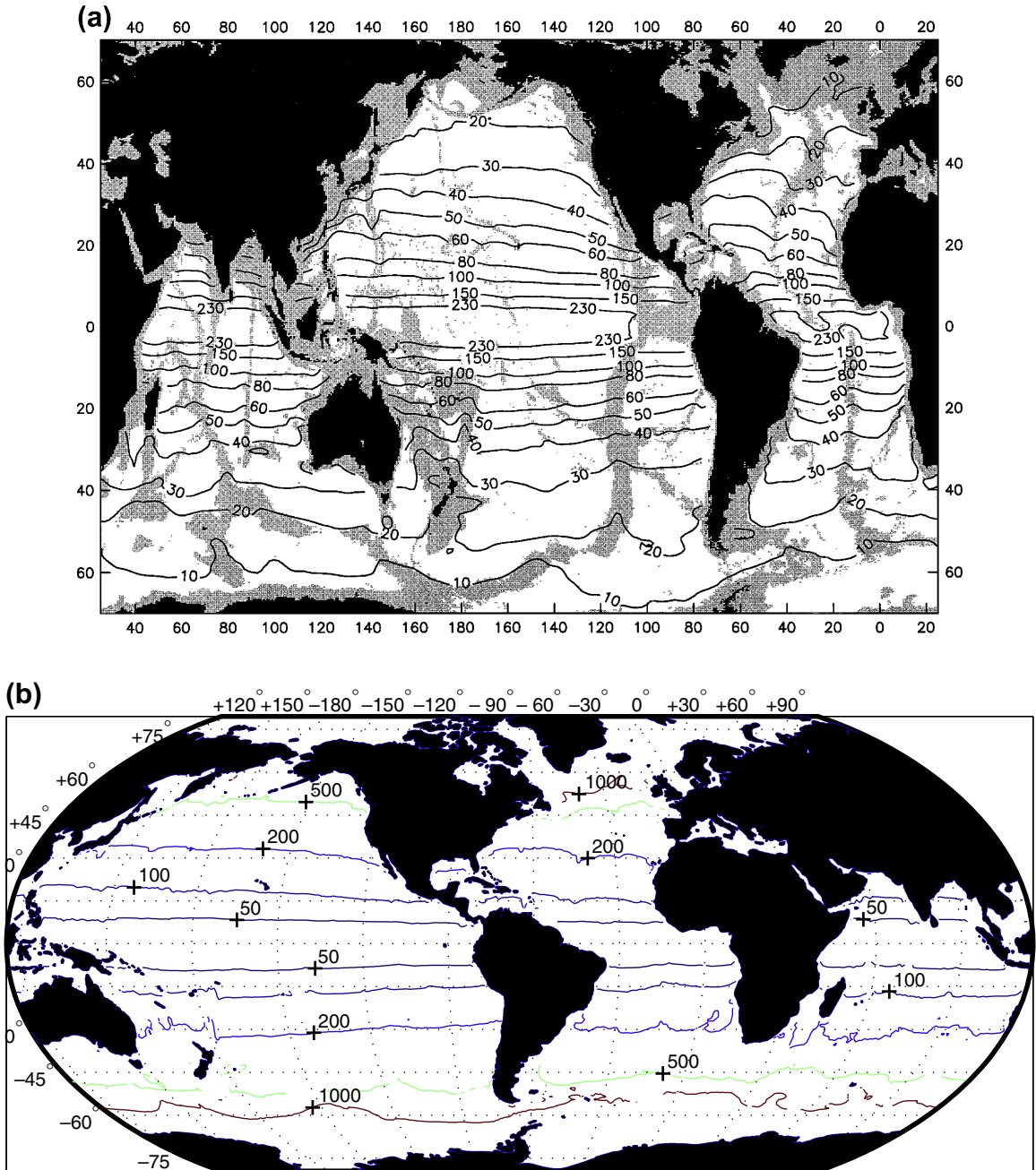


FIGURE S7.30 (a) Rossby deformation radius (km) for the first baroclinic mode. Source: From Chelton *et al.* (1998). (b) Shortest period (in days) for the first baroclinic mode, based on the deformation radius in (a). Note that the annual cycle, at 365 days, occurs around latitudes 40 to 45 degrees; poleward of this, all such waves are slower. Source: From Wunsch (2009).

where  $\omega$  is the wave frequency,  $k$  and  $l$  are the wavenumbers in the east-west ( $x$ ) and north-south ( $y$ ) directions,  $\beta$  is as in Eq. (7.38), and  $R_l$  is as given in Eq. (7.39b). Highest frequency (shortest period) occurs at the wavelength associated with the Rossby deformation radius (Figure S7.31). The shortest periods vary from less than 50 days in the tropics to more than 2 to 3 years at high latitudes (Figure S7.30b from Wunsch, 2009). Poleward of about 40 to 45 degrees latitude there is no first baroclinic mode at the annual cycle, so seasonal atmospheric forcing cannot force the first baroclinic mode at these higher latitudes. This results in a fundamentally different response to atmospheric variability at higher latitudes than in the tropics and at mid-latitudes.

In much of the ocean away from the equator, the barotropic and first baroclinic modes dominate the variability, and hence the space and timescales of the eddy field. At the equator, a much larger set of baroclinic modes is typically observed, resulting in much more complex vertical velocity structure than at higher latitudes. Equatorial Rossby waves are slightly different from non-equatorial Rossby waves since geostrophy does not hold at the equator, but the vertical structures and behavior are similar, with the restoring force for the equatorial Rossby waves the same as at mid-latitude — the change in Coriolis parameter with latitude.

### 7.7.5. Instability of Geostrophic Ocean Currents

Almost all water flows are unsteady. When gyre-scale flows break up, they do so into large eddies, on the order of tens to hundreds of kilometers in diameter or larger (see Section 14.5). The size of the eddies is often approximately the Rossby deformation radius. The eddies usually move westward, like Rossby waves.

Instabilities of flows are often studied by considering a mean flow and then finding the small perturbations that can grow exponentially. This

approach is called “linear stability theory”; it is linear because the perturbation is always assumed to be small relative to the mean flow, which hardly changes at all. When perturbations are allowed to grow to maturity, when they might be interacting with each other and affecting the mean flow, the study has become nonlinear.

We define three states: *stable*, *neutrally stable*, and *unstable*. A stable flow returns to its original state after it is perturbed. A neutrally stable flow remains as is. In an unstable flow, the perturbation grows.

The two sources of energy for instabilities are the *kinetic energy* and the *potential energy* of the mean flow. Recall from basic physics that kinetic energy is  $\frac{1}{2}mv^2$  where  $m$  is mass and  $v$  is speed; for a fluid we replace the mass with density  $\rho$ , or just look at the quantity  $\frac{1}{2}v^2$ . Also recall from basic physics that potential energy comes from raising an object to a height; the work done in raising the object gives it its potential energy. In a stratified fluid like the ocean, there is no *available potential energy* if isopycnals are flat, which means that nothing can be released. For there to be usable or available potential energy, isopycnals must be tilted.

*Barotropic instabilities* feed on the kinetic energy in the horizontal shear of the flow. For instance, the Gulf Stream and similar strong currents are jet-like, with large horizontal shear. Their speeds exceed 100 cm/sec in the center of the jet and decay to 0 cm/sec over about 50 km on either side of the jet. Such currents also have large kinetic energy because of their high speeds. The kinetic energy can be released if special conditions on the potential vorticity structure of the current are met. These conditions are that the horizontal shear be “large enough” compared with a restoring  $\beta$ -effect (Eq. 7.38), which creates Rossby waves in the absence of sheared flow (previous subsection). Barotropic instabilities can be thought of as the (unstable) waves that occur in the presence of a horizontally sheared current and possibly

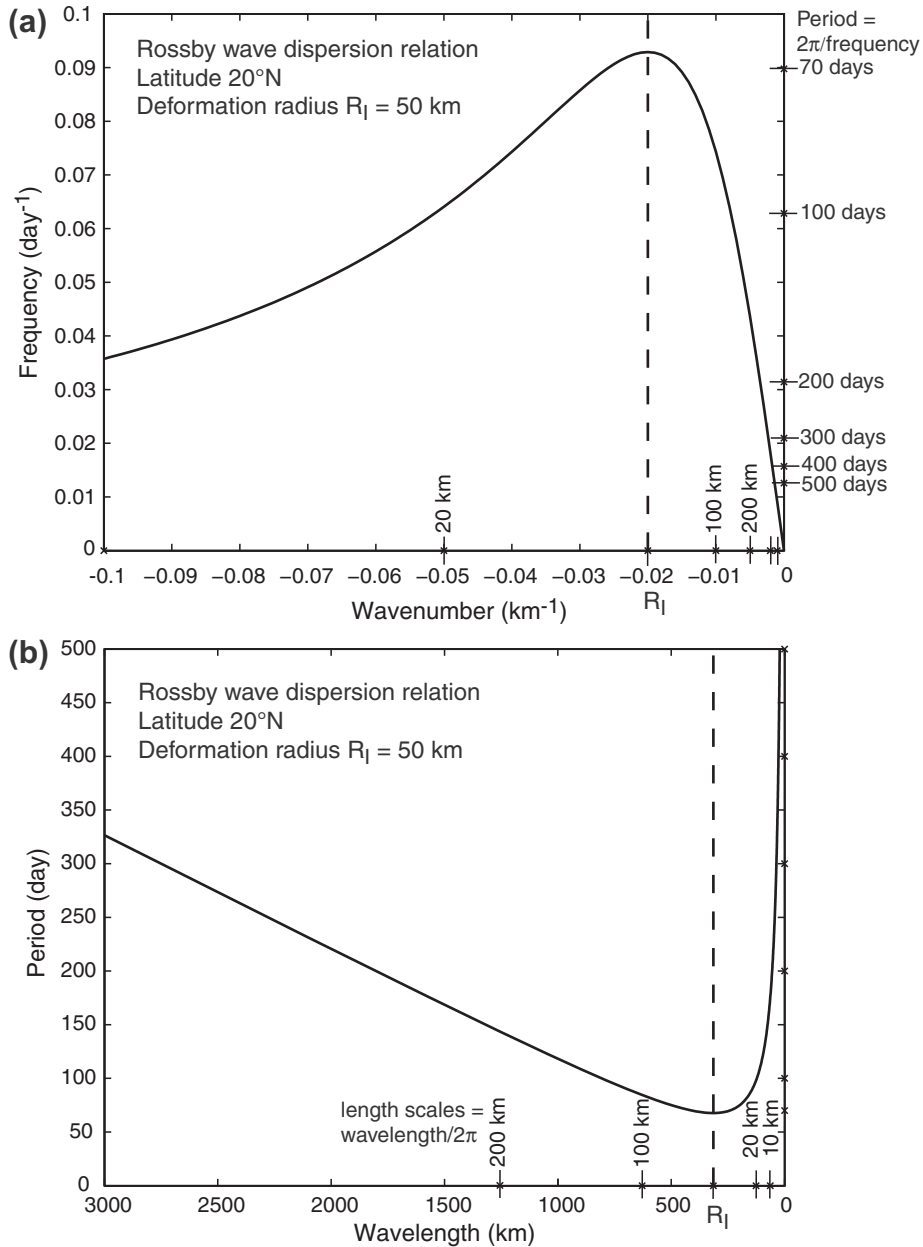


**FIGURE S7.31** Dispersion relation for first mode baroclinic Rossby waves (Eq. 7.40), assuming a deformation radius  $R_1$  of 50 km, latitude 20 degrees (north or south) and  $y$ -wavenumber  $l = 0$ . (a) Frequency  $\omega$  versus  $x$ -wavenumber  $k$  and (b) period versus wavelength. The Rossby radius is shown with the dashed line. The highest frequency and shortest period are at the Rossby radius length scale.

also the  $\beta$ -effect; see Pedlosky (1987). The net effect of the barotropic instability is to reduce the size of the horizontal shear. For the Gulf Stream, for instance, this results in decreasing the maximum speed at the core of the jet, and inducing flows in the opposite direction on the outskirts of the jet. These flows look like “recirculations” (Section 9.3.2).

*Baroclinic instabilities* draw on the available potential energy of the flow. The relatively recent study of sub-mesoscale eddies and instabilities generated in the ocean’s mixed layer is essentially that of baroclinic instability operating on density fronts within the mixed layer (Boccaletti et al., 2007). The fronts are strongly tilted isopycnals, which are then subject to this kind of potential energy release.

Baroclinic instability is peculiar to geostrophic flows, because Earth’s rotation makes it possible to have a mean geostrophic flow with mean tilted isopycnals. On the other hand, barotropic instability is similar to instabilities of all sheared flows including those without Earth’s rotation.

### 7.7.6. Kelvin Waves

Coastlines and the equator can support a special type of hybrid wave called a “Kelvin wave,” which includes both gravity wave and Coriolis effects. Kelvin waves are “trapped” to the coastlines and trapped at the equator, which means that their amplitude is highest at the coast (or equator) and decays exponentially with offshore (or poleward) distance. Kelvin waves are of particular importance on eastern boundaries since they transfer information poleward from the equator. They are also central to how the equatorial ocean adjusts to changes in wind forcing, such as during an El Niño (Chapter 10).

Kelvin waves propagate with the coast to the right in the Northern Hemisphere and to the left in the Southern Hemisphere. At the equator, which acts like a boundary, Kelvin waves propagate only eastward. In their alongshore

direction of propagation, Kelvin waves behave just like surface gravity waves and obey the gravity wave dispersion relation (Section 8.3). However, unlike surface gravity waves, Kelvin waves can propagate in only one direction. Kelvin wave wavelengths are also very long, on the order of tens to thousands of kilometers, compared with the usual surface gravity waves at the beach. Although the wave propagation speed is high, it can take days to weeks to see the transition from a Kelvin wave crest to a Kelvin wave trough at a given observation point.

In the across-shore direction, Kelvin waves differ entirely from surface gravity waves. Their amplitude is largest at the coast. The offshore decay scale is the Rossby deformation radius (Section 7.7.4).

Lastly, Kelvin wave water velocities in the direction perpendicular to the coast are exactly zero. The water velocities are therefore exactly parallel to the coast. Moreover, the alongshore velocities are geostrophic, so they are associated with pressure differences (pressure gradient force) in the across-shore direction.

## 7.8. WIND-DRIVEN CIRCULATION: SVERDRUP BALANCE AND WESTERN BOUNDARY CURRENTS

The large-scale circulation in the ocean basins is asymmetric, with swift, narrow currents along the western boundaries, and much gentler flow within the vast interior, away from the side boundaries. This asymmetry is known as *westward intensification* of the circulation; it occurs in both the Northern and Southern Hemispheres and in the subtropical and subpolar gyres.

The Gulf Stream is the prototype of these western boundary currents, as the first that was extensively studied, and as the example for which theories of westward intensification were developed. In a book that summarizes

these theories, [Stommel \(1965\)](#) reviewed early knowledge of the Gulf Stream, dating back to the first explorations of the North Atlantic, and summarized theoretical attempts to understand it, dating back to the nineteenth century. When the subtropical gyre and Gulf Stream were finally modeled theoretically in the mid-twentieth century, the resulting theory was breathtakingly simple. The long delay in arriving at this theory was due to the similarity between the wind patterns above the subtropical North Atlantic and the circulation — both are high pressure systems — with anticyclonic flow (clockwise in the Northern Hemisphere). But the winds are clearly not westward intensified relative to the ocean boundaries.

The primary originators of the theories that provide our present understanding were Harald Sverdrup, Henry Stommel, Walter Munk, and Nicholas Fofonoff. [Sverdrup \(1947\)](#) first explained the mid-ocean vorticity balance, created by variations in Ekman transport, that creates what we now call the “Sverdrup interior” solution (Section 7.8.1). Just a few years earlier, [Sverdrup et al. \(1942\)](#) were still suggesting that the Ekman transport variations would simply pile water up in the central gyre, with a resulting geostrophic flow around the pile. [Stommel \(1948\)](#) and [Munk \(1950\)](#) provided the first (frictional) explanations for the western boundary currents (Section 7.8.2), and [Fofonoff \(1954\)](#) showed how very different the circulation would be without friction.

Most of the physical effects described in this section occur because the Coriolis parameter varies with latitude, that is, because of the  $\beta$ -effect (Eq. 7.38).

### 7.8.1. Sverdrup Balance

The gentle interior flow of the (non-equatorial) oceans can be described in terms of their meridional (north-south) direction. In the subtropical gyres, the interior flow is toward the equator in both the Northern and Southern

Hemispheres. In the subpolar gyres, the interior flow is poleward in both hemispheres. These interior flow directions can be understood through a potential vorticity argument introduced by [Sverdrup \(1947\)](#), so we call the applicable physics the “Sverdrup balance.”

Consider a schematic of the subtropical North Pacific ([Figure S7.32](#)). The winds at the sea surface are not spatially uniform ([Figure 5.16](#) and [Figure S10.2](#) in the online supplement). South of about  $30^\circ\text{N}$ , the Pacific is dominated by easterly trade winds. North of this, it is dominated by the westerlies. This causes northward Ekman transport under the trade winds, and southward Ekman transport under the westerlies. As a result, there is Ekman convergence throughout the subtropical North Pacific ([Figures 5.16d](#) and [S10.2](#)).

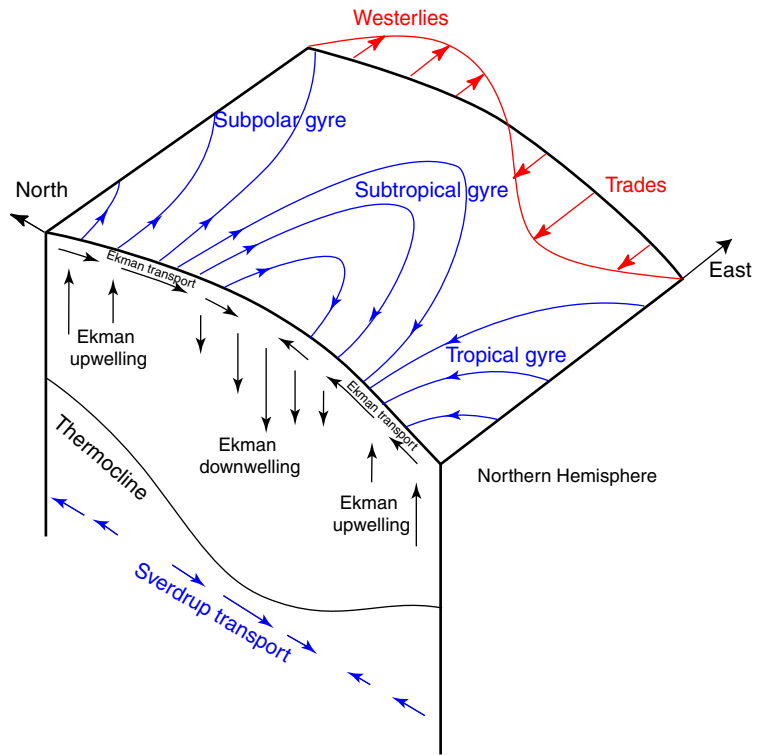
The convergent surface layer water in the subtropics must go somewhere so there is downward vertical velocity at the base of the (50 m thick) Ekman layer. At some level between the surface and ocean bottom, there is likely no vertical velocity. Therefore there is net “squashing” of the water columns in the subtropical region (also called *Ekman pumping*; Section 7.5.4).

This squashing requires a decrease in either planetary or relative vorticity (Eq. 7.35). In the ocean interior, relative vorticity is small, so planetary vorticity must decrease, which results in the equatorward flow that characterizes the subtropical gyre ([Figure S7.28](#)).

The subpolar North Pacific lies north of the westerly wind maximum at about  $40^\circ\text{N}$ . Ekman transport is therefore southward, with a maximum at about  $40^\circ\text{N}$  and weaker at higher latitudes. Therefore there must be upwelling (*Ekman suction*) throughout the wide latitude band of the subpolar gyre. This upwelling stretches the water columns (Eq. 7.35), which then move poleward, creating the poleward flow of the subpolar gyre.

The *Sverdrup transport* is the net meridional transport diagnosed in both the subtropical

**FIGURE S7.32** Sverdrup balance circulation (Northern Hemisphere). Westerly and trade winds force Ekman transport creating Ekman pumping and suction and hence Sverdrup transport.



and subpolar gyres, resulting from planetary vorticity changes that balance Ekman pumping or Ekman suction.

All of the meridional flow is returned in western boundary currents, for reasons described in the following sections. Therefore, subtropical gyres must be anticyclonic and subpolar gyres must be cyclonic.

Mathematically, the Sverdrup balance is derived from the geostrophic equations of motion with variable Coriolis parameter  $f$  (Eq. 7.23a,b). The  $x$ - and  $y$ -momentum equations are combined to form the vorticity equation, recalling that  $\beta = df/dy$ :

$$f(\partial u/\partial x + \partial v/\partial y) + \beta v = 0 \quad (7.41)$$

Using the continuity equation

$$\partial u/\partial x + \partial v/\partial y + \partial w/\partial z = 0 \quad (7.42)$$

Eq. (7.41) becomes the potential vorticity balance

$$\beta v = f \partial w/\partial z. \quad (7.43)$$

This important equation states that water column stretching in the presence of rotation is balanced by a change in latitude (Figure S7.28).

In Eq. (7.43), the vertical velocity  $w$  is due to Ekman pumping. From Eqs. (7.20) and (7.21):

$$\begin{aligned} w &= \partial/\partial x (\tau^{(y)}/\rho f) - \partial/\partial y (\tau^{(x)}/\rho f) \\ &= \text{"curl } \tau \text{"} \end{aligned} \quad (7.44)$$

where  $\tau$  is the vector wind stress,  $\tau^{(x)}$  is the zonal wind stress, and  $\tau^{(y)}$  is the meridional wind stress. Assuming that the vertical velocity  $w$  is zero at great depth, Eq. (7.43) can be vertically integrated to obtain the *Sverdrup balance*:

$$\begin{aligned} \beta \left( M^{(y)} - \left( \tau^{(x)} / f \right) \right) &= \partial / \partial x \left( \tau^{(y)} \right) - \partial / \partial y \left( \tau^{(x)} \right) \\ &= \text{“curl } \tau \text{”} \end{aligned} \quad (7.45)$$

where the meridional (south-north) mass transport  $M^{(y)}$  is the vertical integral of the meridional velocity  $v$  times density  $\rho$ . The second term on the left side is the meridional Ekman transport. Thus, the meridional transport in the Sverdrup interior is proportional to the wind stress curl corrected for the Ekman transport.

The meridional transport  $M^{(y)}$  is the Sverdrup transport. A global map of the Sverdrup transport integrated from the eastern to the western boundary is shown in Figure 5.17. The size of the integral at the western boundary gives the western boundary current transport since Sverdrup’s model must be closed with a narrow boundary current that has at least one additional physical mechanism beyond those in the Sverdrup balance (a shift in latitude because of water column stretching driven by Ekman transport convergence). Physics of the boundary currents are discussed in the following sections.

### 7.8.2. Stommel’s Solution: Westward Intensification and Western Boundary Currents

In the late 1940s, Henry Stommel (1948) added simple linear friction to Sverdrup’s

model of the gentle interior flow in a basin with eastern and western boundaries (Section 7.8.1). Mathematically this is an addition of dissipation of potential vorticity  $Q$  on the right-hand side of Eq. (7.37). The remarkable result was that the returning flow can only be in a narrow jet along the western boundary (Figure S7.33). The potential vorticity balance in this jet is change in planetary vorticity balanced by bottom friction.

Figure S7.33a shows the ocean circulation if there were no latitudinal variation in Coriolis parameter (no  $\beta$ -effect; Stommel, 1965). This is the solution if Earth were a rotating, flat disk with westerlies in the north and trades in the south. In this solution, the potential vorticity input from the wind cannot be balanced by a change in latitude, so the flow builds up relative vorticity (negative sign) that is balanced throughout the basin by bottom friction; the Sverdrup balance (Eq. 7.40) cannot apply. In Figure S7.33b, for the realistic spherical Earth with a  $\beta$ -effect, the flow is southward throughout the interior (Sverdrup balance), and returns northward in a swift jet on the western boundary. This idealized circulation resembles the Gulf Stream and Kuroshio subtropical gyres in which the Gulf Stream and Kuroshio are the narrow western boundary currents returning all southward Sverdrup interior flow back to the north.

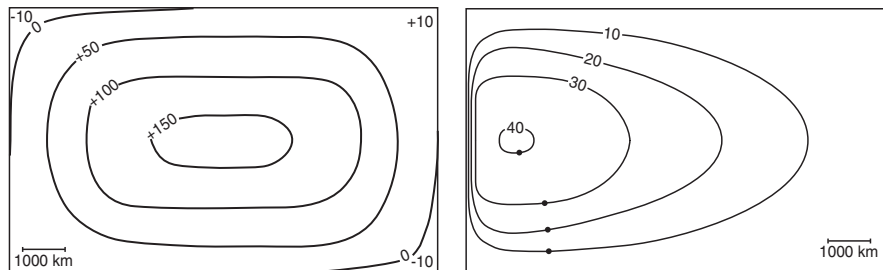


FIGURE S7.33 Stommel’s wind-driven circulation solution for a subtropical gyre with trades and westerlies like the central latitudes of Figure S7.32: (a) surface height on a uniformly rotating Earth and (b) westward intensification with the  $\beta$ -effect. After Stommel (1965).

Stommel's frictional solution is somewhat unrealistic since the friction is between the boundary current and the ocean bottom. This means that the wind-driven flow must reach to the ocean bottom. However, with stratification, it is not at all obvious that the circulation reaches so deep (although in fact one characteristic of strong western boundary currents such as the Gulf Stream system is that the narrow current does reach to the bottom even if the Sverdrup interior flow does not). A subsequent study by Walter Munk avoids this restriction and still yields westward intensification, as seen next.

### 7.8.3. Munk's Solution: Western Boundary Currents

A few years after Stommel's work, Walter Munk considered the effect of more realistic friction on the ocean gyre circulations between the currents and the side walls rather than between the currents and the ocean bottom. Munk's (1950) result was very similar to Stommel's result, predicting westward intensification of the circulation. A narrow, swift jet along the western boundary returns the Sverdrup interior flow to its original latitude (Figure S7.34).

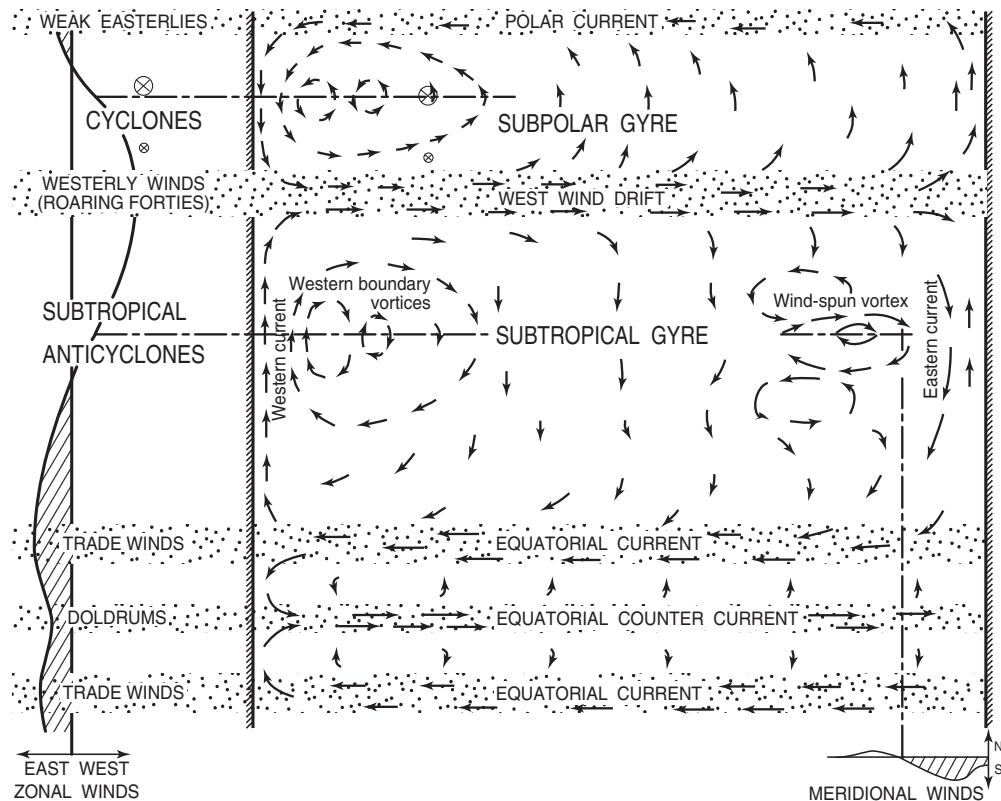


FIGURE S7.34 Munk's wind-driven circulation solution: zonal wind profiles on left and circulation streamlines in the center. After Munk (1950).

How does the potential vorticity balance work in Munk's model (which is combined with Sverdrup's model)? Why do we find the boundary current on the western side rather than the eastern side, or even within the middle of the basin (if considering Stommel's bottom friction)? In the Sverdrup interior of a subtropical gyre, when the wind causes Ekman pumping, the water columns are squashed, they move equatorward to lower planetary vorticity.

To return to a higher latitude, there must be forcing that puts the higher vorticity back into the fluid. This cannot be in the form of planetary vorticity or very, very narrow wind forcing, since the first is already contained in the Sverdrup balance, and the second is unphysical except in one or two extremely special locations (e.g., Arabian coast, Chapter 11). Therefore, the input of vorticity must affect the relative vorticity.

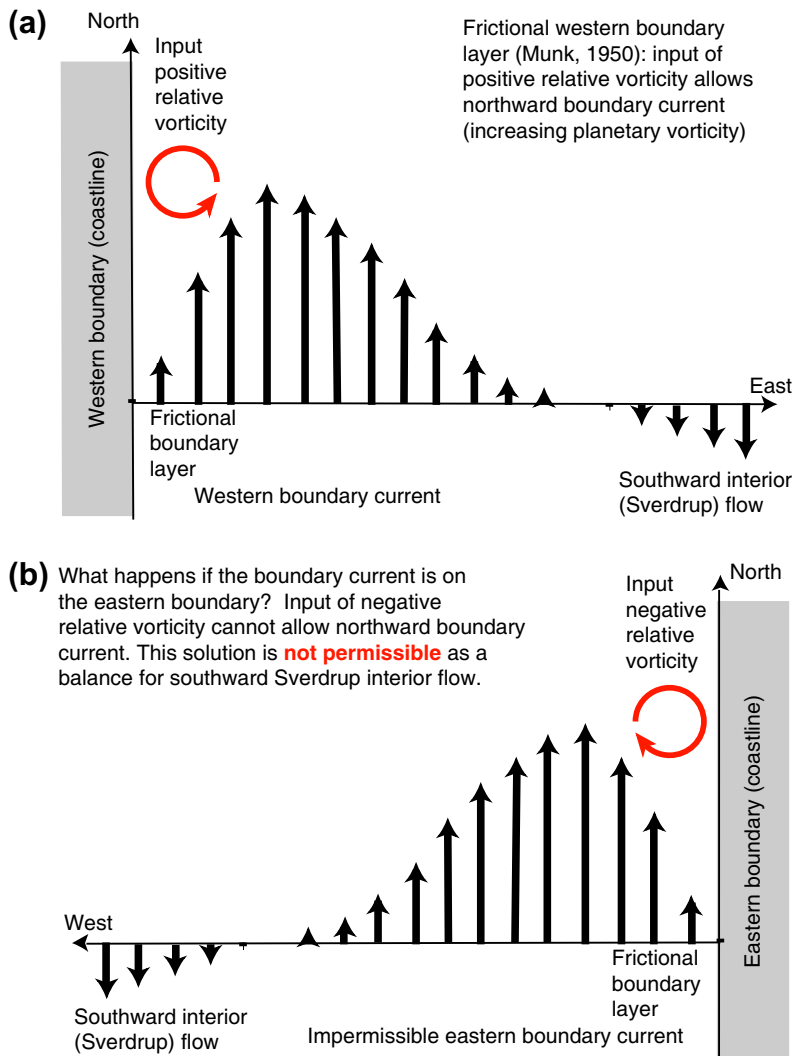


FIGURE S7.35 (a) Vorticity balance at a western boundary, with side wall friction (Munk's model). (b) Hypothetical eastern boundary vorticity balance, showing that only western boundaries can input the positive relative vorticity required for the flow to move northward.

Consider a western boundary current for a Northern Hemisphere subtropical gyre (Figure S7.35), with friction between the current and the side wall (Munk's model). The effect of the side wall is to reduce the boundary current velocity to zero at the wall. Therefore, the boundary current has positive relative vorticity. This vorticity is injected into the fluid by the friction at the wall, and allows the current to move northward to higher Coriolis parameter  $f$ . (Note that there is negative relative vorticity in the boundary current offshore of its maximum speed, but the current changes much more slowly and the negative relative vorticity there is much lower than the positive relative vorticity at the boundary.) On the other hand, if the narrow jet returning flow to the north were on the eastern boundary, the side wall friction would inject negative relative vorticity, which would make it even more difficult for the boundary current fluid to join the interior flow smoothly. Therefore, vorticity arguments require that frictional boundary currents be on the western boundary. The reader can go through this exercise for subpolar gyres as well as for both types of gyres in the Southern Hemisphere and will find that a western boundary current is required in all cases.

#### 7.8.4. Fofonoff's Solution: Large-Scale Inertial Currents

In one further important simplified approach to large-scale ocean circulation, Nicholas Fofonoff, in 1954, showed that circulation can arise as a free, unforced mode. The idea is that a very small amount of wind, with very little friction anywhere in the system, could set up such a circulation. Indeed, aspects of the Fofonoff solution are found in highly energetic regions, such as in the neighborhood of the Gulf Stream (which in actuality is not highly frictional, and which is stronger than predicted from the Sverdrup interior balance). This type of circulation is called an "inertial circulation." It is

easiest to describe using Fofonoff's own figure (Figure S7.36).

In the Fofonoff circulation, there is no Sverdrup interior with flow moving northward or southward. The interior flow is *exactly* zonal (east-west). This is because there is no wind input of vorticity, so flow cannot change latitude since it would then have to change its planetary vorticity. This exact zonality therefore results from the  $\beta$ -effect. However, there are strong boundary currents on both the western and eastern boundaries, and there can be strong, exactly zonal jets crossing the ocean in its interior.

How do these strong currents with so much relative vorticity connect to each other? Consider westward flow across the middle of the ocean, as illustrated in Figure S7.36. This reaches the western boundary and must somehow get back to the eastern boundary to feed back into the westward flow. It can do this by moving along the western boundary in a very narrow current that has a large amount of relative vorticity. This current can be to either the north or the south. Suppose it is to the north. Then the relative vorticity of this frictionless current is positive, allowing it to move to higher latitude. It then jets straight across the middle of the ocean, reaches the eastern boundary, and moves southward, feeding into the westward flow in the interior. There is no net input of vorticity anywhere in this model (no wind, no friction).

Following the Sverdrup, Stommel, Munk, and Fofonoff models, a number of theoretical papers explored various combinations of the different types of friction, inertia, and boundary geometries on the mean ocean flow, but their results can all be understood in terms of these basic models. Some of the earliest ocean circulation models (Veronis, 1966; Bryan, 1963) illustrated the dynamical processes for various strengths of friction and inertia. Further real breakthroughs in theoretical understanding of wind-driven ocean circulation occurred thirty to forty years later, with treatment of the effect of stratification, as discussed next.

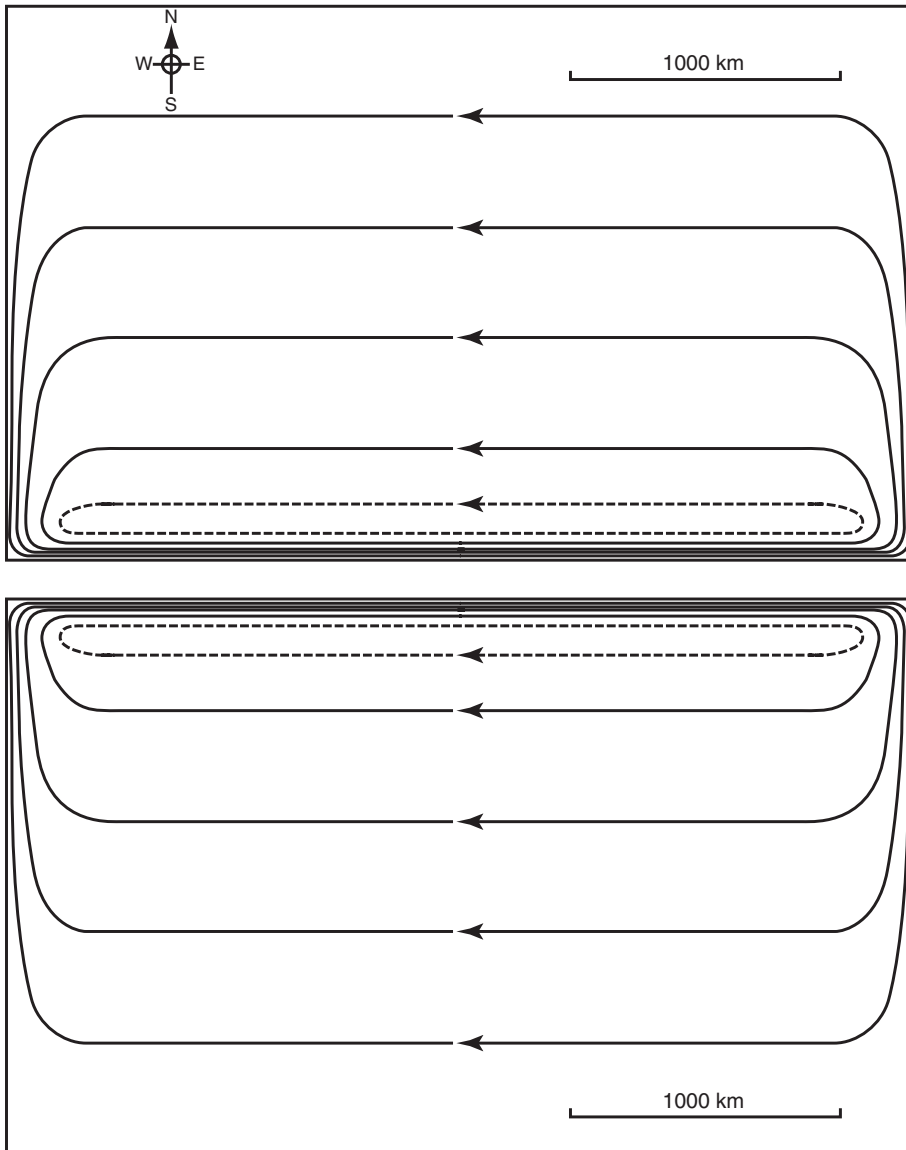


FIGURE S7.36 Inertial circulation, in the absence of friction and wind, but in the presence of the  $\beta$ -effect. Source: From Fofonoff (1954).

### 7.8.5. Wind-Driven Circulation in a Stratified Ocean

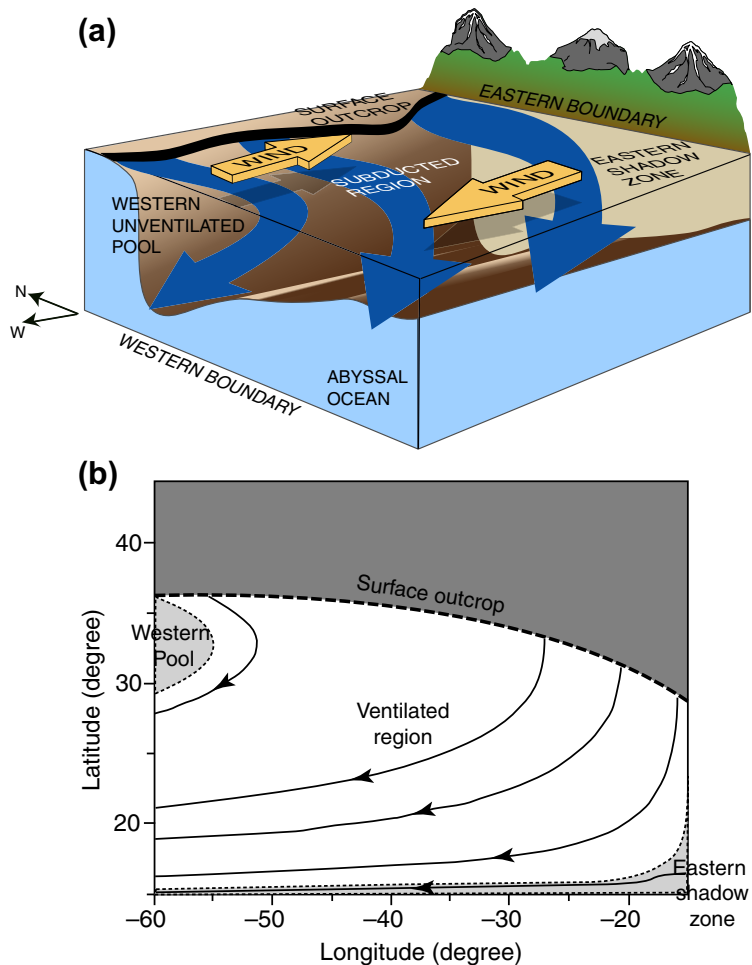
What happens to the wind-driven circulation theories in a stratified ocean? Water moves

down into the ocean, mostly along very gradually sloping isopycnals. Where streamlines of flow are connected to the sea surface, we say the ocean is directly *ventilated* (Figure S7.37). Where there is Ekman pumping (negative wind stress curl), the

Sverdrup interior flow is equatorward (Section 7.8.1). Water columns at the local mixed layer density move equatorward and encounter less dense water at the surface. They slide down into the subsurface along isopycnals, still moving equatorward. This process is called *subduction* (Luyten, Pedlosky, & Stommel, 1983), using a term borrowed from plate tectonics. The subducted waters then flow around the gyre and enter the western boundary current if they do not first enter the tropical circulation. The details of this process are beyond the scope of this text.

In each subducted layer, there can be three regions (Figure S7.37): (1) a *ventilated region* connected from the sea surface as just described, (2) a western unventilated pool with streamlines that enter and exit from the western boundary current without entering the surface layer, and (3) an eastern quiet (*shadow*) zone between the easternmost subducting streamline and the eastern boundary. A continuous range of surface densities is found in the subtropical gyre; the water column is directly ventilated over this full range, with waters at each density coming from a different sea-surface location

**FIGURE S7.37** (a) Subduction schematic (Northern Hemisphere). (b) Streamlines for idealized subduction on an isopycnal surface. The light gray regions are the western pool and eastern shadow zone, where streamlines do not connect to the sea surface. The heavy dashed contour is where the isopycnal meets the sea surface (surface outcrop); in the dark gray area there is no water of this density. After Williams (1991).



depending on the configuration of streamlines on that isopycnal. This is called the “*ventilated thermocline*”; in water mass terms, this process creates the Central Water. The maximum density of the ventilated thermocline is set by the maximum winter surface density in the subtropical gyre (Stommel, 1979). This usually occurs at the most poleward edge of the gyre, around 40 to 50 degrees latitude. The maximum depth of the ventilated thermocline is the depth of this densest isopycnal, and is between 500 and 1000 m depending on the ocean (see Chapters 9–11).

Subducting waters can leave the surface layer in two distinct ways: they can be pushed downward along isopycnals by Ekman pumping, and they can also be included in the subsurface layer through seasonal warming and cooling of the surface layer while they flow southward. In winter the surface layer is of uniform density. Entering spring and summer, this is glazed over by a surface layer of much lower density. All the while the geostrophic flow is southward. When the next winter arrives, the water column is farther south and winter cooling does not penetrate down to it. Therefore it has effectively entered the subsurface flow and does not re-enter the surface layer until it emerges from the western boundary, possibly many years later. Therefore the properties of the subsurface flows are set by the late winter conditions. The other seasons have no impact other than to provide seasonal isolation of the winter layer until it has subducted. Stommel (1979) called this phenomenon the “Ekman demon,” analogous to Maxwell’s demon of thermodynamics, which is a thought experiment about separating higher and lower energy molecules.

The opposite of subduction is *obduction*, borrowed again from plate tectonics by Qiu and Huang (1995). In obducting regions, waters from subsurface isopycnals come up and into the surface layer. These are generally upwelling regions such as the cyclonic subpolar gyres and the region south of the ACC.

Wind-driven circulation occurs in unventilated stratified regions as well. It is most vigorous in regions connected to the western boundary currents where water can enter and exit the western boundary. In these regions, the western boundary currents and their separated extensions usually reach to the ocean bottom. In a region that is closer and closer to the western boundary with increasing depth, there can be a closed circulation region that connects in and out of the western boundary without connection to the sea surface; such regions are characterized by constant potential vorticity (stretching and planetary portions only, or  $f/H$ ). These dynamics are beyond the scope of this text.

## 7.9. WIND-DRIVEN CIRCULATION: EASTERN BOUNDARY CURRENTS AND EQUATORIAL CIRCULATION

### 7.9.1. Coastal Upwelling and Eastern Boundary Currents

The eastern boundary regions of the subtropical gyres have strong but shallow flow that is dynamically independent of the open ocean gyre regimes. Upper ocean eastern boundary circulation is driven by alongshore wind stress that creates onshore (or offshore) Ekman transport that creates upwelling (or downwelling; Section 7.5.4). Beneath or inshore of the equatorward eastern boundary currents there is a poleward undercurrent or countercurrent. Coastal upwelling systems are not restricted to eastern boundaries; the southern coast of the Arabian peninsula has the same kind of system. These circulations are fundamentally different from western boundary currents, which are tied to potential vorticity dynamics (Section 7.8).

The classical explanation of eastern boundary currents is that equatorward winds force Ekman flow offshore, which drives a shallow upwelling

(on the order of 200 m deep) in a very narrow region adjacent to the coast (on the order of 10 km; Figure S7.13c). The upwelling speed is about 5–10 m/day. Because of stratification, the source of upwelled water is restricted to layers close to the sea surface, usually between 50 and 300 m.

The zone of coastal upwelling can be extended to more than 100 km offshore by an increase in longshore wind strength with distance offshore; this is observed in each eastern boundary upwelling system due to topographic steering of the winds by the ocean–land boundary. The offshore Ekman transport therefore increases with distance offshore, which requires upwelling through the whole band (Bakun & Nelson, 1991). The zone is identified by positive wind stress curl, notably in the California Current and Peru-Chile Current regions and the Arabian upwelling zone (Figure 5.16d).

Upwelled water is cooler than the original surface water. It originates from just below the euphotic zone and therefore is also rich in nutrients, which results in enhanced biological productivity characterized by high chlorophyll content (Section 4.6). Cool surface temperatures and enhanced biological productivity are clear in satellite images that record sea-surface temperature and ocean color (Figure 4.28).

Upwelling is strongly seasonal, due to seasonality in the winds. Onset of upwelling can be within days of arrival of upwelling-favorable winds. In one example, off the coast of Oregon, the surface temperature dropped by 6°C in two days after a longshore wind started.

Coastal upwelling is accompanied by a rise in upper ocean isopycnals toward the coast (Figure 7.6). This creates an equatorward geostrophic surface flow, the *eastern boundary current*. These currents are narrow (<100 km width and near the coast), shallow (upper 100 m), strong (40–80 cm/sec), and strongly seasonal. The actual flow in an eastern boundary current system includes strong, meandering eddies

and offshore jets/filaments of surface water, often associated with coastline features such as capes (Figure 10.6). Actual eastern boundary currents are some distance offshore at the axis of the upwelling front created by the offshore Ekman transport.

*Poleward undercurrents* are observed at about 200 m depth beneath the equatorward surface currents in each eastern boundary upwelling system. When upwelling-favorable winds weaken or disappear, the equatorward flow also disappears and the poleward undercurrent extends up to the surface (there is no longer an undercurrent). Poleward undercurrents are created mainly by the alongshore pressure gradient that drives the onshore subsurface geostrophic flow that feeds the upwelling. There may also be a contribution from positive wind stress curl throughout the eastern boundary region that leads to poleward Sverdrup transport (Section 7.8.1; Hurlburt & Thompson, 1973).

The only ocean without an equatorward eastern boundary current is the Indian Ocean. The Leeuwin Current along the west coast of Australia flows poleward, even though the winds are upwelling favorable and would drive a normal eastern boundary current there in the absence of other forces. However, there is a much larger poleward pressure gradient force along this boundary than along the others, due to the flow of water westward through the Indonesian archipelago from the Pacific to the Indian Ocean.

### 7.9.2. Near-Surface Equatorial Currents and Bjerknes Feedback

Circulation within about 2 degrees latitude of the equator is very different from non-equatorial circulation because the Coriolis parameter  $f$  vanishes at the equator. The narrowness of this equatorial influence, that is, the equatorial baroclinic deformation radius, is set by the variation in Coriolis parameter with latitude and the

stratification of the ocean. Equatorial circulation is driven by easterly trade winds in the Pacific and Atlantic and by the seasonally reversing monsoonal winds in the Indian Ocean. We describe here only the equatorial circulation that results from trade winds.

Since the Coriolis parameter vanishes and there is no frictional Ekman layer, the easterly trade winds drive equatorial surface flow due westward in a frictional surface layer (Figure S7.38a). The westward surface current is shallow (50 to 100 m) and of medium strength (10 to 20 cm/sec). In each of the three oceans, this westward surface flow is a part of the *South Equatorial Current*. The water piles up gently in the west (to about 0.5 m height) and leaves a depression in the east. This creates an eastward pressure gradient force (from high pressure in the west to low pressure in the east). The pressure gradient force drives an eastward flow called the *Equatorial Undercurrent* (EUC). The EUC is centered at 100 to 200 m depth, just below the frictional surface layer. The EUC is only about 150 m thick. It is among the strongest ocean currents (>100 cm/sec). (See illustrations of the Pacific EUC in Section 10.7.3 and of the Atlantic EUC in Section 9.4.)

The pileup of waters in the western equatorial region results in a deepened pycnocline called the *warm pool* and a shallow pycnocline in the eastern equatorial region. Coriolis effects become important a small distance from the equator; the resulting off-equatorial Ekman transport enhances upwelling in the equatorial band. This creates upwelling along the equator and shoaling of the pycnocline toward the equator that drives a westward, nearly geostrophic flow at the sea surface. This broadens the frictional westward flow found right on the equator.

Upwelling in the eastern equatorial region draws cool water to the surface because of the shallow thermocline there. This creates a cold surface feature along the equator called the *cold*

*tongue* (see the sea-surface temperature map in Figure 4.1). Because of the thickness of the warm pool in the west, even intense upwelling cannot cause cold surface temperatures. The warm pool's high surface temperature, in excess of 28 °C, is maintained through radiative equilibrium with the atmosphere (Jin, 1996).

The east-west contrast in temperature along the equator maintains the atmosphere's *Walker circulation*, which has ascending air over the warm pool and descending over the eastern colder area. The Walker circulation is an important part of the trade winds that creates the warm pool and cold tongue, so there can be a feedback between the ocean and atmosphere; this is called the *Bjerknes feedback* (Bjerknes, 1969; Figure S7.38b). If something weakens the trade winds, as at the beginning of an El Niño event (Chapter 10), the westward flow at the equator weakens and upwelling weakens or stops. Surface waters in the eastern regions therefore warm. Water in the deep warm pool in the west sloshes eastward along the equator, thinning the pool. The change in sea-surface temperature weakens the Walker circulation/trade winds even more, which further exacerbates the ocean changes. This is an example of a *positive feedback*.

In the Indian Ocean, the prevailing equatorial winds are monsoonal, meaning that trade winds are only present for part of the year. This creates seasonally reversing equatorial currents and inhibits the formation of the warm pool/cold tongue structure. The Indian Ocean sea-surface temperature is high at all longitudes.

## 7.10. BUOYANCY (THERMOHALINE) FORCING AND ABYSSAL CIRCULATION

Heating and cooling change the ocean's temperature distribution, while evaporation, precipitation, runoff, and ice formation change the ocean's salinity distribution (Chapters 4

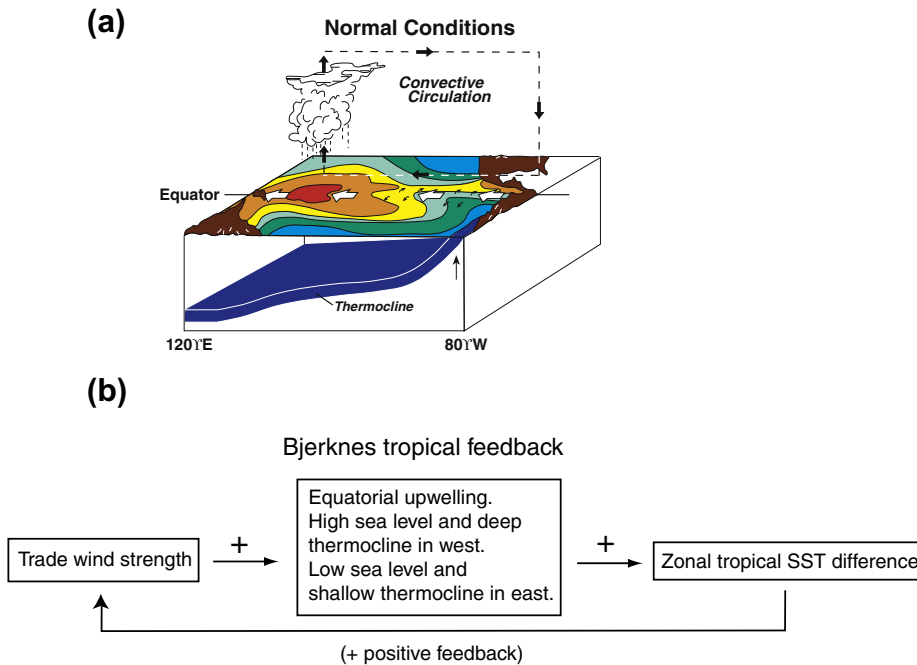


**FIGURE S7.38** (a) Schematic of upper ocean equatorial circulation (large white arrows), surface temperature (red is warm, blue is cold), and thermocline depth and upwelling, driven by the Walker circulation (“convective loop”). *Source: From NOAA PMEL (2009b).* (b) “Bjerknes feedback” between the trade wind strength and zonal (east-west) difference in tropical surface temperature. (Arrows mean that increase in one parameter results in an increase in the second parameter.) In this positive feedback loop, increased trade winds cause a larger sea-surface temperature difference, which in turn increases the trade wind strength.

and 5). Collectively, these are referred to as *buoyancy*, or *thermohaline*, forcing. Buoyancy processes are responsible for developing the ocean’s stratification, including its abyssal properties, pycnocline, thermocline, halocline, and upper layer structure (other than in wind-stirred mixed layers). Advection by currents also changes temperature and salinity locally, but it cannot change the overall inventory of either.

*Abyssal circulation* refers to the general category of currents in the deep ocean. The *overturning circulation*, also called the *thermohaline circulation*, is the part of the circulation associated with buoyancy changes, and overlaps spatially with the wind-driven upper ocean circulation; it also includes shallow elements

that are independent of the abyssal circulation. In the overturning circulation, cooling and/or salinification at the sea surface causes water to sink. This water must rise back to the warm surface, which requires diffusion of heat (buoyancy) downward from the sea surface. The source of eddy diffusion is primarily wind and tidal energy. Thus aspects of the thermohaline circulation depend on the magnitude of non-buoyancy processes through the eddy diffusivity (Wunsch & Ferrari, 2004).

Studies of the overturning circulation originated in the 1800s and early 1900s with German, British, and Norwegian oceanographers. J. Sandström (1908) presented experiments and ideas about the simplest overturning cells driven by high-latitude cooling and a deep

tropical warm source that we now identify with downward heat diffusion (see Figure S7.40). H. Stommel, in the 1960s, produced a series of elegant papers on abyssal flow driven by isolated sources of deep water and broad scale upwelling that returns the water back to the upper ocean (Section 7.10.2). At the same time, Stommel presented simple theories of the complementary idea of ocean flows driven by the very large-scale density contrasts (warm, saline tropics and cold, fresh poles: Section 7.10.3).

### 7.10.1. Buoyancy Loss Processes (Diapycnal Downwelling)

Water becomes denser through net cooling, net evaporation, and brine rejection during sea ice formation. We have already described brine rejection (Section 3.9.2); it is responsible for creating the densest bottom waters in the global ocean (Antarctic Bottom Water and parts of the Circumpolar Deep Water) and also in the regional basins where it is operative (Arctic Ocean, Japan Sea, etc.). Here we focus on *convection* created by net buoyancy loss in the open ocean, when surface water becomes denser than water below, and advects and mixes downward. Convection creates a mixed layer, just like wind stirring (Section 7.3). However, a convective mixed layer can be hundreds of meters thick by the end of winter, whereas a wind-stirred mixed layer is limited to about 150 m by the depth of wind-driven turbulence.

Convection happens on different timescales. Diurnal (daily) convection occurs at night in areas where the surface layer restratifies strongly during the day. During the annual cycle, cooling usually starts around the autumnal equinox and continues almost until the spring equinox. The resulting convection eats down into the surface layer, reaching maximum depth and density at the end of winter when the cumulative cooling reaches its maximum (February–March in the Northern

Hemisphere and August–September in the Southern Hemisphere).

Ocean convection is usually driven by surface cooling. Excess evaporation can also create convection, but the latent heat loss associated with evaporation is usually stronger. “Deep” convection is a loose term that usually refers to creation of a surface mixed layer that is thicker than about 1000 m. Deep convection has three phases: (1) preconditioning (reduction in stratification), (2) convection (violent mixing), and (3) sinking and spreading. Preconditioning for deep convection includes reduced stratification through the water column and some sort of dynamical feature that allows stratification to become even more. The convection phase occurs when there is large heat loss, usually due to high wind speeds along with very cold, dry air usually blowing from the land. Adjustment or restratification, followed by spreading, occurs as the convective features collapse (Killworth, 1983; Marshall & Schott, 1999.)

Convective regions have a typical structure (Figure S7.39). These include: (1) a *chimney*, which is a patch of tens to more than hundreds of kilometers across within which preconditioning can allow convection and (2) convective *plumes* that are the actual sites of convection and are about 1 km or less across (Killworth, 1979; Marshall & Schott, 1999).

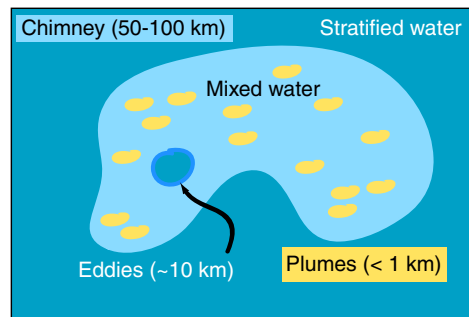


FIGURE S7.39 Processes in a deep convection region. After Marshall and Schott (1999).

The plumes are about the same size across as they are deep. It is not yet clearly known what the vertical velocity structure is within the convective plumes. Observations in the Labrador Sea have suggested that there is more downward motion than upward motion, and that the required upward motion might occur more slowly over a broader area within the chimney.

Deep convection occurs only in a few special locations around the world: Greenland Sea, Labrador Sea, Mediterranean Sea, Weddell Sea, Ross Sea, and Japan (or East) Sea. These sites, with the exception of the isolated Japan Sea, ventilate most of the deep waters of the global ocean. (The denser bottom waters, particularly in the Southern Hemisphere, result from the brine rejection process around Antarctica.)

### 7.10.2. Diapycnal Upwelling (Buoyancy Gain)

The structure of the basin and global scale overturning circulations depends on both the amount of density increase in the convective source regions and the existence of a buoyancy (heat) source at lower latitudes that is at least as deep as the extent of the cooling (Sandström, 1908; Figure S7.40). Since there are no significant local deep heat sources in the world ocean, waters that fill the deep ocean can only return to the sea surface as a result of diapycnal eddy diffusion of buoyancy (heat and freshwater)

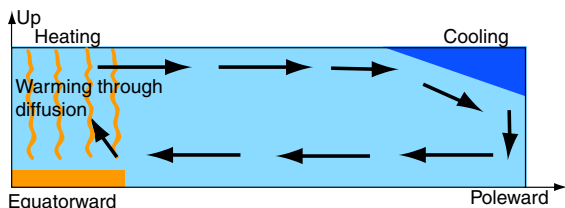


FIGURE S7.40 The role of vertical (diapycnal) diffusion in the MOC, replacing Sandström's (1908) deep tropical warm source with diapycnal diffusion that reaches below the effect of high latitude cooling.

downward from the sea surface (Sections 5.1.3 and 7.3.2).

Munk's (1966) diapycnal eddy diffusivity estimate of  $\kappa_v = 1 \times 10^{-4} \text{ m}^2/\text{sec}$  (Section 7.3.2) was based on the idea of isolated sources of deep water and widespread diffusive upwelling of this deep water back to the surface. From all of the terms in the temperature and salt equations (7.12–7.13), Munk assumed that most of the ocean is dominated by the balance

$$\text{vertical advection} = \text{vertical diffusion} \quad (7.46a)$$

$$w \partial T / \partial z = \partial / \partial z (\kappa_v \partial T / \partial z) \quad (7.46b)$$

Munk obtained his diffusivity estimate from an average temperature profile and an estimate of about 1 cm/day for the upwelling velocity  $w$ , which can be based on deep-water formation rates and an assumption of upwelling over the whole ocean. The observed diapycnal eddy diffusivity in the open ocean away from boundaries is an order of magnitude smaller than Munk's estimate, which must be valid for the globally averaged ocean structure. This means that there must be much larger diffusivity in some regions of the ocean — now thought to be at the boundaries — at large seamount and island chains, and possibly the equator (Section 7.3).

### 7.10.3. Stommel and Arons' Solution: Abyssal Circulation and Deep Western Boundary Currents

Deep ocean circulation has been explained using potential vorticity concepts that are very familiar from Sverdrup balance (Section 7.8.1). Stommel (1958), Stommel, Arons, and Faller (1958), and Stommel & Arons (1960a,b) considered an ocean with just two layers, and solved only for the circulation in the bottom layer. They assumed a source of deep water at the northernmost latitude, and then assumed that this water upwells uniformly (at the same rate) everywhere (Figure S7.41). This upwelling stretches the deep ocean water columns.

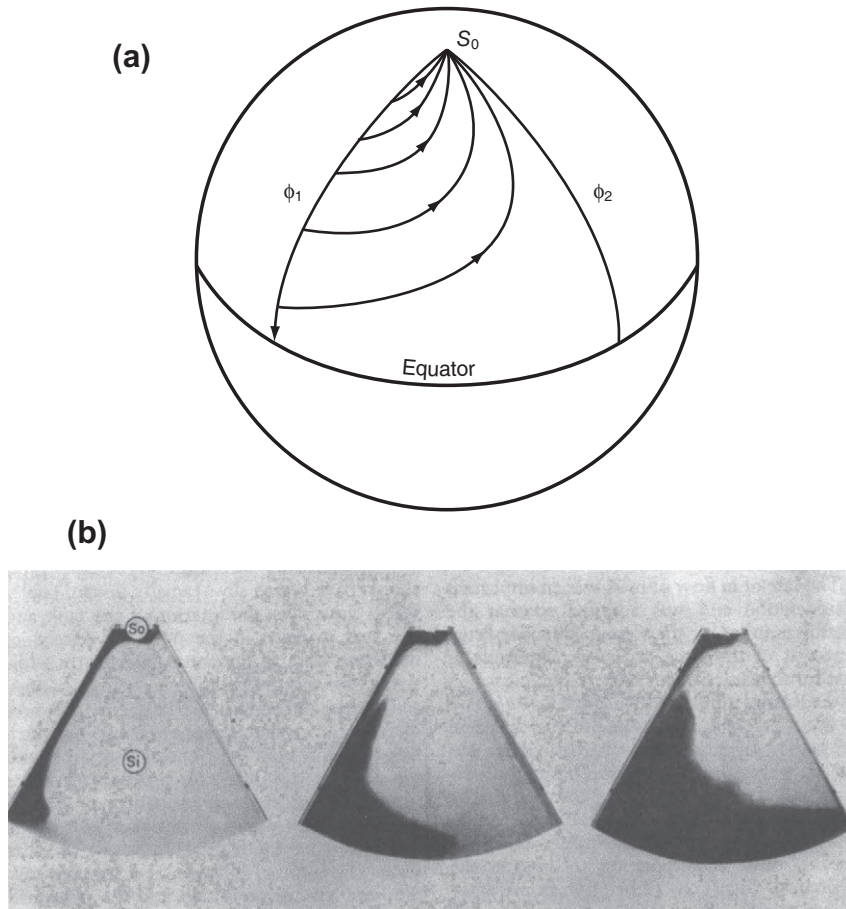


**FIGURE S7.41** (a) Abyssal circulation model. After Stommel and Arons (1960a). (b) Laboratory experiment results looking down from the top on a tank rotating counterclockwise around the apex ( $S_0$ ) with a bottom that slopes towards the apex. There is a point source of water at  $S_0$ . The dye release in subsequent photos shows the Deep Western Boundary Current, and flow in the interior  $S_i$  beginning to fill in and move towards  $S_0$ . Source: From Stommel, Arons, & Faller (1958).

Stretching requires a poleward shift of the water columns to conserve potential vorticity (Eq. 7.35). The predicted interior flow is therefore counterintuitive — it runs toward the deep-water source. (Actual abyssal flow is strongly modified from this by the major topography that modifies the  $\beta$ -effect by allowing stretched columns to move toward shallower bottoms rather than toward higher latitude.)

*Deep Western Boundary Currents* (DWBCs) connect the isolated deep-water sources and

the interior poleward flows. Whereas unambiguous poleward flow is not observed in the deep ocean interior (possibly mostly because of topography), DWBCs are found where they are predicted to occur by the Stommel and Arons abyssal circulation theory (Warren, 1981). One such DWBC runs southward beneath the Gulf Stream, carrying dense waters from the Nordic Seas and Labrador Sea. Swallow and Worthington (1961) found this current after being convinced by Stommel to go search for

it. Maps from the 1920s Meteor expedition (Wüst, 1935) show the large-scale consequences of this particular DWBC for deep salinity and oxygen distributions over the whole length of the Atlantic (see Chapter 9). Stommel's (1958) map (Figure S7.42), revisited later by Kuo and Veronis (1973) using a numerical ocean model, shows the conceptual global pattern of DWBCs and abyssal circulation, including the deep-water source in the northern North Atlantic (the source of North Atlantic Deep Water, Chapter 9) and in the Antarctic (the source of Antarctic Bottom Water, Chapter 13).

#### 7.10.4. Thermohaline Oscillators: Stommel's solution

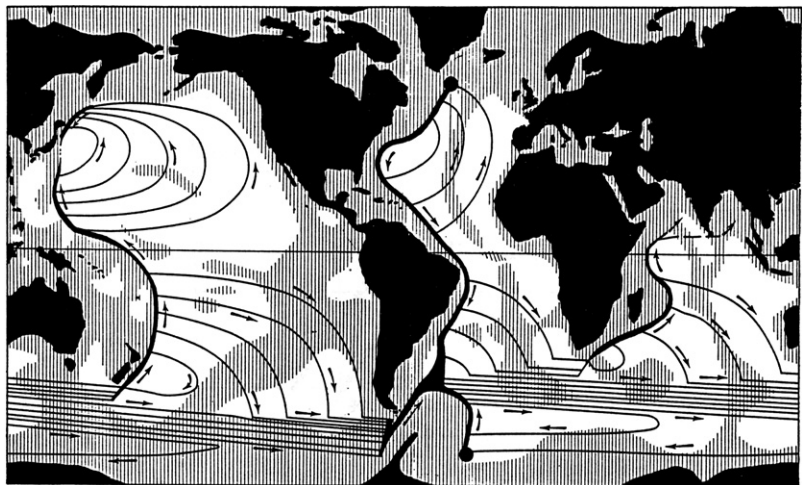
An entirely different approach to the MOC from the Stommel-Arons abyssal circulation model considers changes in overturn associated with changing rates of dense water production. The prototype of these models is a very simple reduction of the ocean to just a few boxes, and was also developed by Stommel (1961), who can be appreciated at this point as a giant of ocean general circulation theory. Such box models show how even the simplest model of climate change, for example, can lead to

complex results. In this case, *multiple equilibria* result, that is, the system can jump suddenly between quite different equilibrium states.

Stommel (1961) reduced the ocean to two connected boxes representing dense, cold, fresh high latitudes and light, warm, saltier low latitudes (Figure S7.43). The boxes are connected, with the amount of flow between them dependent on the density difference between the boxes. (This is a simplification of sinking of dense water to the bottom and flowing toward a region of lower bottom density, to be fed in turn by upwelling in the lower density box, and return flow at the sea surface.) In each box, the temperature and salinity are set by (1) flux of water between the boxes (thermohaline circulation) that depends on the density difference between the boxes and (2) restoring temperature and salinity to a basic state over some set time period. Then the effects on the flow between the boxes of slow heating and cooling, or of freshwater fluxes (evaporation and precipitation for instance), are studied.

Stommel (1961) found that several different thermohaline circulation strengths exist for a given set of choices of model parameters (externally imposed temperature and salinity,

FIGURE S7.42 Global abyssal circulation model, assuming two deep water sources (filled circles near Greenland and Antarctica). Source: From Stommel (1958).



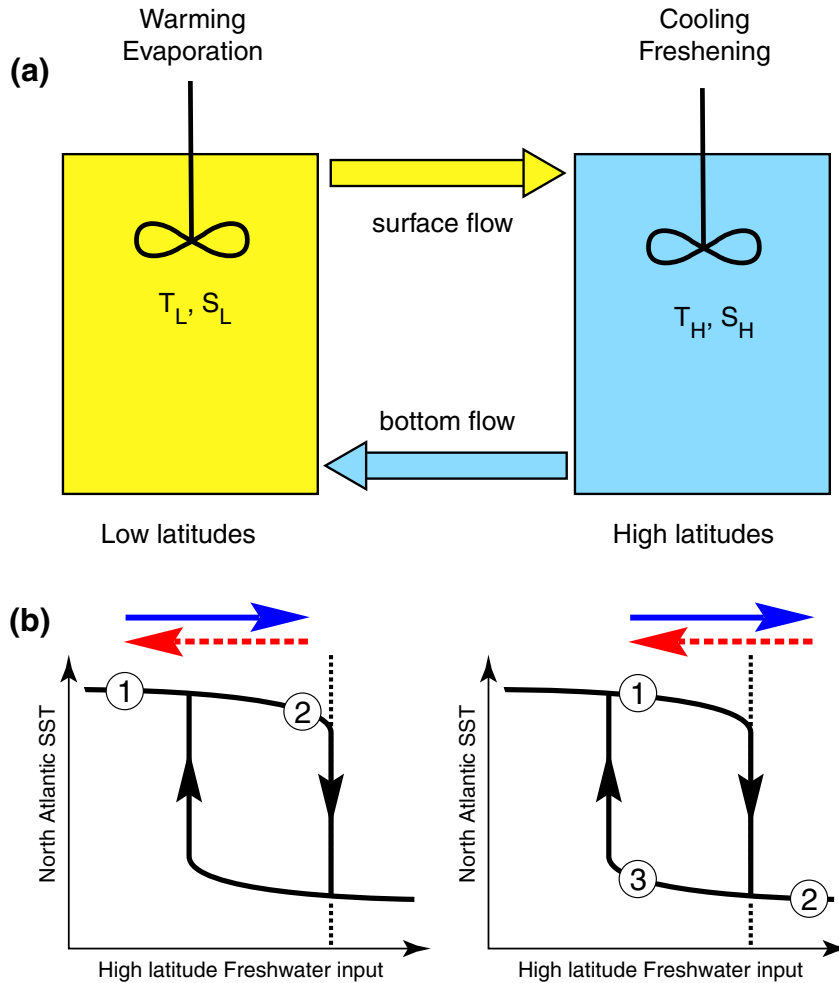


**FIGURE S7.43** (a) Schematic of the [Stommel \(1961\)](#) two-box model of the meridional overturning circulation. The direction of the arrows assumes that the higher latitude box (blue) has higher density water. Each box is well mixed. (b) Schematic of the hysteresis in North Atlantic sea-surface temperature resulting from hysteresis in MOC strength. The starting point in freshwater is denoted by 1; starting at lower freshwater, hence higher salinity, in the left panel. Freshening is denoted by the blue arrow, with the same total amount in both panels. Salinification is denoted by red arrow, and should be exactly opposite to the freshwater arrow. In the left panel, starting at higher salinity, the freshening allows the system to remain on the top branch, and so subsequent evaporation returns the system to original state. In the right panel, with a fresher starting point, the same freshening causes transition to lower curve (2), and subsequent evaporation returns system to a different state, denoted by 3. *After [Stocker and Marchal \(2000\)](#).*

restoration timescales for temperature and salinity, and factor relating the flow rate to the density difference between the boxes). As the basic state was slowly changed, perhaps by reduction of the basic high-latitude

(which reduces its density), the flow rate slowly changed and then suddenly jumped to a different equilibrium rate. When the basic state salinity was then slowly increased, the system jumped back to a higher flow rate but

at a very different basic salinity than during its decreasing phase. Thus this system exhibits *hysteresis*: it has different equilibrium states depending on whether the state is approached from a much higher salinity or a much lower salinity.

The coupled atmosphere-sea-ice-land-physics-biology-chemistry climate system is far more complex than the two simple boxes in this very simple Stommel oscillator model. Yet its multiple equilibria and hysteresis behavior have been useful in demonstrating the potential for abrupt and relatively large changes in climate and, more specifically, for interpretation of numerical models of the changes in overturning circulation that could result from changes in external forcing.

## References

- Armi, L., 1978. Some evidence for boundary mixing in the deep ocean. *J. Geophys. Res.* 83, 1971–1979.
- Assaf, G., Gerard, R., Gordon, A., 1971. Some mechanisms of oceanic mixing revealed in aerial photographs. *J. Geophys. Res.* 76, 6550–6572.
- Bakun, A., Nelson, C.S., 1991. The seasonal cycle of wind-stress curl in subtropical eastern boundary current regions. *J. Phys. Oceanogr.* 21, 1815–1834.
- Bjerknes, J., 1969. Atmospheric teleconnections from the equatorial Pacific. *Mon. Weather Rev.* 97, 163–172.
- Boccaletti, G., Ferrari, R., Fox-Kemper, B., 2007. Mixed layer instabilities and restratification. *J. Phys. Oceanogr.* 37, 2228–2250.
- Brink, K.H., 2005. Coastal physical processes overview. In: Robinson, A.F., Brink, K.H. (Eds.), *The Sea, Vol. 13: The Global Coastal Ocean: Multiscale interdisciplinary Processes*. Harvard University Press, Cambridge, MA, pp. 37–60.
- Bryan, K., 1963. A numerical investigation of a nonlinear model of a wind-driven ocean. *J. Atm. Sci.* 20, 594–606.
- Chelton, D.B., deSzoeke, R.A., Schlax, M.G., El Naggar, K., Siwertz, N., 1998. Geographical variability of the first baroclinic Rossby radius of deformation. *J. Phys. Oceanogr.* 28, 433–460.
- Chereskin, T.K., 1995. Direct evidence for an Ekman balance in the California Current. *J. Geophys. Res.* 100, 18261–18269.
- Cushman-Roisin, B., 1994. *Introduction to Geophysical Fluid Dynamics*. Prentice Hall, Englewood Cliffs, N.J., 320 p.
- d'Asaro, E.A., Eriksen, C.C., Levine, M.D., Paulson, C.A., Niiler, P., Van Meurs, P., 1995. Upper-ocean inertial currents forced by a strong storm. Part 1: Data and comparisons with linear theory. *J. Phys. Oceanogr.* 25, 2909–2936.
- Davis, R.E., deSzoeke, R., Niiler, P., 1981. Variability in the upper ocean during MILE. Part II: Modeling the mixed layer response. *Deep-Sea Res.* 28A, 1453–1475.
- Doron, P., Bertuccioli, L., Katz, J., Osborn, T.R., 2001. Turbulence characteristics and dissipation estimates in the coastal ocean bottom boundary layer from PIV data. *J. Phys. Oceanogr.* 31, 2108–2134.
- Egbert, G.D., Ray, R., 2001. Estimates of M2 tidal energy dissipation from TOPEX/Poseidon altimeter data. *J. Geophys. Res.* 106, 22475–22502.
- Ekman, V.W., 1905. On the influence of the Earth's rotation on ocean currents. *Arch. Math. Astron. Phys.* 2 (11), 1–53.
- Eriksen, C.C., 1982. Geostrophic equatorial deep jets. *J. Mar. Res.* 40 (Suppl), 143–157.
- Fofonoff, N.P., 1954. Steady flow in a frictionless homogeneous ocean. *J. Mar. Res.* 13, 254–262.
- Gent, P.R., McWilliams, J.C., 1990. Isopycnal mixing in ocean circulation models. *J. Phys. Oceanogr.* 20, 150–155.
- Gill, A.E., 1982. *Atmospheric-Ocean Dynamics*. Academic Press, New York, 662 p.
- Gill, A.E., Niiler, P., 1973. The theory of seasonal variability in the ocean. *Deep-Sea Res.* 20, 141–177.
- Gregg, M.C., 1987. Diapycnal mixing in the thermocline: a review. *J. Geophys. Res.* 94, 5249–5286.
- Huang, R.-X., 2010. *Ocean Circulation: Wind-driven and Thermohaline Processes*. Cambridge University Press, Cambridge, UK, 806 p.
- Hurlburt, H.E., Thompson, J.D., 1973. Coastal upwelling on a  $\beta$ -plane. *J. Phys. Oceanogr.* 19, 16–32.
- Jin, F.F., 1996. Tropical ocean-atmosphere interaction, the Pacific cold tongue, and the El Niño-Southern Oscillation. *Science* 274, 76–78.
- Kelley, D.E., Fernando, H.J.S., Gargett, A.E., Tanny, J., Özsoy, E., 2003. The diffusive regime of double-diffusive convection. *Progr. Oceanogr.* 56, 461–481.
- Killworth, P.D., 1979. On chimney formation in the ocean. *J. Phys. Oceanogr.* 9, 531–554.
- Killworth, P.D., 1983. Deep convection in the world ocean. *Rev. Geophys.* 21, 1–26.
- Knauss, J.A., 1997. *Introduction to Physical Oceanography*, second ed., Waveland Press, Long Grove, IL, 309 pp.
- Kraus, E.B., Turner, J.S., 1967. A one-dimensional model of the seasonal thermocline, II. The general theory and its consequences. *Tellus* 19, 98–105.
- Kunze, E., Firing, E., Hummon, J.M., Chereskin, T.K., Thurnherr, A.M., 2006. Global abyssal mixing Inferred from Lowered ADCP shear and CTD strain profiles. *J. Phys. Oceanogr.* 36, 1553–1576.

- Kuo, H.-H., Veronis, G., 1973. The use of oxygen as a test for an abyssal circulation model. *Deep-Sea Res.* 20, 871–888.
- Langmuir, I., 1938. Surface motion of water induced by wind. *Science* 87, 119–123.
- Large, W.G., McWilliams, J.C., Doney, S.C., 1994. Oceanic vertical mixing: A review and a model with a non-local K-profile boundary layer parameterization. *Rev. Geophys.* 32, 363–403.
- Ledwell, J.R., Watson, A.J., Law, C.S., 1993. Evidence for slow mixing across the pycnocline from an open-ocean tracer–release experiment. *Nature* 364, 701–703.
- Ledwell, J.R., Watson, A.J., Law, C.S., 1998. Mixing of a tracer in the pycnocline. *J. Geophys. Res.* 103, 21499–21529.
- Lentz, S.J., 1995. Sensitivity of the inner-shelf circulation to the form of the eddy viscosity profile. *J. Phys. Oceanogr.* 25, 19–28.
- Levitus, S., 1988. Ekman volume fluxes for the world ocean and individual ocean basins. *J. Phys. Oceanogr.* 18, 271–279.
- Levitus, S., Boyer, T.P., Antonov, J., 1994a. World ocean atlas: Volume 5: Interannual variability of upper ocean thermal structures. NOAA/NESDIS, Tech. Rpt., OSTI ID: 137204.
- Lien, R.-C., Gregg, M.C., 2001. Observations of turbulence in a tidal beam and across a coastal ridge. *J. Geophys. Res.* 106, 4575–4591.
- Luyten, J.R., Pedlosky, J., Stommel, H., 1983. The ventilated thermocline. *J. Phys. Oceanogr.* 13, 292–309.
- Marshall, J., Schott, F., 1999. Open-ocean convection: observations, theory, and models. *Rev. Geophys.* 37, 1–64.
- Munk, W., 1966. Abyssal recipes. *Deep-Sea Res.* 13, 707–730.
- Munk, W.H., 1950. On the wind-driven ocean circulation. *J. Atm. Sci.* 7, 80–93.
- Nansen, F., 1922. In: Brodhaus, F.U. (Ed.), *Nacht und Eis*. Leipzig, Germany, 355 pp. (in German).
- NOAA National Weather Service, 2005. Hydrometeorological Prediction Center (HPC) Home Page. National Weather Service. <http://www.hpc.ncep.noaa.gov/> (accessed 1.3.05).
- NOAA PMEL TAL Project Office, 2009b. El Niño theme page: access to distributed information on El Niño. NOAA Pacific Marine Environmental Laboratory. [http://www.pmel.noaa.gov/tao/el\\_nino/nino-home.html](http://www.pmel.noaa.gov/tao/el_nino/nino-home.html) (accessed 3.26.09).
- Olberson, D.J.M., Wenzel, Willebrand, J., 1985. The inference of North Atlantic circulation patterns from climatological hydrographic data. *Rev. Geophys.* 23, 313–356.
- Osborn, T.R., Cox, C.S., 1972. Oceanic fine structure. *Geophys. Astrophys. Fluid Dyn.* 3, 321–345.
- Pedlosky, J., 1987. *Geophysical Fluid Dynamics*, second ed., Springer-Verlag, New York, 732 p.
- Polton, J.A., Smith, J.A., MacKinnon, J.A., Tejada-Martínez, A.E., 2008. Rapid generation of high-frequency internal waves beneath a wind and wave forced oceanic surface mixed layer. *Geophys. Res. Lett.* 35, L13602. doi:10.1029/2008GL033856.
- Polzin, K.L., Toole, J.M., Ledwell, J.R., Schmitt, R.W., 1997. Spatial variability of turbulent mixing in the abyssal ocean. *Science* 276, 93–96.
- Pond, S., Pickard, G.L., 1983. *Introductory Dynamical Oceanography*, second ed., Pergamon Press, Oxford. 329 p.
- Price, J.F., Baringer, M.O., 1994. Outflows and deep water production by marginal seas. *Progr. Oceanogr.* 33, 161–200.
- Price, J.F., Weller, R.A., Pinkel, R., 1986. Diurnal cycling: Observations and models of the upper ocean response to diurnal heating, cooling and wind mixing. *J. Geophys. Res.* 91, 8411–8427.
- Qiu, B., Huang, R.X., 1995. Ventilation of the North Atlantic and North Pacific: Subduction versus obduction. *J. Phys. Oceanogr.* 25, 2374–2390.
- Ralph, E.A., Niiler, P.P., 1999. Wind-driven currents in the tropical Pacific. *J. Phys. Oceanogr.* 29, 2121–2129.
- Redi, M.H., 1982. Oceanic isopycnal mixing by coordinate rotation. *J. Phys. Oceanogr.* 12, 1154–1158.
- Reid, J.L., 1994. On the total geostrophic circulation of the North Atlantic Ocean: Flow patterns, tracers and transports. *Progr. Oceanogr.* 33, 1–92.
- Reid, J.L., 1997. On the total geostrophic circulation of the Pacific Ocean: Flow patterns, tracers and transports. *Progr. Oceanogr.* 39, 263–352.
- Rudnick, D.L., Boyd, T.J., Brainard, R.E., Carter, G.S., Egbert, G.D., Gregg, M.C., Holloway, P.E., Klymak, J.M., Kunze, E., Lee, C.M., Levine, M.D., Luther, D.S., Martin, J.P., Merrifield, M.A., Moum, J.N., Nash, J.D., Pinkel, R., Rainville, L., Sanford, T.B., 2003. From tides to mixing along the Hawaiian Ridge. *Science* 301, 355–357.
- Salmon, R., 1998. *Lectures on Geophysical Fluid Dynamics*. Oxford University Press, New York, 378 p.
- Sandström, J., 1908. *Dynamische Versuche mit Meerwasser*. *Annalen der Hydrographie und Maritimen Meteorologie*, pp. 6–23 (in German).
- Simpson, J.H., 1998. Tidal processes in shelf seas. In: Brink, K.H., Robinson, A.R. (Eds.), *The Sea*, Vol. 10: The Global Coastal Ocean: Processes and Methods. Harvard University Press, Boston, MA, pp. 113–150.
- Smith, J.A., 2001. Observations and theories of Langmuir circulation: a story of mixing. In: Lumley, J.L. (Ed.), *Fluid Mechanics and the Environment: Dynamical Approaches*. Springer, New York, pp. 295–314.

- Smith, R.D., Maltrud, M.E., Bryan, F.O., Hecht, M.W., 2000. Numerical simulation of the North Atlantic Ocean at  $1/10^\circ$ . *J. Phys. Oceanogr.* 30, 1532–1561.
- Stewart, R.H., 2008. Introduction to Physical Oceanography. Open-source textbook. [http://oceanworld.tamu.edu/ocean410/ocng410\\_text\\_book.html](http://oceanworld.tamu.edu/ocean410/ocng410_text_book.html) (accessed 3.28.09).
- Stocker, T.F., Marchal, O., 2000. Abrupt climate change in the computer: Is it real? *Proc. Natl. Acad. Sci., USA* 97, 1362–1365.
- Stommel, H., 1948. The westward intensification of wind-driven currents. *Trans. Am. Geophys. Union* 29, 202–206.
- Stommel, H.M., 1958. The abyssal circulation. *Deep-Sea Res.* 5, 80–82.
- Stommel, H.M., 1961. Thermohaline convection with two stable regimes of flow. *Tellus* 13, 224–230.
- Stommel, H.M., 1965. *The Gulf Stream: A Physical and Dynamical Description*, second ed., University of California Press, Berkeley, and Cambridge University Press, London, 248 p.
- Stommel, H.M., 1979. Determination of water mass properties of water pumped down from the Ekman layer to the geostrophic flow below. *Proc. Nat. Acad. Sci., USA* 76, 3051–3055.
- Stommel, H.M., Arons, A., 1960a. On the abyssal circulation of the World Ocean — I. Stationary planetary flow patterns on a sphere. *Deep-Sea Res.* 6, 140–154.
- Stommel, H.M., Arons, A., 1960b. On the abyssal circulation of the World Ocean — II. An idealized model of the circulation pattern and amplitude in oceanic basins. *Deep-Sea Res.* 6, 217–233.
- Stommel, H.M., Arons, A., Faller, A., 1958. Some examples of stationary planetary flow patterns in bounded basins. *Tellus* 10, 179–187.
- Stommel, H.M., Niiler, P.P., Anati, D., 1978. Dynamic topography and recirculation of the North Atlantic. *J. Mar. Res.* 36, 449–468.
- Sverdrup, H.U., 1947. Wind-driven currents in a baroclinic ocean. *Proc. Nat. Acad. Sci., USA* 33, 318–326.
- Sverdrup, H.U., Johnson, M.W., Fleming, R.H., 1942. *The Oceans: Their Physics, Chemistry and General Biology*. Prentice-Hall Inc., Englewood Cliffs, NJ, 1057 pp.
- Swallow, J.C., Worthington, L.V., 1961. An observation of a deep countercurrent in the western North Atlantic. *Deep-Sea Res.* 8, 1–19.
- Thorpe, S.A., 2004. Langmuir circulation. *Annu. Rev. Fluid Mech.* 36, 55–79. doi:10.1146/annurev.fluid.36.052203.071431.
- Tomczak, M., Godfrey, J.S., 1994. *Regional Oceanography, An Introduction*. Pergamon Press, Oxford, England, 422 p.
- Treguier, A.M., 2006. Ocean models. In: Chassignet, E.P., Verron, J. (Eds.), *Ocean Weather Forecasting: An Integrated View of Oceanography*. Springer, The Netherlands.
- Vallis, G.K., 2006. *Atmospheric and Oceanic Fluid Dynamics: Fundamentals and Large-scale Circulation*. Cambridge University Press, Cambridge, UK, 745 p.
- Veronis, G., 1966. Wind-driven ocean circulation — part II. Numerical solution of the nonlinear problem. *Deep-Sea Res.* 13, 30–55.
- Warren, B.A., 1981. Deep circulation of the world ocean. In: Warren, B.A., Wunsch, C. (Eds.), *Evolution of Physical Oceanography*. MIT Press, Cambridge MA, pp. 6–41.
- Weller, R., Dean, J.P., Marra, J., Price, J., Francis, E.A., Boardman, D.C., 1985. Three-dimensional flow in the upper ocean. *Science* 118, 1–22.
- Williams, R.G., 1991. The role of the mixed layer in setting the potential vorticity of the main thermocline. *J. Phys. Oceanogr.* 21, 1803–1814.
- Wunsch, C., 1996. *The Ocean Circulation Inverse Problem*. Cambridge University Press, New York, 458 pp.
- Wunsch, C., 2009. The oceanic variability spectrum and transport trends. *Atmosphere–Ocean* 47, 281–291.
- Wunsch, C., Ferrari, R., 2004. Vertical mixing, energy, and the general circulation of the oceans. *Annu. Rev. Fluid Mech.* 36, 281–314.
- Wüst, G., 1935. Schichtung und Zirkulation des Atlantischen Ozeans. Die Stratosphäre. In *Wissenschaftliche Ergebnisse der Deutschen Atlantischen Expedition auf dem Forschungs- und Vermessungsschiff "Meteor" 1925-1927, 6 1st Part 2*, 109–288 (in German).
- Wyrtki, K., 1975. Fluctuations of the dynamic topography in the Pacific Ocean. *J. Phys. Oceanogr.* 5, 450–459.